

Infrastructures near Seismic Faults

Data archives prepared for the
Report of JSPS Research Project
2004-2006 Grant-in-Aid for Scientific Research (A) (No. 16208048)
**Key Points for Rational Design of Civil Infrastructures near
Seismic Faults Reflecting Soil-Structure Interaction Features**
and
Final Report of the
Technical Committee for Fault-related Geotechnical Issues about
Civil-infrastructures, Japan Geotechnical Society (JGS).

Aug, 2007

Technical Committee for Fault-related Geotechnical Issues about Civil-infrastructures
Japan Geotechnical Society (JGS),
and Members of the
JSPS Research Project 2004-2006 Grant-in-Aid for Scientific Research (A) (No. 16208048)

Infrastructures near Seismic Faults: Data archives prepared by the Technical Committee for Fault-related Geotechnical Issues about Civil-infrastructures, Japan Geotechnical Society (JGS).

Kazuo KONAGAI, Leader, Institute of Industrial Science, University of Tokyo,
Sunao KUNIMATSU, Active Fault Research Center,
Keiichi UETA, Central Research Institute of Power Electric Industry,
Fumiaki UEHAN, Railway Technical Research Institute,
Nobuhiro ONIZUKA, Assoc. Professor, Kisarazu National College of Technology,
Hiroyoshi KIKU, Assoc. Professor, Kanto Gakuin University,
Takeyasu SUZUKI, Research Fellow, IIS, University of Tokyo,
Hitoshi NAKASE, Tokyo Electric Power Services Co. Ltd.,
Atsushi NOZU, Port and Airport Research Institute,
Takashi MATSUSHIMA, Assoc. Professor, Tsukuba University and
Jörgen JOHANSSON, Assistant Professor, Inst., Industrial Science, University of Tokyo.

Overseas collaborators:

Dr. Cheng-Hsing CHEN, Professor, National Taiwan University (NTU) and Deputy Director of National Center for Research of Earthquake Engineering (NCREE),
Dr. Wei F. Lee, Taiwan Construction Research Institute (TCRI), and
Mr. Travis MEI, ditto,

REPORT OF JSPS RESEARCH PROJECT
2006 GRANT-IN-AID FOR SCIENTIFIC RESEARCH (A)
Project No. 16208048
Title of the Project:

Key Points for Rational Design for Civil-Infrastructures near Seismic Faults Reflecting Soil-Structure Interaction Features

(地盤との相互作用を考慮した社会基盤施設の断層対策の合理的なガイドラインの提案)

Head investigator: Kazuo KONAGAI, Institute of Industrial Science, University of Tokyo
Investigators: Muneo HORI, Earthquake Research Institute, University of Tokyo
Kimiro MEGURO, Institute of Industrial Science, University of Tokyo
Junichi KOSEKI, Institute of Industrial Science, University of Tokyo
Takashi MATSUSHIMA, Institute of Engineering Mechanics and Systems, Tsukuba University
Jörgen JOHANSSON, Institute of Industrial Science, University of Tokyo,
and
Osamu MURATA, Dr. Eng., Railway Technical Research Institute (for the first fiscal year of 2005)

Grant-in-aid:	12,500,000JPY	2004
	9,800,000JPY	2005
	3,800,000JPY	2006

Publication list

(Peer-reviewed papers)

- Hossein Tahghighi and Kazuo Konagai. Numerical analysis of non-linear soil-pile interaction under lateral loads. *Soil Dynamics and Earthquake Engineering*, **27(4)**, 463-474, 2007.
- Johansson, J. and Konagai, K., Fault induced permanent ground deformations: An experimental comparison of wet and dry soil and implications for buried structures. *Soil Dynamics and Earthquake Engineering*, **26(1)**, 45-53, 2006.
- Johansson, J. and Konagai, K. Fault induced permanent ground deformations: Experimental verification of wet and dry soil, numerical findings' relation to field observations of tunnel damage and implications for design, *Soil Dynamics and Earthquake Engineering*, **27(10)**, 938-956, 2007.
- Kim D.S. and Konagai K., Simple approach to obtain ground amplification motion of surface soil deposits with a radical change of depth, *Canadian Geotechnical Journal*, **42(2)**, 491-498, 2005.
- Konagai, K., Yoshimi, M., Meguro, K., Yoshimura, M., Mayorca, P., Takashima, M., Farahani, A., Tahghighi, H. and Keshavarz, M.: Strain induced in cracked utility poles and damage to dwellings from the Dec. 26. 2003, Bam Earthquake, *Bull., Earthquake Research Institute*, University of Tokyo, **79(3/4)**, 59-68, 2004.
- Konagai, K., Numada, M., Zafeirakos, A., Johansson, J., Sadr, A. and Katagiri, T.: An example of landslide-inflicted damage to tunnel in the 2004 Mid-Niigata Prefecture earthquake, *Landslides* **2(2)**, 159-163, 2005.
- Konagai, K.: Data archives of seismic fault-induced damage, *Soil Dynamics and Earthquake Engineering*, **25(7-10)**, 559-570, 2005.
- Konagai, K., Johansson, J., Zafeirakos, A., Numada, A. and Sadr, A. (2005b). "Damage to tunnels in the October 23, 2004 CHUETSU earthquake," *JSCE Journal of Earthquake Engineering*, **28**, 75-127.
- Konagai, K., Numada, M., Zafeirakos, A., Johansson, J. Sadr, A. and Katagiri, T. (2005a). "An example of landslide-inflicted damage to tunnel in the 2004 Mid-Niigata Prefecture earthquake," *Landslides* **2(2)**, pp. 159-163.

(Field survey reports of massive earthquakes)

- Konagai, K., Johansson, J., Zafeirakos, A., Numada, A. and Sadr, A. and Katagiri, T. (2005c) "Geotechnical hazard for civil-infrastructures in the October 23, 2004, Niigata Chuetsu Earthquake, Japan," *Bull., ERS*, **38**, 3-18.
- Konagai, K. et al. (2007). "Annual Report of the Research and Development program for Resolving Critical Issues, "Earthquake damage in active-folding areas: creation of a comprehensive data archive and suggestions for its application to remedial measures for civil-infrastructure systems," Special Coordination Funds for Promoting Science and Technology, Ministry of Education, Culture, Sports, Science and Technology."
- Konagai, K., et al. (2006). "Quick Report of the JSCE Mission for Geotechnical Survey along Jehlum and Kunhar Valleys (Ver. 1.2)," JSCE, http://www.jsce.or.jp/report/41/ss-JSCE-IDI_Pakistan.pdf.

PREFACE

A large earthquake of local magnitude 7.3 (moment magnitude 7.6) struck the west-central Taiwan September 21, 1999. The epicenter was located close to the city Chi-Chi with a very shallow hypocenter at about 7 km depth. It is the largest in-land earthquake and the most destructive to hit Taiwan in over hundred years. Among the most extraordinary phenomena during this earthquake were the extremely large displacement of the fault ruptures along the 105-km long Chelungpu Fault. Highway No. 3 was under-construction when the earthquake occurred. The highway crosses the activated fault rupture trace at four points including Bauweishan, where a viaduct for the highway shoots 3 ramps leading to Nanto rest area. About 300 piles for the viaduct and its ramps were reportedly deformed and cracked by large deformations of soils caused by the fault rupturing. Since they are still preserving their deformed shapes in the soil, investigating remaining piles was considered to provide a clear perspective for designing pile-supported structures in vicinities of active fault traces.

A study of fault-inflicted damage is in itself nothing new. But with highly advanced recent technologies for field and geophysical surveys, lessons that can be learned from recent massive earthquakes surely gain importance in developing more rational design procedures especially in over-populated countries such as Japan and Taiwan. This report summarizes essential fruits of the 3-years JSPS project (No. 16208048) and activities of the Technical Committee for Fault-related Geotechnical Issues about Civil-infrastructures (preparatory phase: 2001-2002, actual phase: 2003-2005), Japan Geotechnical Society (JGS). Maintenance tasks of the data archive have been performed by members, and will be continued. Therefore the present version just shows the one facet in the course of its development. As is the case of many reports, this report is an outgrowth of different peer-reviewed papers published in both domestic and international journals and survey reports from recent massive earthquakes. Chapters in this report thus contain a lot of works done by the members and many collaborators.

The overseas collaborators include:

Dr. Cheng-Hsing CHEN, Professor, National Taiwan University (NTU) and Deputy Director of National Center for Research of Earthquake Engineering (NCREE),

Dr. Wei F. Lee, Taiwan Construction Research Institute (TCRI), and

Mr. Travis MEI, ditto,

for developing a data archive of piles of Baweishan viaduct deformed in the 1999 ChiChi Earthquake (**Chapter 2**).

The following members of the Technical Committee for Fault-related Geotechnical Issues about Civil-infrastructures, Japan Geotechnical Society (JGS), provided important materials for preparing the data archives of fault-inflicted damages. **Boldfaced** materials in parentheses are included in this English version of the data archive, while the others appeared in the Japanese version of the committee report for the preparatory phase (2002):

Dr. Sunao KUNIMATSU, Active Fault Research Center, (**Chapter 2**)

Dr. Keiichi UETA, Central Research Institute of Power Electric Industry, (**Chapter 3, 3.5**)

Dr. Fumiaki UEHAN, Railway Technical Research Institute, (**Chief Secretary**)

Dr. Nobuhiro ONIZUKA, Assoc. Professor, Kisarazu National College of Technology, (**Chapter 2** and Distinct Element Method)

Dr. Hiroyoshi KIKU, Assoc. Professor, Kanto Gakuin University, (Submerged areas in the 1999

Izmit Earthquake)

Dr. Takeyasu SUZUKI, Research Fellow, IIS, University of Tokyo, (bore-holing at Sannokai, Japan, **Chapter 3, 3.3**)

Dr. Hitoshi NAKASE, Tokyo Electric Power Services Co. Ltd., (DEM simulations, Pore water pressure effect on embedded and/or buried structures)

Dr. Atsushi NOZU, Port and Airport Research Institute, (Velocity pulses in **Chapter 6, 6.2**)

Dr. Takashi MATSUSHIMA, Assoc. Professor, Tsukuba University (DEM simulations of binary granular assemblies) and

Dr. Jorgen JOHANSSON, Assistant Professor, Inst., Industrial Science, University of Tokyo (Numerical simulations and experiments on wet and dry sands over dip-slip faults).

I am indebted to many people whose suggestions and criticisms have helped us with this project. Especially, Dr. Hiroyuki Kameda and Dr. Neil Briton, Director General and EqTAP Chief Coordinator, Earthquake Disaster Mitigation Research Center, National Research Institute for Earth Science and Disaster Prevention, gave us important pieces of advice for a possible integrated approach involving social sciences. We had frequent opportunities to discuss with Dr. Akira Sangawa, National Institute of Advanced Industrial Science and Technology (AIST), Guest Professor at IIS, University of Tokyo, Prof. Takashi Nakata, Hiroshima University, Dr. Yoshitaka Murono, Railway Technical Research Center. The discussions were very constructive. In 2001 and 2003 two workshops on Seismic fault-induced failures were organized by the project leader and held at the Institute Industrial Science at the University of Tokyo, Japan. The proceedings contain valuable pieces of information, which are also included in this final report. Keynote lectures in these workshops were provided by the following outstanding researchers, Prof. Jonathan Bray, University of California, Berkeley, USA, Prof. Risat Ulusay, Hacettepe University, Turkey, Prof. Derin URAL, Istanbul Technical University, Turkey, Dr. Kung Chen Shan, Vice President, SINOTECH, Taiwan, Prof. Yasutaka IKEDA, Univ. of Tokyo, Prof. C.H. Chen, National Taiwan University, Dr. Takefumi Takahashi, Executive Director, Metropolitan Expressway Public Corporation (former Director General for Disaster Management, Cabinet Office), Prof. Masanori Hamada, Waseda University and Dr. Raymundo Punongbayan, Executive Director, Earthquake and Megacities Initiative, Metro Manila, Philippines. It was sad and shocking news on April 28, 2005, that Dr. Punongbayan and eight others died in a helicopter crash at Gabaldon, Nueva Ecija. He was an acknowledged authority on volcanic, seismic, and lahar hazards evaluation. It was also a sad that Mr. Hidetoshi Miura, Managing Director at Terra Corporation was killed in the snowcapped mountain accident. Mr. Miura had dedicated great efforts to geophysical surveys at Bauweishan. May they rest in peace!

Kazuo KONAGAI

Leader of the project

EqTAP: Development of Earthquake and Tsunami Disaster Mitigation Technologies and their Integration to the Asia-Pacific Region

AIST: National Institute of Advanced Industrial Science and Technology

EDM: Earthquake Disaster Mitigation Research Center, National Research Institute for Earth Science and Disaster Prevention

CONTENTS

1	INTRODUCTION	1
2	DAMAGE TO FOUNDATIONS	
2.1	BAUWEISHAN VIADUCT AND ITS RAMPS	5
	Location: 23° 54'02"N, 120° 42'21"E	
	Earthquake: Sept. 23, 1999, ChiChi Earthquake, Taiwan, M=7.6	
3	DAMAGE TO TUNNELS	25
3.1	TANNA TUNNEL	25
	Location: 35° 6'14"N, 139° 0'55"E	
	Earthquake: Nov. 26, 1930, North-Izu Earthquake, Japan, M=7.2	
3.2	INATORI TUNNEL	27
	Location: 34° 46'20"N, 139° 1'53"E	
	Earthquake: Jan. 14, 1978, Off-Izu Oshima Earthquake, Japan, M=7.0	
3.3	OUTLET TUNNEL OF 2 nd KAKKONDA HYDROPOWER STATION	30
	Location: 39° 46'49"N, 140° 56'48"E	
	Earthquake: Sept. 3, 1998, Mid-North Iwate Earthquake, Japan, M=6.1	
3.4	INTAKE TUNNEL OF SHIHKANG DAM	33
	Location: 24° 16'42"N, 120° 46'14"E	
	Earthquake: Sept. 23, 1999, ChiChi Earthquake, Taiwan, M=7.6	
3.5	INTAKE TUNNEL OF OMIYA DAM	34
	Location: 35° 13'46"N, 133° 22'39"E	
	Earthquake: Oct. 6, 2000, West Tottori Earthquake, Japan, M=7.3	
3.6	UONUMA TUNNEL OF JOETSU SHINKANSEN RAILWAY	37
	Location: 37° 17'19"N, 138° 51'43"E	
	Earthquake: Oct. 23, 2004, Chuetsu Earthquake, Japan, M=6.8	
3.7	BERKELEY-HILL BART TUNNEL	45
	Location: 37° 51'04"N, 127° 14'16"W	
	Earthquake: Cracking is due to continuous creeping movement of the Hayward fault.	
3.8	BOLU TUNNEL	47
	Location: 40°45'18"N, 31°27'04"E	
	Earthquake: August 17, 1999, Izmit Earthquake, Turkey, M=7.4	
4	DAMAGE TO DAMS	
4.1	SHIHKANG DAM	49
	Location: 23° 54'02"N, 120° 42'21"E	
	Earthquake: Sept. 23, 1999, ChiChi Earthquake, Taiwan, M=7.6	
5	LANDSLIDES/ LANDFORM CHANGES	
5.1	TIGER HEAD HILL SLIDE	61
	Location: 24° 07'52"N, 120° 44'18"E	
	Earthquake: Sept. 23, 1999, ChiChi Earthquake, Taiwan, M=7.6	
5.2	LANDFORM CHANGES IN MID-NIIGATA REGION	63
	Location: 7 km (North-South) × 11 km (East-West) area in Mid-Niigata with its center at 37°18'41"N, 138°53'03"E	
	Earthquake: Oct. 23, 2004, Chuetsu Earthquake, Japan, M=6.8	
5.3	STRAINS INDUCED WITHIN SOILS NEAR FAULT RUPTURE PLANES	66
	Location: 40°43'32"N, 29°49'02"E for Fig. 5.8(b) and 40°43'21"N, 29°50'55"E for Fig. 5.8(c)	
	Earthquake: August 17, 1999, Izmit Earthquake, Turkey, M=7.4	
5.4	LONG LASTING LANDFORM CHANGES IN PAKISTAN	67
	Location: 23° 54'02"N, 120° 42'21"E	
	Earthquake: Oct. 8, 2005, Kashmir Earthquake, Pakistan, M=7.6	

6	INTENSE SHAKES	
6.1	VELOCITY PULSES	69
6.2	DAMAGE TO QUAY WALLS	71
	<i>Kobe Port in the 1995 Great Hanshin Earthquake</i>	
	Location: 34° 39'33"N, 135° 13'22"E for Port island and 34° 40'37"N, 135° 16'19"E for Rokko island	
	Earthquake: Jan. 17, 1995, Great Hanshin Earthquake, Japan, M=7.2, and <i>Sakai Port in the 2000 West Tottori Earthquake</i>	
	Location: Port island N35° 32'41", E133° 14'55" for Station F-1493	
	Earthquake: Oct. 6, 2000, West Tottori Earthquake, Japan, M=7.3	
6.3	ABDARREH VILLAGE, IRAN, IN THE 2002 CHANGUREH EARTHQUAKE	73
	Location: 35° 47'43"N, 49° 01'16"E	
	Earthquake: June 22, 2002, Changureh Earthquake, Iran, M=6.4-6.5	
6.4	BAM CITY, IRAN, IN THE 2003 BAM EARTHQUAKE	80
	Location: 29° 06'18"N, 58° 21'31"E	
	Earthquake: Dec. 26, 2003, Bam Earthquake, Iran, M=6.6-6.6	
7	FAULT PROVISIONED DESIGN EXAMPLES	
7.1	MITIGATION MEASURES	89
7.2	WATER SUPPLY OF EAST BAY MUNICIPAL UTILITY DISTRICT, CALIFORNIA, U.S.A.	89
7.3	TOKYO, JAPAN – SAKHALIN, RUSSIA PIPELINE	91
	Location: off-shore, Shirako, Chiba, Japan	
7.4	COUNTERMEASURES FOR SHINKANSEN (bullet train) STATION AND BRIDGE	92
	Location: 34° 42'24"N, 135° 11'46"E	
7.5	FREEWAY PROJECT SAN BERNARDINO, CALIFORNIA, 2002	94
	Location: 34° 08'43"N, 117° 19'09"W	
7.6	CLYDE DAM IN NEW ZEALAND	96
	Location: 45° 10'47"S, 169° 18'19"E	
7.7	FLEXIBLE ALASKAN PIPELINE	98
	Location: 63° 23'00"N, 145° 44'00"E	
	Earthquake: Nov. 3, 2002, Denali Fault Earthquake, USA, M=7.9	
8	KEY POINTS FOR RATIONAL DESIGNS	
8.1	INTRODUCTION	101
8.2	SEQUENTIAL APPEARANCE OF THRUST FAULT RUPTURE PLANES	101
8.3	SOIL STRAIN PAPERETER DETERMINING RESTRICTION LEVEL	104
8.4	SEQUENCE OF DYNAMIC AND STATIC SOIL DEFORMATIONS	105
8.5	ACTIVE LENGTH OF UNDERGROUND PIPES AND TUNNELS	107
Appendix 1	BOREHOLE DATA AT BAUWEISHAN	109

Cut and paste any location (latitude and longitude) of the above examples that you are looking for on the "Fly To" search box of the Google Earth, and you will reach there.



Google Earth can be downloaded from the following URL: <http://earth.google.com/>

Chapter 1

INTRODUCTION

In terms of death toll, we had had some quiet 40 years in Japan since the devastating Fukui Earthquake of 1948 (M=7.3), which killed 3,769 people. Seismic activity in Japan, however, has seemingly increased since the 1993 Kushiro Earthquake, which was then followed by intense earthquakes in rapid succession. And the January 17, 1995, South Hyogo Earthquake (Kobe Earthquake hereafter) was responsible for the total of 6432 deaths and serious destruction of urban facilities in Kobe, a mega city spreading over a bundle of hidden faults along the Rokko Mountains.

The 1999 Chi-Chi and Kocaeli earthquakes in Taiwan and Turkey, the 2002 Central Alaska (USA), and the more recent 2004 Mid Niigata earthquake, have shown how human lives, buildings and infrastructure are endangered by fault surface ruptures. Even though fault surface rupturing is not a new problem, there are very few building codes in the world containing any type of provisions for reducing the risks. This may be due to the infrequent occurrence of fault surface ruptures, the great difficulty in preventing damage to infrastructure and buildings affected by the ruptures and also the difficult task of estimating the related permanent deformations due to many unknown factors such as possible fault location, geometry and motion; and mechanical properties of the soil deposit.

In California, United States; New Zealand; and also in Taiwan, after the 1999 Chichi earthquake, so called fault zoning acts have been established. Current fault zoning acts prevent or restrict construction within a certain distance from a known fault line and may be one way of reducing the risks for new buildings and infrastructure, but for structure already built along a fault line other remedial measures are needed, further more current fault zoning acts do not say anything about the possible extent of deformations and/or the probability of occurrence of these deformations.

In densely populated countries such as Japan and other east and south-east Asian countries it is difficult to impose such fault-zoning act due to the lack of space (**Figs. 1.1 and 1.2**). Furthermore, damage in recent earthquakes in Japan was caused by unknown faults, even though fault mapping is very thorough. In these countries building code provisions based on engineering principles are needed as to allow for construction along fault-lines if certain design requirements are met. Such building code provisions would also be attractive for less populated countries, such as United States and New Zealand, as well, since it may allow for more economical construction.

Another issue is the difference between strike-slip and dip-slip faults. The deformations along a strike-slip seem to be concentrated in a narrower zone along the fault line whereas the deformations along a dip-slip fault may affect areas further away from the fault line, (Mukoyama, 2000). In Japan there are some 90 dip-slip fault systems with several faults included in each system and with a lot of buildings and infrastructure along them.

The first part of the report covers the damage examples (Fault-inflicted Damage Data Archive), and emphasis is given to the damage in the recent massive earthquakes in Japan and Taiwan. The original prototype of the data archive was launched in the 3-years JSPS project of (No. 12355020). During this term of the JSPS project (16208048), the data archive has been further enriched adding some updated examples. Fault-related failures will fall into two broad categories: ground rupture-induced and ground shaking-induced failures. The collected materials are listed in **Tables 1.1** and **1.2**. The examples taken herein include damage to bridges (their foundations), tunnels, dams and slope failures. Among all, the project members devoted greater part of their efforts to the survey of Bauweishan area, Taiwan, where about 300 piles for a highway viaduct and its ramps were deformed in the 1999 ChiChi Earthquake. Invaluable supports were from Dr. Chen, C.H., at the Department of Civil Engineering, National Taiwan University, Dr. Lee, W. and Wang, C. at the Taiwan Construction Research Institute (TCRI), who have jointly investigated the displacement built up in piles and soils at Bauweishan. Putting together all available data, a digital 3D model of soils and piles was prepared for Bauweishan viaducts.

In the second part, a few fault provisioned design case histories and the recent success story of the Trans-Alaskan pipeline are introduced. In 2001 and 2003 two workshops on Seismic fault-induced failures were organized by the project leader and held at the Institute Industrial Science at the University of Tokyo, Japan. The proceedings of these two workshops contain valuable information and some examples from them are also included.

REFERENCES

Watanabe, M. and Suzuki, Y (1999): 3D photographs of seismic fault traces, *Kokon Shoin Press*.
White paper of the Metropolis (1999).

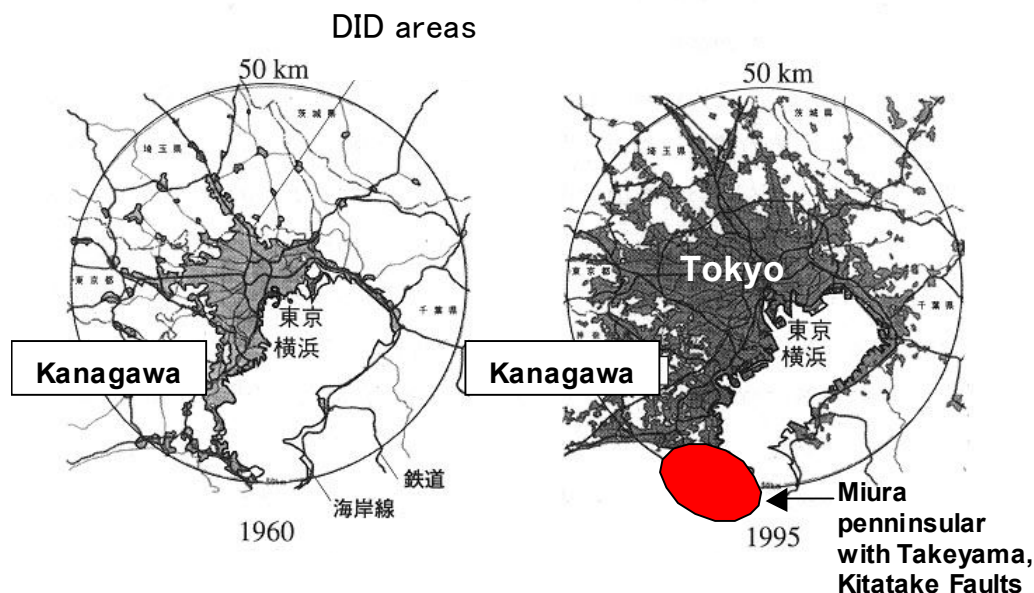
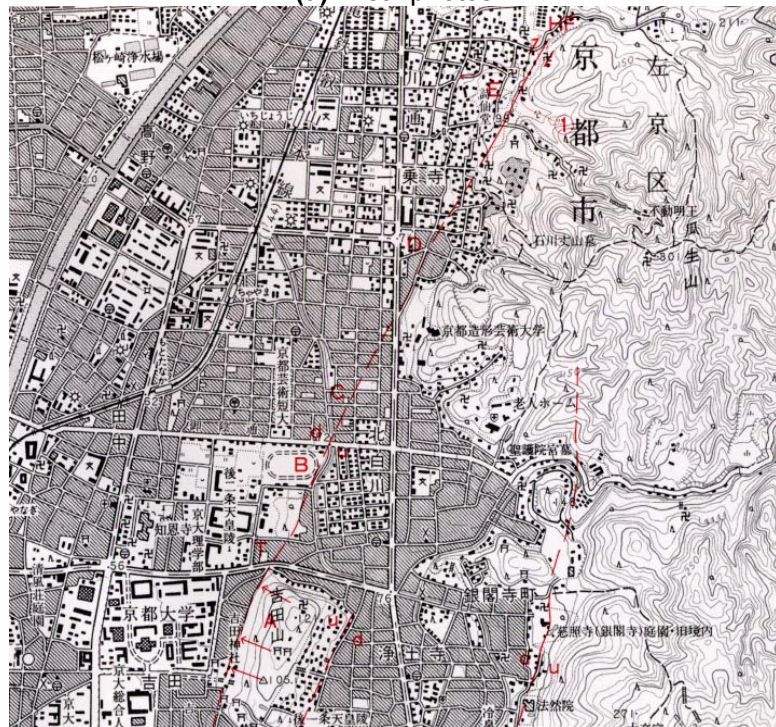


Fig. 1.1: Expansion of DID area in Metro Tokyo and Yokohama (White paper of the Metro police, 1999)
DID: Densely Inhabited District, a district consisting of mutually adjoining National Census areas, each of which has a population density larger than 4000 inhabitants per square kilometer, and having a combined population larger than 5000.



(a) Areal photos



(b) Location of Hanaore fault

Fig. 1.2: Hanaore Fault crossing Kyoto
(Watanabe, M. and Suzuki, Y., 1999.)

(a) The pair of photographs can be perceived as a single image in terms of depth. (b) Based on 14C dating of exposures at three trenches excavated across the fault, a surface-rupturing earthquake is estimated to have occurred on the northeastern splay of the Hanaore fault an around mid 16th century. As for its southern part, however, at least one event seems to have occurred since 2000B.C. And Kyoto, a historical city with 2.6 millions population, has never experienced this fault activation.

Table 1.1. Examples of ground rupture-inflicted damage:
Examples with * are newly added.

Structure	Contents
Bridges/ Foundations	* Baweishan Viaduct and its ramps (1999 ChiChi Eq., Taiwan)
	Bol viaduct (1999 Duzce Eq., Turkey) (from Kawashima K.)
	ShiWei Bridge (1999 ChiChi Eq., Taiwan) Rigid body motions of piers (from Kosa, K. and Yamaguchi, E.)
	BeiFong Bridge (1999 ChiChi Eq., Taiwan) Movement of piers, Ground movement along the bridge (from Kawashima K.)
	WuShi Bridge (1999 ChiChi Eq., Taiwan) Movement of piers, Ground movement along the bridge (from Kawashima K. and Kosa, K.)
Tunnels	Tanna Tunnel (1930 North Izu Eq., Japan), Crack map of the tunnel etc. (from RTRI)
	Inatori Tunnel (1978 Off the IzuOshima island Eq.) Crack map of the tunnel, Buckled rail: Even off the fault rupture plane, buckling of rails can occur, and cause derailment etc. (from RTRI)
	Rokko Tunnel (1995 Kobe Eq.), Crack maps etc. (from RTRI)
	Outlet tunnel of Kakkonda hydropower station (1998 Mid-North Iwate Eq, Japan), Crackmap of the damaged tunnel etc. (from Tohoku Electric Power Co. Ltd)
	Intake tunnel of ShihKang Dam (1999 ChiChi Eq., Taiwan, from JSCE reconnaissance team etc.).
	* Intake Tunnel of Unoike reservoir (2001 West Tottori Earthquake), Crack map from Dr. Ueta
	* Uonuma Tunnel of Shinkansen Joetsu Railway (2004 Chuetsu Earthquake)
Dam	ShihKang area (1999 ChiChi Eq., Taiwan), Taiwan: Survey map of Sihkang area . (from Collaborators in Taiwan incl. Kung C.S.), Crack map of the dam (from Konagai K., Sugimura Y., Miura S.) etc
Soils	Yalova-Izmit areas (1999 Kocaeli Eq., Turkey), Survey map etc. showing subsidence of ground (from ULSAY, R., Hacettepe Univ., URAL, D., Istanbul Technical Univ. and the Japan Geotechnical Society team)
	Tiger Head Hill landslide (1999 ChiChi Eq., Taiwan), Sketch of the landslide mass, etc. (from Collaborators in Taiwan and from Kamai, T.)
Others	Traces of faulting found at ruins (from Sangawa, A, AIST)

Table 1.2. Examples of ground shaking-inflicted damage

Dam & reservoir	Kasho dam (2001 West Tottori Eq., Japan) Analysis of seiche (from Ohmachi, T.)
Dwellings	Abdarreh village (2002 Changureh Eq., Iran)
	* Bam city (2003 Bam Eq., Iran)

Abbreviations RTRI Railway Technical Research Institute
 AIST National Research Institute of Advanced Industrial Science and Technology

Chapter 2

DAMAGE TO FOUNDATIONS

2.1 BAUWEISHAN VIADUCT AND ITS RAMPS (1999 Chichi Earthquake Taiwan)

Location: 23° 54'02"N, 120° 42'21"E

Earthquake: Sept. 23, 1999, ChiChi Earthquake, Taiwan, M=7.6

Introduction

The trace of the surface rupture that appeared in the 1999 ChiChi earthquake closely followed the frontal slope of the north-south trending local mountain range (**Fig. 2.1**). Highway No. 3 was under-construction when the Sept. 21, 1999, ChiChi Earthquake occurred. The highway crosses the activated fault rupture trace at four points including Bauweishan, Pinlinchi, Fuanglishan, and Choshuishan (Chen 2003). At Bauweishan, the viaduct for the highway shoots 3 ramps leading to Nanto rest area. All viaducts for main highway and its ramps were simply supported by piers with piles, and about 300 piles were reportedly deformed and cracked by large deformations of soils caused by the fault rupturing. After the earthquake, new viaducts for this highway were constructed shifting the original plan about 11m south, and there are still many piles for the original structures remaining in the deformed soil mass. Since they are still preserving their deformed shapes in the soil, investigating remaining piles was considered to provide a clear perspective for designing pile-supported structures in vicinities of active fault traces. A discussion on this issue must be based on a quite different scenario from those for ordinary designs; in the ordinary design, ground accelerations and/or velocities are always crucial factors. Due attention should be paid to deformation buildup in un-cemented soils that cover hidden faults. When a base rock comes steadily up into an un-cemented soil deposit, strains can be distributed over some wide zones, which extent depends largely on the material properties, dip of the fault rupture plane, etc. Consequently an embedded foundation can be shifted from its original location, and deformed even though it is located off the major rupture plane. With this as a background, Konagai, K. and his team at Institute of Industrial Science, University of Tokyo, Chen, C.H. and his team at the Department of Civil Engineering, National Taiwan University, Lee, W. and Wang, C. at the Taiwan Construction Research Institute (TCRI) jointly surveyed the displacement built up in piles and soils at Bauweishan. Putting together all available data, a digital 3D model of soils and piles was prepared for Bauweishan viaducts.

Overview of Field Survey

The layout of the 4 viaducts is shown in **Fig. 2.2**. Piles for the main highway and ramps are respectively 1.5m and 1.2m in diameters. When the Chi-Chi earthquake occurred, most piles had been completely driven in the soil, and some of them were at the stages of constructing their pile caps, piers, and/or cap beams. No pier supported bridge girders, and therefore, kinematic soil-pile interaction with little inertia forces from superstructures was considered to have been the major cause of damage to the piles.

Every subsurface exploration should be preceded by a review of all available information concerning the geological and subsurface conditions at or near the site. In most instances, this information is desirable to be supplemented by the results of direct investigations. The first direct step is usually to drill several holes into the ground by an expedient method and to obtain fairly intact samples of soil from every stratum encountered by the drilling tools. However the dislocated fault and several hundreds abandoned and used piles are all perplexity for estimating soil profiles only from one available borehole. Therefore the strategy was made in such a way that drilling of several boreholes would be conducted to locate the fault rupture plane, and then geophysical exploration for locating some hidden foundations. As contrasted with direct methods, geo-physical explorations such as electric resistivity tomography and ground penetrating radar surveys provide rather in-direct vague images of subsurface soil conditions. However together with the real soil samples taken point-wise from the boreholes, it was also expected to supplement information that could help to interpolate and/or extrapolate soil profiles where direct methods were not applicable nor allowed.

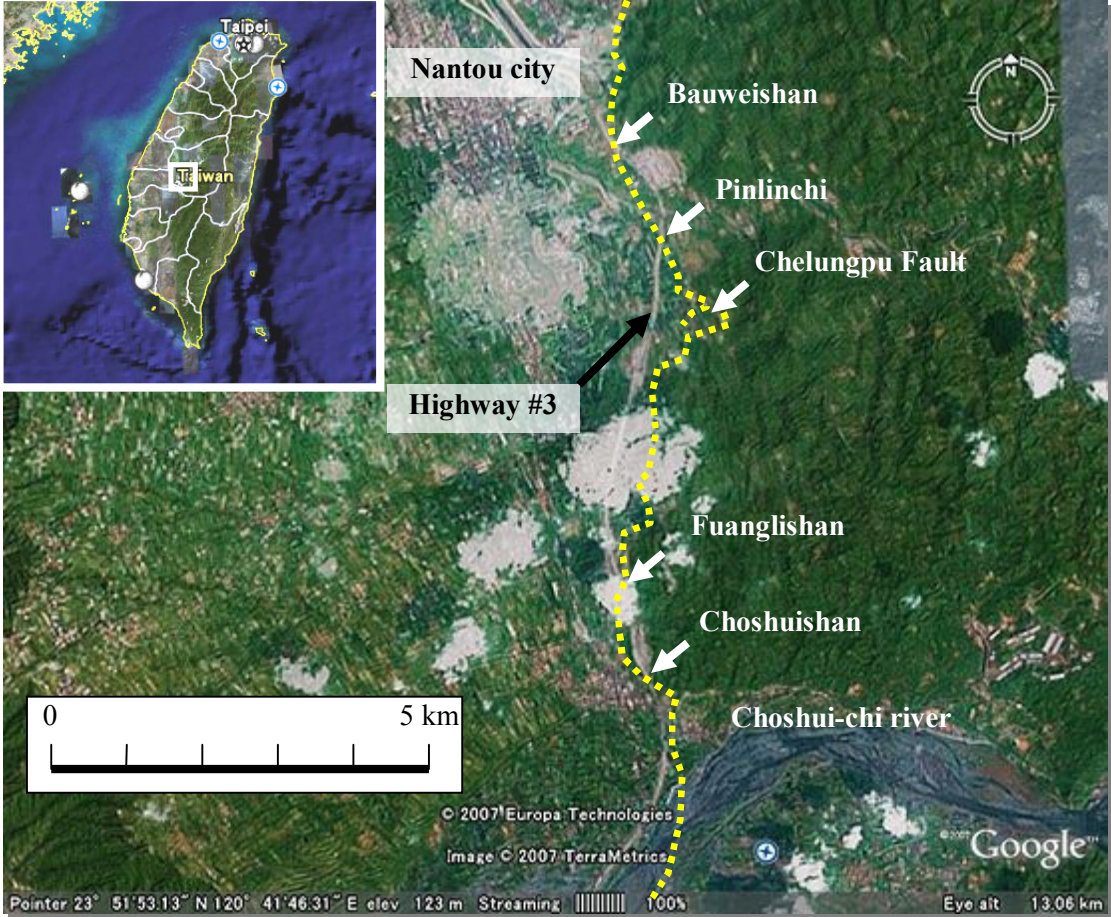


Fig. 2.1: Highway No.3 and Chelungpu Fault

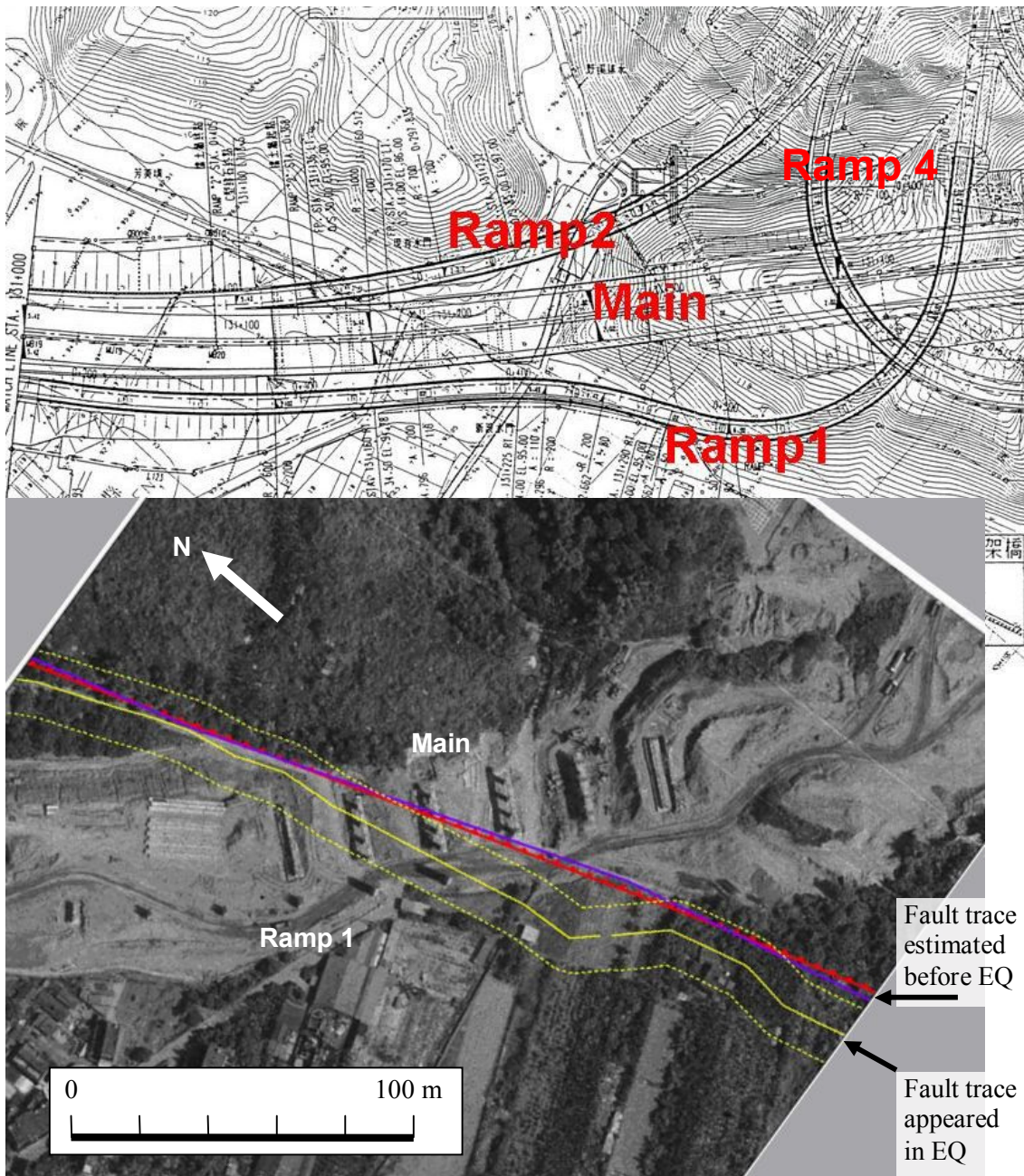


Fig. 2.2: Original plan for Bauweishan viaducts (above) and aerial photo of the same area (below): When the earthquake occurred, all pile caps for the main viaduct and 5 for Ramp #1 from the north (left in the photo) supported piers.

Boreholing

Fig. 2.3 shows the locations of the bore holes. Boreholes A1, A2 and A3 are lined up in the transverse direction with respect to the estimated fault trace so that hidden fault rupture surface would be found, while Boreholes B1, B2, B3, B4 are arranged in square in such a way that they surround the possible location of an original pier in expectation that the presence of the buried piles for this pier would be located in the 3D geo-resistivity survey.

The outlines of each borehole are described below.

Borehole A1—

- a. Drilled depth: 31 m
- b. for Lithology observation and
- c. 2D cross-hole imaging was conducted using Borehole A3.

Borehole A2—

- a. Drilled depth: 50 m
- b. for Standard Penetration Test at 1~2m interval with piece-wise soil sampling, and
- c. P-S waves logging.

A3—

- a. Drilled depth: 31 m
- b. for all-core sampling to detect possible location of the fault rupture plane, and
- c. 2D cross-hole imaging using Borehole A1.

B1~B4—

- a. Drilled depths: 31 m
- b. for 3D cross-hole imaging
- c. Borehole B2 for all-core sample to detect locations of the fault rupture plane and
- d. the other boreholes for lithology observation.

Observed features of soil samples are summarized in **Table 2.1**:

Table 2.1: Site soil materials and depths.

Borehole	Hanging wall			Foot wall
	Surface stratum		Silty clay zone with stripes	Gravel and Sand
	Fill	Sandy silt with gravels		
A1	0.0-2.9	2.9-10.7	10.7-26.4	26.4-31.0
A2	0.0-5.4	5.4-6.6	6.6-42.4	42.4-50.0
A3	0.0-9.1	9.1-10.5	10.5-	-
B1	0.0-4.8	4.8-11.6	11.6-12.7	12.7-31.0
B2	0.0-5.4	5.4-9.0	9.0-24.4	24.4-31.0
B3	0.0-2.3	2.3-11.8	11.8-12.3	12.3-31.0
B4	0.0-3.2	3.2-10.0	10.0-21.3	21.3-31.0

(unit: m)

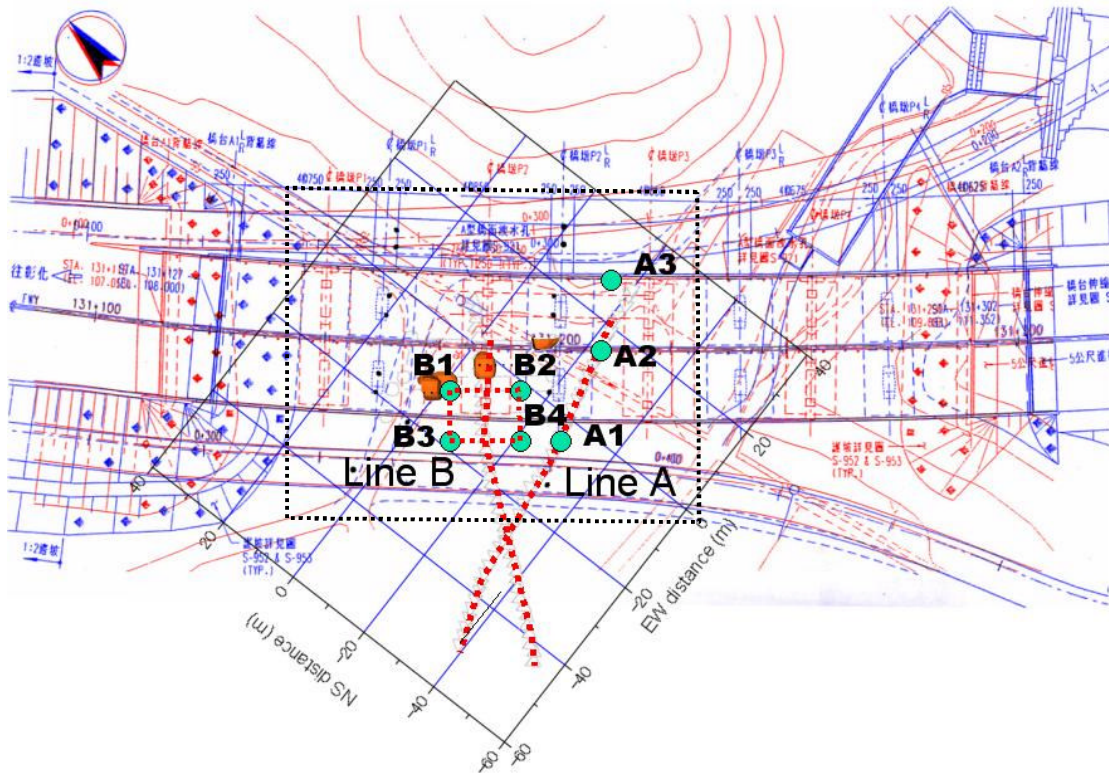


Fig. 2.3: Locations of boreholes: Red and blue drawings are original and post-earthquake plans of viaducts. Orange blocks immediately above are high electric-resistivity zones located in the electric resistivity tomography exploration.

At all boreholes, stiff surface stratum of about 8 to 16m thick sand and gravel spreads over a slightly consolidated but rather softer layer of silt and/or clay. The surface stratum has an artificial surface fill probably from the time of highway construction ranging 2 to 10 m thick over natural deposit of sands and gravels. For the samples taken from the deeper silt-clay layer, one of the most remarkable features was that the samples had diagonal streak marks as shown in **Fig. 2.4** evidencing that shear strains have been continually built up within this zone. This silt-clay zone becomes thicker above a much stiffer deposit of boulders as the distance from the estimated fault trace increases, indicating the zone is on the hanging wall side over the much stiffer footwall layer of dense gravel fabric with its voids completely filled up with sand. The estimated soil profile for the line A (Boreholes A1, A2 and A3) is illustrated in **Fig. 2.5**.

Shear Zone : 7~42 m

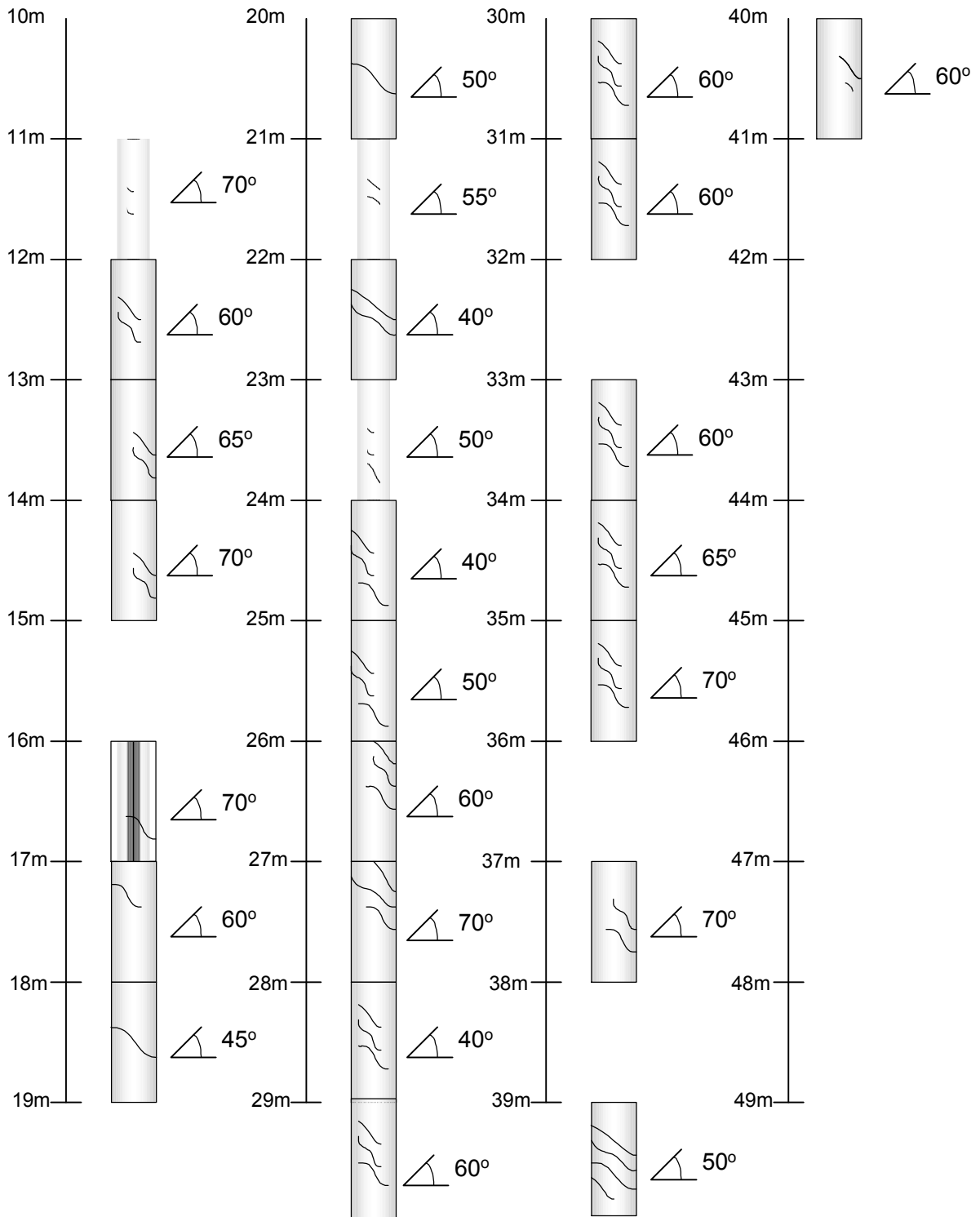


Fig. 2.4: Diagonal streak marks appearing on samples from Borehole A2

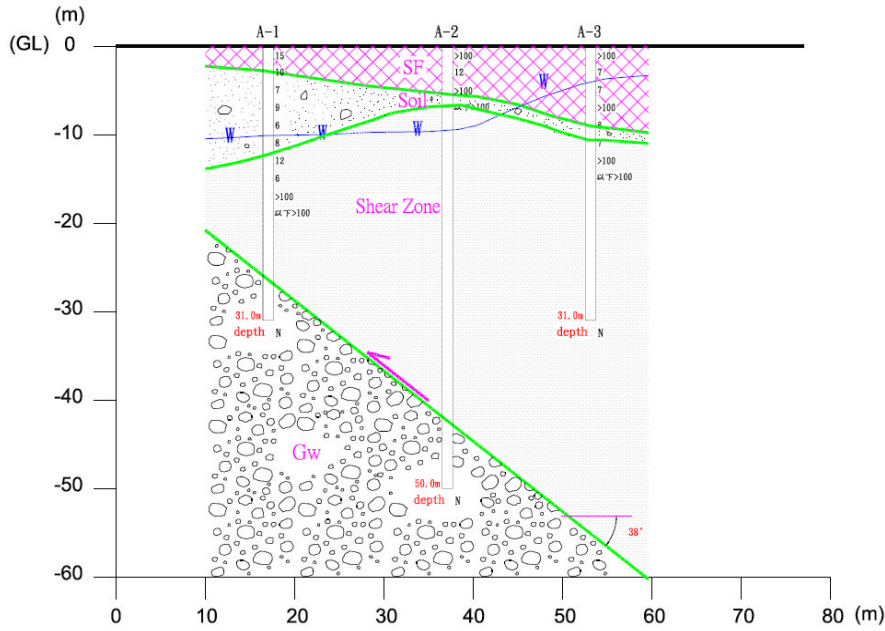


Fig. 2.5: Estimated soil profile along Line A

Electric resistivity tomography and ground penetrating radar (GPR) survey

The exploration was made to detect the presence of abandoned and hidden original piles. Immediately beneath the down-traffic bridge girders between the present piers MP1 and MP2, a 30m×15m rectangular area was surveyed (See **Fig. 2.6**).

Fig. 2.7(a) shows the measured spatial 3D distribution of geo-resistivity ($\text{ohm} \times \text{m}$). With total 84 electrodes arranged in rectangle (21×4) at every 1.5m and 5m intervals in longitudinal and transverse directions of the main viaduct respectively, the deepest range of reliable inversion analysis of about -6 to -7 m was reached. Within this range, there are three cubic (red) zones of high resistivity found at about 8 m interval. Since concrete exhibits higher resistivity than soils, they can be parts of embedded structures. Medium high resistivity (green) spreads rather shallower part of the surveyed area, which zone is seemingly similar in its shape to the anomalies found in the ground penetrating radar survey as explained below.

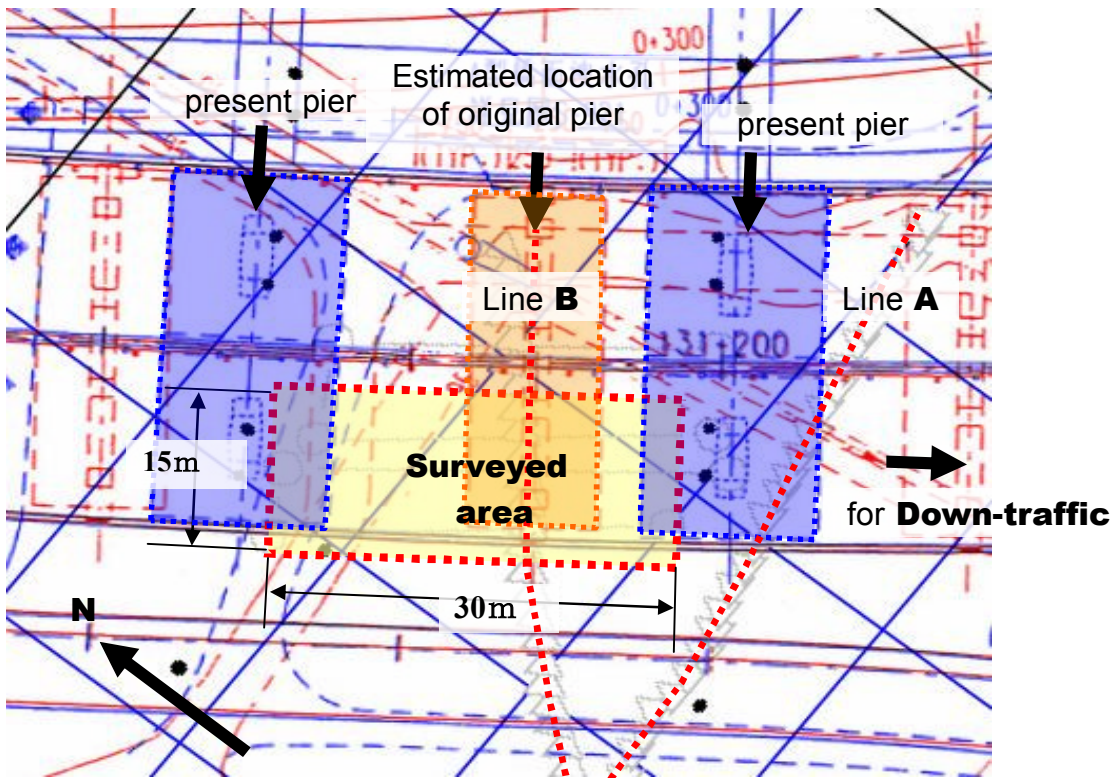
The same area was scanned by using a ground-penetrating radar (GPR, see **Fig. 2.6(a)**) radiating pulses of 400MHz microwave band. The depth range of the GPR was thus limited above -4m by both the conductivity of the rather wet subsurface soil and the transmitting frequency. The stripes of radargrams show a return signal pattern of anomalies as shown in **Fig. 2.7(b)**. The image of anomalies is similar in its shape to the green-colored zone of middle high resistivity in **Fig 2.7(a)**. Since the greater part of the shallow sub-surface soil was from the time of constructing the viaducts, this zone is considered to include artificial fill and debris, and only the presence of the three cubes of high resistivity in **Fig. 2.7(a)** was used as references for determining the layout of Boreholes B1, B2, B3 and B4.



(a) Ground penetrating radar



(b) Electric resistivity survey



(c) Surveyed area

Fig. 2.6: Area for electric resistivity tomography and ground penetrating radar surveys

Using Boreholes B1, B2, B3 and B4, cross-hole ground resistivity tomography was conducted. **Fig. 2.8** (left) shows two representative upright cross-sections of the observed soil column surrounded by the boreholes. At left back of the soil column (below B1), there appeared a red zone of high resistivity suggesting the presence of an artificial object embedded about 10m deep in this soil.

Lines A and B in **Figs.2.1** and **2.6** were also used for the surface 2D resistivity tomography, and detected electro-resistivity images for cross-sections along Lines A and B are shown in **Figs. 2.8** (right). Because the same 2D soil profile is assumed to extend along the estimated fault trace in the inverse analyses, analyzed images are a little too vague for describing real impedance boundaries. However comparing **Fig. 2.8** (right) with **Fig. 2.5** showing the soil profile estimated from borehole

samples, a green zone of middle value of resistivity (10 to several tens ohm*m) spreading over the blue low-resistivity zone on the hanging wall side can include debris from the construction time, while green to yellow zones on the footwall side can be the layer of dense gravel and sand fabric. Along Line B, inclusion of green to yellow colors in the blue shear zone may suggest the presence of an embedded structure.

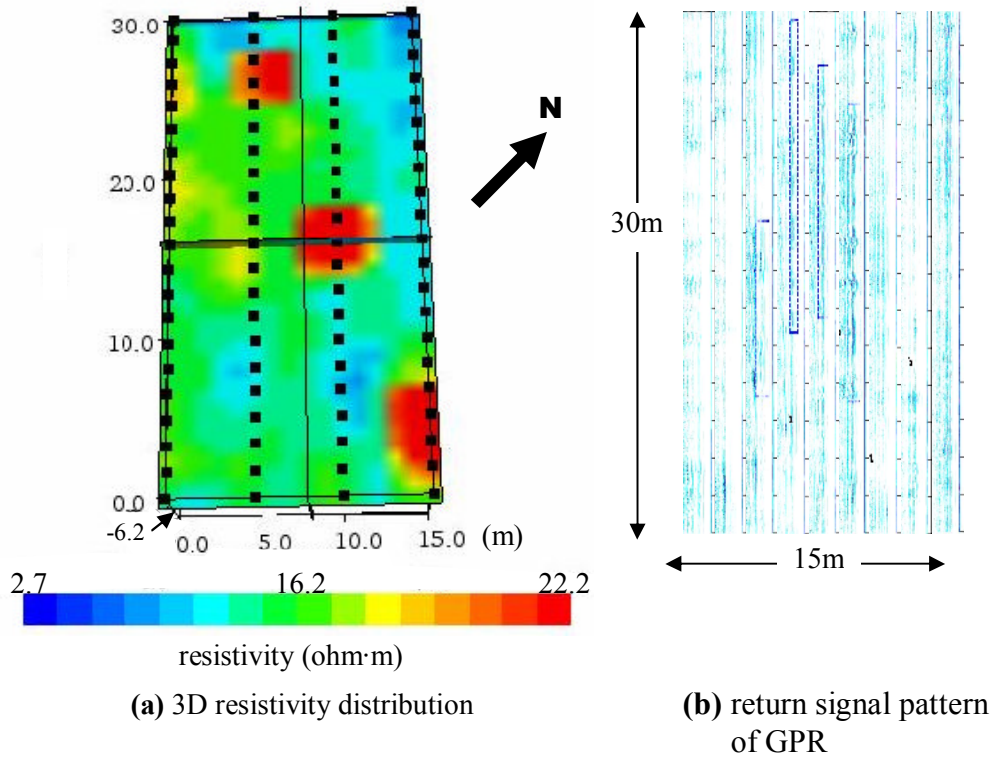


Fig. 2.7. Electric resistivity distribution and reflected return signal pattern of ground penetrating radar

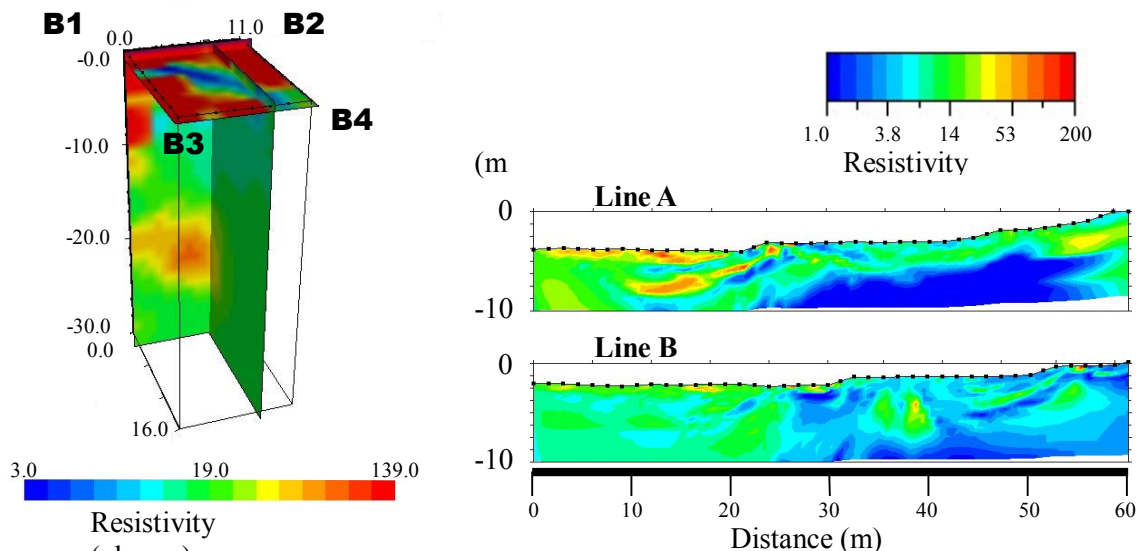
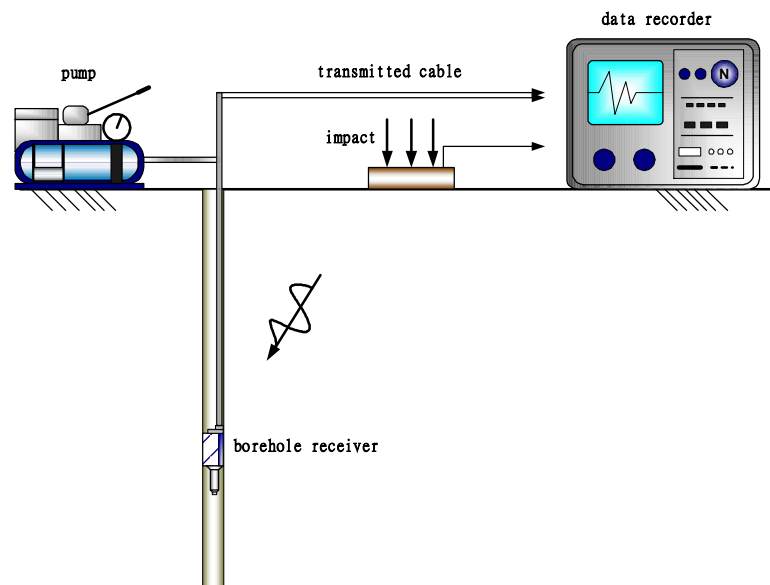


Fig. 2.8: Electric resistivity distribution within the soil column surrounded by Boreholes B1, B2, B3 and B4 (left), and along Lines A and B (right)

PS waves logging

Down-hole velocity logging provides vertical variations of elastic wave velocities along a borehole (**Fig. 2.9**). Waves that can be measured are: (1) primary waves (P-waves hereafter) for P-wave logging, (2) primary and secondary waves (S-waves hereafter) for PS loggings. P and S waves in a high frequency range are often measured in sonic loggings for better special resolutions.

P and S wave velocities along Borehole A2 were measured at every 2 meters regular interval down through the hole to its bottom end of 40m below the ground surface. The measured time-distance curve is shown in **Fig. 2.10**, and analyzed variations of P and S wave velocities as well as dynamic elastic properties for Borehole A2 are shown in **Fig. 2.11** and **Table 2.2**. Seemingly there are four major layers with different seismic wave velocities (**Fig. 2.7**), with top three and the bottom one for the surface strata and sheared clay-silt zone, respectively, as mentioned in the previous section.



(b) Recording units



(c) Source and receiver

Fig. 2.9: System for velocity logging: An Instrument for down-hole velocity logging includes receivers, a data recording unit, wave sources, logging cables, trigger signal detectors, etc.

Receiver unit—Borehole pick consists of three receiver units, one for vertical direction, the others for quarter and horizontal directions. The receiver has the natural frequency of 28Hz.

Recording unit—RAS-24 (Seistronix, United stated).

Seismic resource—hammer.

Table 2.2. Variation of P and S wave velocities along Borehole A2

(m)	Vp (m/sec)	Vs (m/sec)	Dynamic Shear Modulus (kg/cm ²)	Dynamic Young's Modulus (kg/cm ²)	Block Modulus (kg/cm ²)	Dynamic Poisson' Ratio
0~3	1581	636	8337	23402	40404	0.403
3~10	1581	926	17674	43794	27955	0.238
10~16	2082	1243	33423	81759	49206	0.223
16~28	1084	505	4996	13604	16359	0.361
28~40	1084	448	3932	10986	17778	0.397

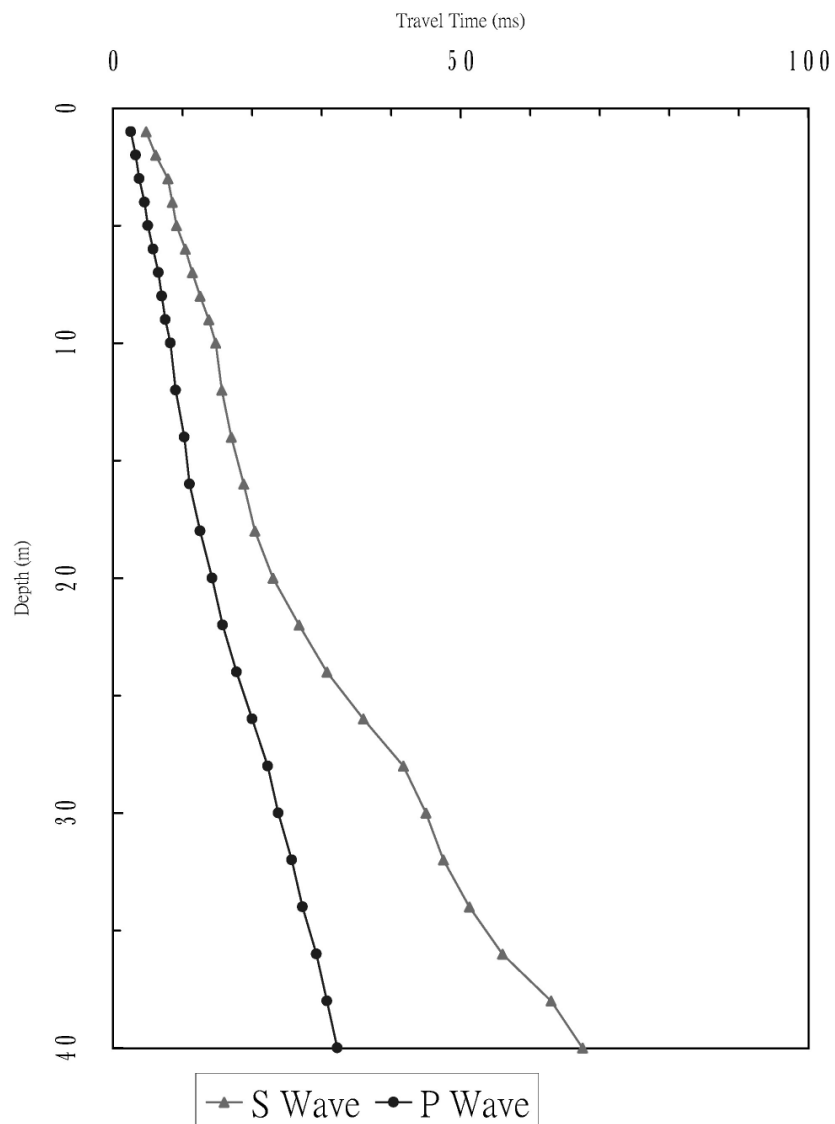


Fig. 2.10: Time-distance curves for P and S waves

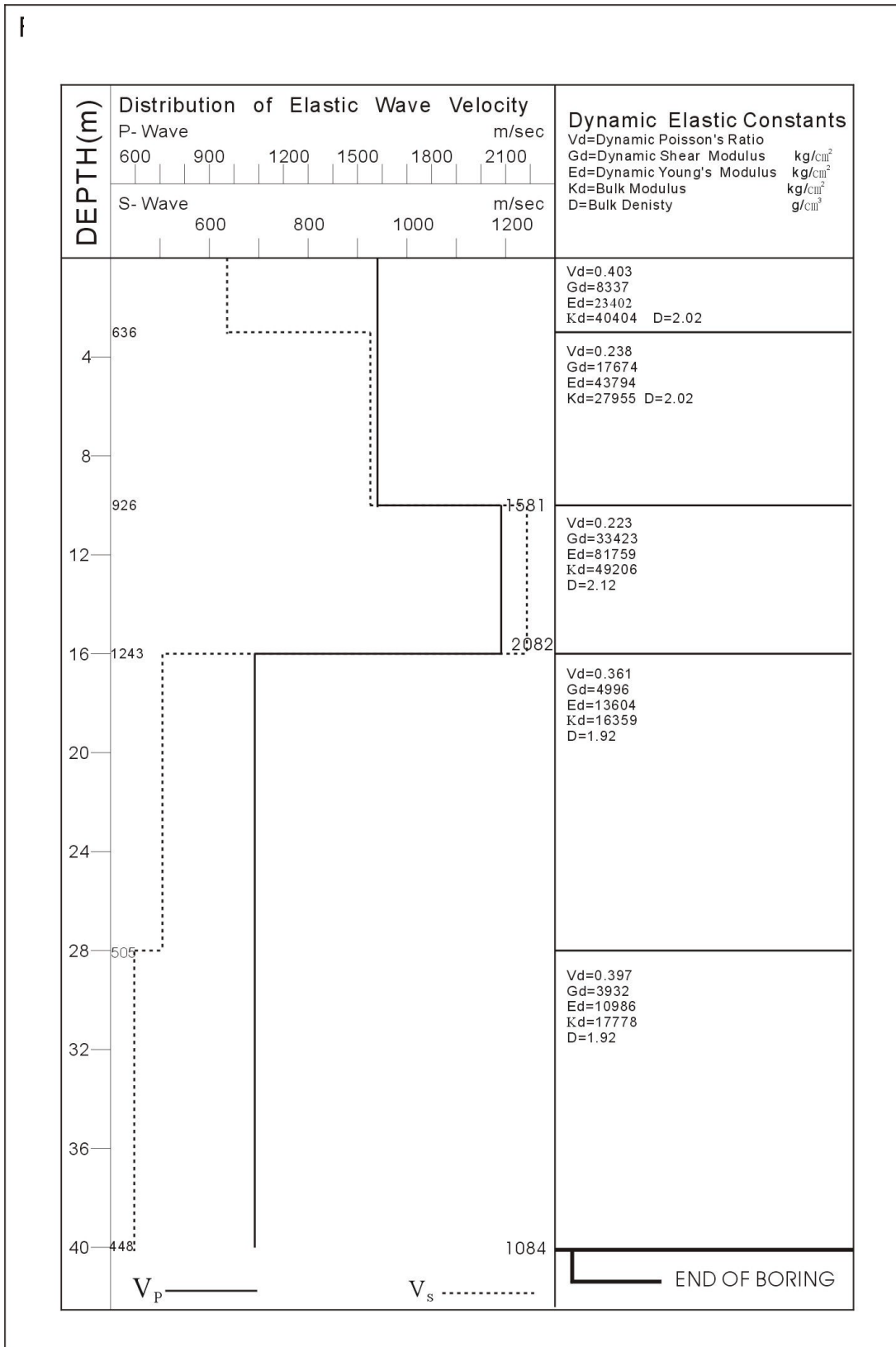


Fig. 2.11: Dynamic elastic constants along borehole A2

Pile cap displacement

Immediately after the earthquake, displacements of pile caps in both horizontal and vertical direction were measured at their centers. **Fig. 2.12** shows locations of pile caps. In this figure, M, R, A, and P put on pile caps stand for “main viaduct”, “ramp”, “abutment”, and “pier”, respectively. Therefore, R2P3 denotes, for example, Pier #3 of Ramp #2. Vertical displacements were obtained for the main viaduct and Ramp #1 because elevations before the earthquake were only available for those pile caps. Measured components are listed in **Table 2.3**.

Pile caps centers on the hanging wall side were displaced all at once about 2.5 m laterally in the normal direction with respect to the estimated fault trace (**Figs. 2.12** and **2.13**). For vertical components, the scatter of vectors is a little too large to conclude that all piles on the hanging wall were pushed up altogether in the same direction to be sure, but displacement vectors near the fault trace seem to be parallel to the presumable fault plane (See **Fig. 2.13**).

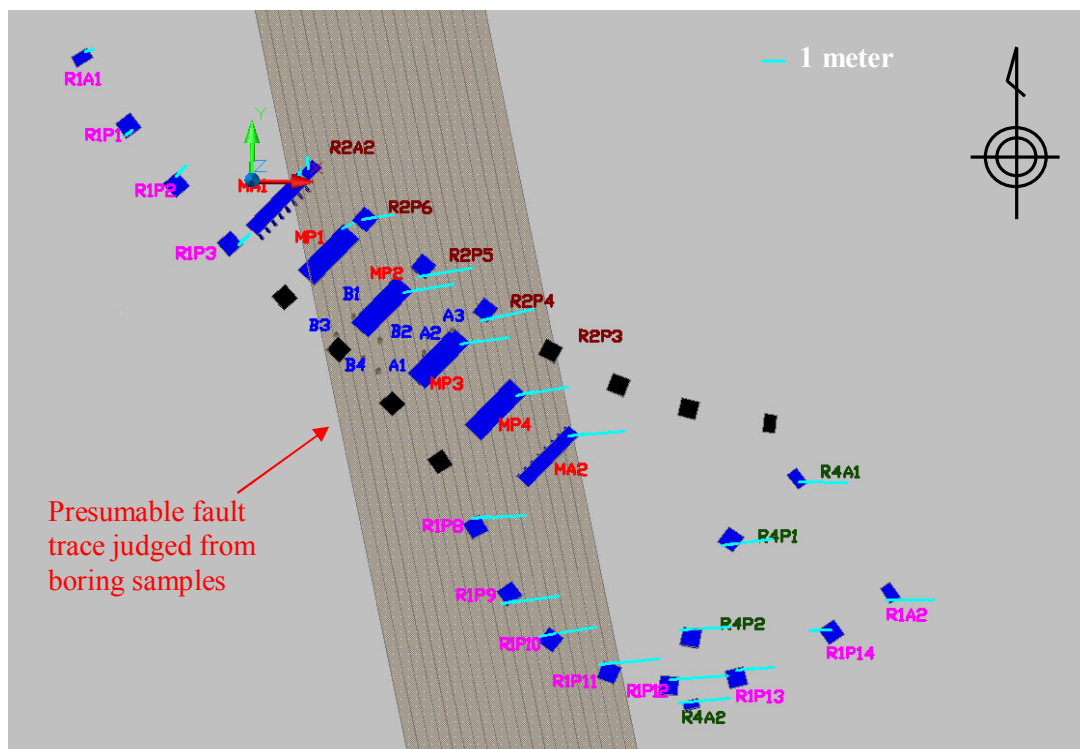


Fig. 2.12: Location of pile caps

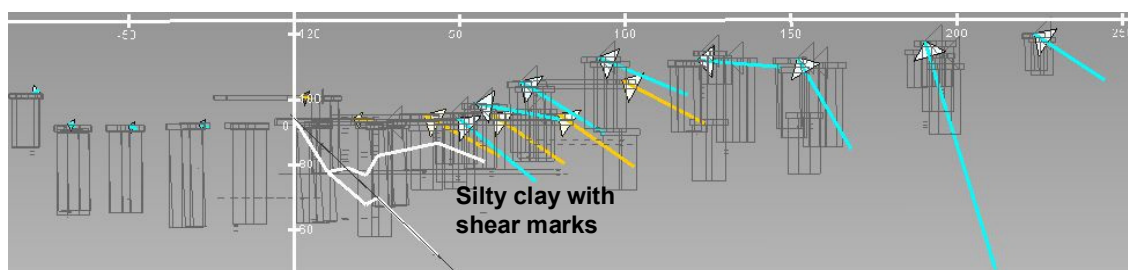


Fig. 2.13: 10-times exaggerated displacement vectors of pile caps for the main viaduct (yellow) and Ramp #1 (blue) looking from south to north in the direction of along the estimated fault trace: This figure was obtained from the 3D digital model for Bauweishan viaducts and their subsurface soils. Details follow this section.

Table 2.3: Displacements of pile caps

Pile cap	Displacements			Directions	Presence of superstructure
	Lateral components		Vertical components		
	North	East			
MA1	-0.403	-0.247	0.22	N148.5W	○
MP1	-0.263	-0.516	0.102	N117W	○
MP2	-0.453	-2.236	1.266	N101.5W	○
MP3	-0.350	-2.175	1.519	N99.1W	○
MP4	-0.450	-2.260	1.633	N101.3W	○
MA2	-0.285	-2.494	1.327	N96.5W	○
R1A1	-0.046	-0.172	-0.136	N105W	○
R1P1	-0.177	-0.197	0.088	N132W	○
R1P2	-0.244	-0.204	0.136	N140W	○
R1P3	-0.248	-0.248	0.154	N134.9W	○
R1P4	N/A	N/A	N/A	N/A	○
R1P5	N/A	N/A	N/A	N/A	○
R1P6	N/A	N/A	N/A	N/A	×
R1P7	N/A	N/A	N/A	N/A	×
R1P8	-0.226	-2.362	1.954	N95.5W	×
R1P9	-0.399	-2.522	0.484	N99W	×
R1P10	-0.505	-2.502	1.597	N101.4W	×
R1P11	-0.324	-2.694	1.154	N96.9W	×
R1P12	-0.233	-2.553	0.208	N95.2W	×
R1P13	-0.223	-1.619	2.806	N97.8W	×
R1P14	-0.132	-2.154	N/A	N93.5W	×
R1A2	-0.107	-2.162	1.426	N92.8W	×
R2A1	N/A	N/A	N/A	N/A	×
R2P1	N/A	N/A	N/A	N/A	×
R2P2	N/A	N/A	N/A	N/A	×
R2P3	N/A	N/A	N/A	N/A	×
R2P4	-0.512	-2.285	N/A	N102.6W	×
R2P5	-0.416	-2.391	N/A	N99.9W	×
R2P6	-0.266	-1.408	N/A	N100.7W	×
R2A2	-0.571	0.051	N/A	N95.1E	×
R4A1	0.047	-2.152	N/A	N88.8W	×
R4P1	-0.286	-2.251	N/A	N97.2W	×
R4P2	-0.172	-2.186	N/A	N94.5W	×
R4A2	-0.257	-2.305	N/A	N96.4W	×

Pile caps on the foot wall side have shifted about 4 to 8 cm away from the fault trace suffering a slight tilts of about 1.5 to 5 degrees. Beyond 100 m away from the fault, the ground subsided only a few centimeters and the piles had no visible damage.

Since only vertical displacements were measured at four corners of every pile cap for the main viaduct, rotations of these pile caps θ_L and θ_T around both two orthogonal axes in a horizontal plane but not around the upright axis were calculated (**Fig. 2.15** and **Table 2.4**). In general, the pile caps for the main viaduct were rotated slightly westwards. Among them, MP2 has experienced the largest rotation of about 1.40%. Abutment MA2 showed the second largest westwards rotation of about 0.82% though it was the farthest among the others from the estimated fault trace. The abutment was under construction, and did not retain its back fill at the time of the earthquake.

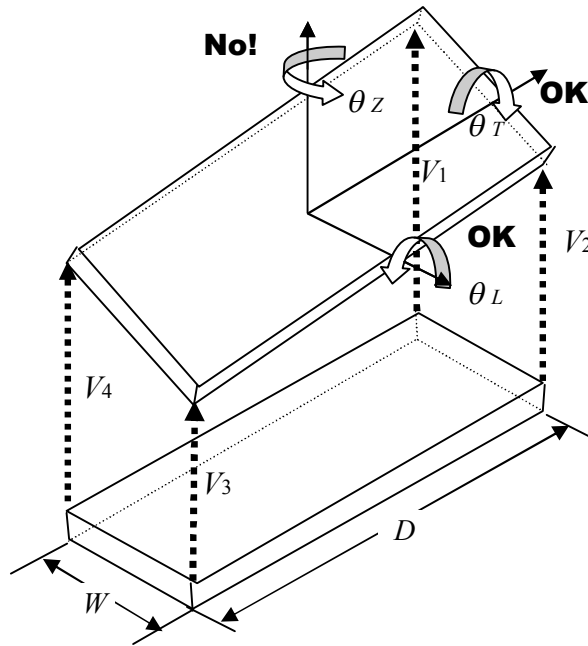


Fig. 2.15. Pile cap rotations around two orthogonal axes in the horizontal plane.

Table 2.4

Pile cap	Vertical displacement at 4 corners (m)				D (m)	W (m)	T (m)	θ_L (%)	θ_T (%)
	V_1	V_2	V_3	V_4					
MA1	0.22	0.26	0.14	0.14	33.10	6.75	1.4	0.3021	-0.296
MP1	0.10	0.09	-0.13	-0.12	29.25	10.5	2.0	0.7521	0.0952
MP2	1.18	1.27	0.81	0.82	29.25	10.5	2.0	1.4017	-0.381
MP3	1.53	1.52	1.54	1.51	29.25	10.5	2.0	0	-0.095
MP4	1.64	1.63	1.65	1.64	29.25	10.5	2.0	-0.034	0
MA2	1.55	1.59	1.33	1.27	33.10	6.75	1.4	0.8157	-0.741

Pile integrity investigation

After the earthquake, piles integrity became one of the major concerns towards continuing construction of the highway viaducts, and direct coring of piles was made at pile caps (MAA 2000, Chen et al. 2003). A triple tube coring system (diameter: 64mm) was used to ensure efficient and reliable core drilling minimizing frictional disturbance. Total 27 piles were subjected to coring and total 547m-long cores were sampled. At every pile cap, one corner pile was taken among those making up a group beneath their cap. Coring started from the center of the top end of the selected pile until the drill went through the pile's bottom and farther 1 m down into the soil, and it was often that the drill reached the side soil before reaching the bottom; the fact indicating that the pile was inclined near the fault rupture plane. There were 11 piles found tilted. Measuring and adjusting errors due to unavoidable inclination of coring through concrete, average inclinations of piles were calculated by dividing the distance from pile's center to the position of side reinforcing bars by the length of the drilled core above the point where the drill hollowed out a part of the side reinforcing bars (see Fig. 2.16). In this estimation, there was nothing to hint the direction of tilt, but pile caps' rotations are considered to be consistent with the tilts of these piles, namely piles are considered to have tilted east. Cores of 6.4 cm in diameter taken from piles were examined for a careful mapping of cracks.

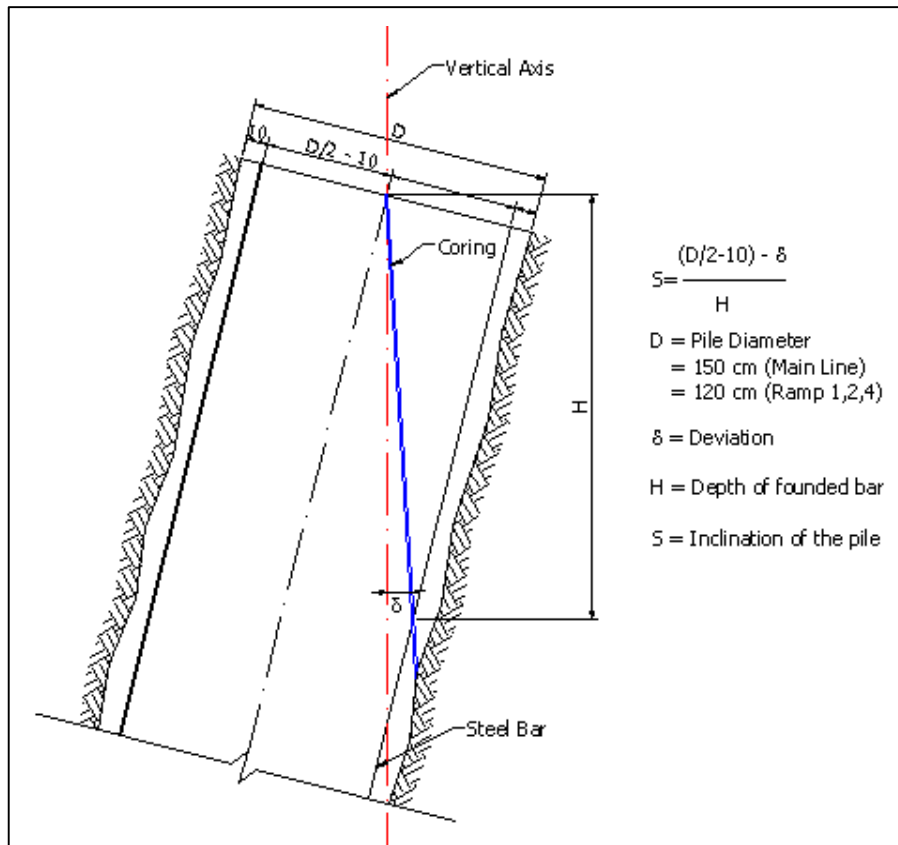


Fig. 2.16: Coring of pile for locating cracks and measuring pile's inclination

Three Dimensional Model of Soils and Foundations

Examining all findings through the conducted sub-surface soil explorations, the most consistent features of soils and foundations at Bauweishan are summarized as follows:

- (1) Rupture plane: The fault rupture plane at Bauweishan has its strike trending N12°W to S12°E, and dips about 45° NEE on average. Pier MP2 for the main viaduct seems to have been crossed by the fault rupture plane at its original location.
- (2) Hanging wall: Greater part of the hanging wall is a thick silty-clay wedge with a 8-16 m thick cap surface stratum spreading over it. The cap surface stratum consists of debris probably from the time of constructing the viaducts and natural sands and gravels. The silty-clay wedge have diagonal strip marks suggesting the wedge have been sheared continually due to thrust fault dislocations. Though slightly consolidated, this silty-clay is softer than the surface cap stratum.
- (3) Footwall: The greater part of the footwall spreading beneath the hanging wall wedge is a dense fabric of boulders and gravels with it voids filled up with sands.

To describe the above-mentioned features in relation with the damage to pile foundations, a 3D digital model of soils and pile foundations was prepared as a CAD (Computer-Aided Design) file.

Download: <http://shake.iis.u-tokyo.ac.jp/active-fault/>.

To view the model, one needs to download Autodesk® Design Review software free-of-charge from the following URL:

<http://usa.autodesk.com/adsk/servlet/index?siteID=123112&id=4086277>

The model (Bauweishan-whole.DWF) is a 3D set of digital data, containing the followings on total 12 layer sets:

- 1) contours: Contour lines describing landforms,

- 2) bore holes: Soil profiles from borehole samples,
- 3) N-values: Number of blows in STP tests,
- 4) fault: The fault rupture plane estimated from borehole samples
- 5) piles-main pre EQ, piles-ramp1 pre EQ, piles-ramp2 pre EQ, and piles-ramp4 pre EQ: piles and their caps for the main highway, ramp #1, ramp #2 and ramp #4 viaducts before the earthquake.
- 6) Piles-main post EQ, piles-ramp1 post EQ, piles-ramp2 post EQ and piles-ramp4 post EQ: piles and their caps for the main highway, ramp #1, ramp #2 and ramp #4 viaducts after the earthquake.
- 7) vectors-main, vectors ramp1, vectors ramp2, vectors ramp4: 10 times exaggerated vectors of pile cap displacements
- 8) captions main, captions ramp1, captions ramp2, captions ramp4: Captions for viaducts (for showing numbers, inclinations etc).
- 9) cracks main, cracks ramp1, cracks ramp2, cracks ramp4: Locations of cracks (yellow) and fractures (green). They are clearly displayed being superimposed on layers “simple-p main postEQ, simple-p 2Dramp1 postEQ, simple-p 2Dramp2 postEQ and simple-p 2Dramp4 postEQ”, representations of piles in a simple line-drawing way.
- 10) 2Dmain postEQ, 2Dramp1 postEQ, 2Dramp2 postEQ, 2Dramp4 postEQ: representations of piles with pile caps in a simple line-drawing way. Red lines show those remaining upright, while pink lines suffered some inclinations.
- 11) Cores-main, cores-ramp1, cores-ramp2, cores-ramp4: sketches of concrete cores, and
- 12) scale: scale for displaying projections of all above on a plane normal to the estimated fault rupture plane.

Discussions

Showing necessary layers and hiding the others in the 3D digital model, one can highlight some important features of soil-pile interaction in the vicinity of the activated seismic fault. Some discussions about the inertia and kinematic soil-pile interactions follow:

When the Bauweishan section of the Highway #3 suffered seismic fault dislocation during its construction, some pile caps sustained their piers, while the others did not. Many piles loaded with piers were cracked around their top ends immediately beneath their caps, while those without piers did not suffer serious cracking at their top ends (**Figs. 2.17** and **2.18**). For the latter piles, clusters of cracks were found rather deeper locations, which were closer to the boundary between the deeper clay layer with sheared marks and shallower and stiffer soil sediment above it (**Fig. 2.18**).

This fact suggests that the piles bearing superstructures can be cracked due to inertia forces from their superstructures, while for those without superstructures, soil deformations can be the major cause of cracking (kinematic interaction). Soil deformations will become less serious as the distance from the fault rupture plane increases. **Figs. 2.18** and **2.19** for Ramps #1 and 4 seemingly indicate this tendency with less seriously cracked piles in the off distance.

Taking into account fault rupturing process, the piles could have experienced dynamic inertia interaction first, which was then followed by rather slow kinematic interaction due to fault-induced large soil deformation. Eventually pile-cap interface cracked due to the inertia interaction can be moment-free, and the pile cap will be moved by the piles experiencing slow and steady soil deformations. To discuss possible pile caps movements near a seismic fault, which movements can affect the function of their viaduct; due attentions should be paid to this scenario.

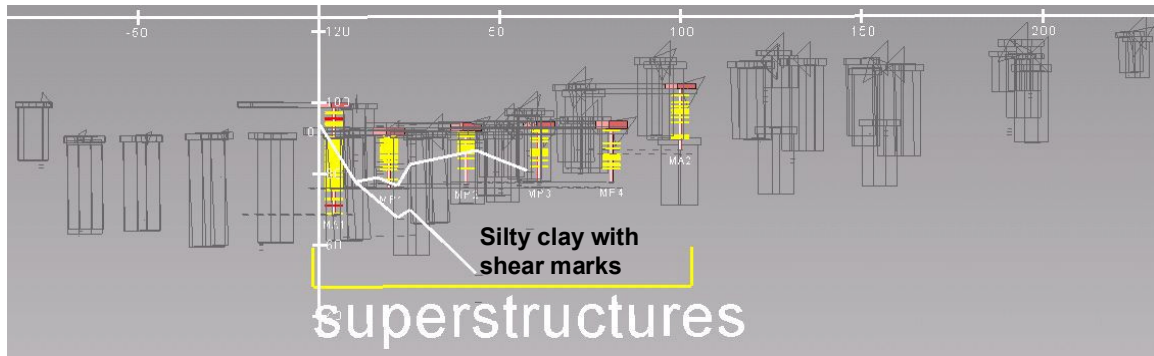


Fig. 2.17. Location of cracks in cores from piles for the main viaduct piers and abutments looking from south to north in the direction of along the estimated fault trace: This figure is prepared from the 3D model of Bauweishan, displaying Layers “2D-main Post EQ”, “captions-main”, “cracks-main”, “scale” and hiding the others. Cracks are densely distributed within the surface stratum of natural sand and gravel covered up with fills from the time of construction. These piles sustained piers when the Chi-Chi Earthquake occurred.

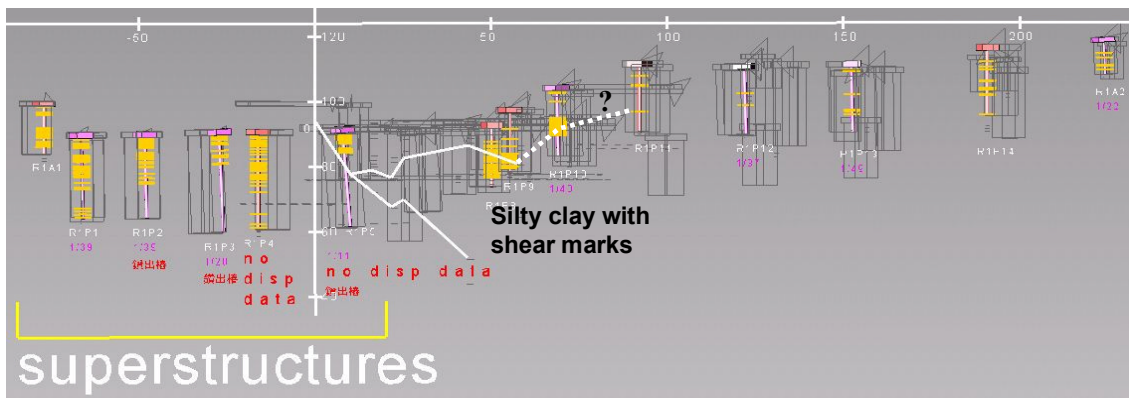


Fig. 2.18. Location of cracks in cores from piles for the Ramp #1 viaduct piers and abutments looking from south to north in the direction of along the estimated fault trace: This figure is prepared from the 3D model of Bauweishan, displaying Layers “2D-ramp1 Post EQ”, “captions-ramp1”, “cracks-ramp1”, “scale” and hiding the others. It is remarkable that piles near the estimated fault, regardless of their locations on either hanging wall side or foot wall side, were severely cracked. However those on the hanging wall side appeared rather deeper locations and seemingly close to boundary between the surface stratum and the silt-clay wedge with shear marks. The farther the piles were on the hanging wall side, the sparser the cracks were. Note those on the hanging wall side sustained no pier when the earthquake occurred.

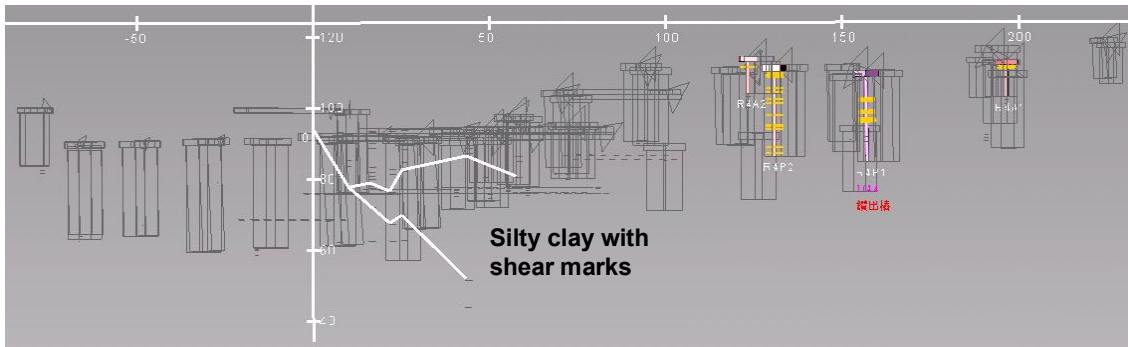


Fig. 2.19. Location of cracks in cores from piles for the Ramp #4 viaduct piers and abutments looking from south to north in the direction of along the estimated fault trace: This figure is prepared from the 3D model of Bauweishan, displaying Layers “2D-ramp4 Post EQ”, “captions-ramp4”, “cracks-ramp4”, “scale” and hiding the others. The cracks were rather sparse as contrasted with those in **Fig. 2.17** and **2.18**.

REFERENCES

- Moh and Associates (MAA), Inc. (2000). “Earthquake Investigation Report for Piles at the Nantou Section (C335) of Freeway Route No. 3.”
- Chen Cheng-Hsing, Chow Hung-Sheng, Yang Chin-Yuan, Shieh Baih-Jung, and Kao Yao-Hung (2003) “Chelungpu fault inflicted damages of pile foundations on FWY Route 3 and fault zoning regulations in Taiwan,” 2nd JSCE/EqTAP/JSPS Workshop on Seismic Fault-induced Failures, -- Possible Remedies for Damage to Urban Facilities --, Konagai, K. Hori, M. and Meguro. K. eds., Feb. 22, 2003, Inst. Of Industrial Science, University of Tokyo.
- Taiwan Construction Research Institute and Institute of Industrial Science University of Tokyo (2006) “Report of Bauweishan Viaduct Geophysical Survey”.

Chapter 3

DAMAGE TO TUNNELS

3. 1 TANNA TUNNEL

Location: 35° 6' 14"N, 139° 0' 55"E

Earthquake: Nov. 26, 1930, North-Izu Earthquake, Japan, M=7.2

Construction of 7.8km-long Tanna Tunnel was planned to bypass a railway route winding up across mountains in Hakone and Tanzawa area. The construction started in 1918 and was making little progress when it was crossing the fault-fracture zone beneath the Tanna basin (**Fig. 3.1**). The most serious problem there was water inflow through fractured rocks, and measures taken included injecting grout, and using pressurized excavation chamber. In addition, a number of branch holes were excavated to drain waters, and the total length of these branches reached 16 km, two times as long as the main tunnel. An intense earthquake (M7.0) occurred at 4:03AM JST, Nov. 26, 1930, exactly when two of the branches (drainage holes) reached its fault rupture plane.

There were four points **(a)-(d)** seriously damaged:

(a) & (b) Cut surfaces of two drainage holes, South #2 and #3, reaching the fault rupture surface at 3660m and 3662m depths respectively from the western entrance (Fig. 3.2): Since these tunnels were pushed through a fractured rock, they were needed to be supported soon after the excavation. In Drainage hole #3, Pi-shaped steel frame were quickly set up at a regular interval of about 1.5m, and the wall was then boarded up with many pieces of wood. The dislocated rock drew both the end frame and several pieces of wood into the mountain. **Fig. 3.3** shows the cut surface of Drainage hole #3. Several pieces of wood were seen half embedded in the left side of the rock.

(c) Point at 3265-3325m from the west entrance:

About a 60 m stretch of the tunnel crown at this point had not been covered up with concrete yet, and therefore exposed frames could not sustain a large soil pressure. A soil mass of about 1200 m³ fell all of sudden into the main tunnel killing 3 persons.

(d) Point at 3050 m from the west: A branch of the Tanna fault seems to have dislocated, and cracked the concrete lining. The east side of this point has subsided by about 23 cm.

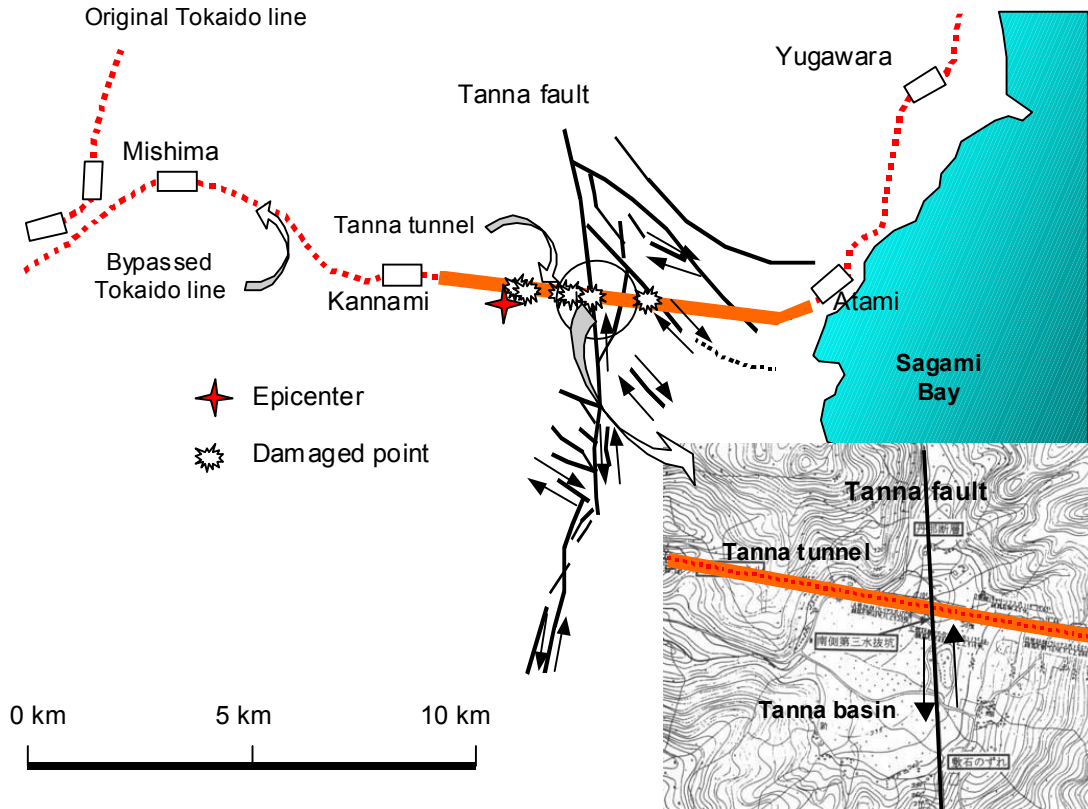


Fig. 3.1: Tanna tunnel and the Tanna fault system.

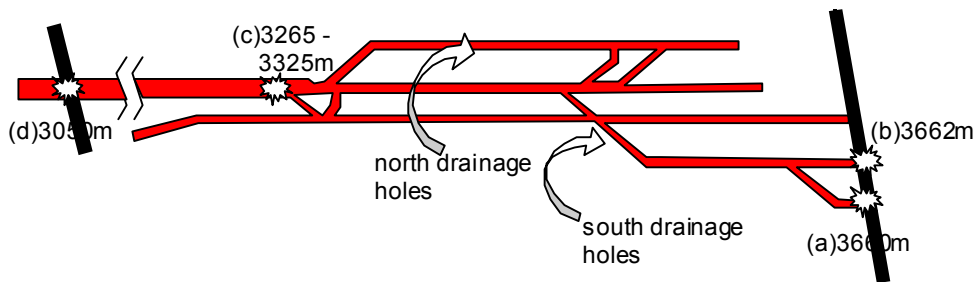


Fig. 3.2: Drainage holes and damaged points

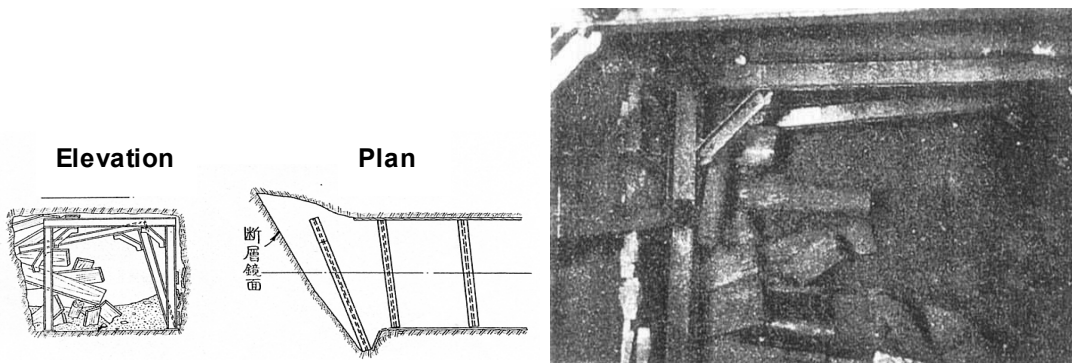


Fig. 3.3: Drainage hole #3

3.2. INATORI TUNNEL

Location: 34° 46'20"N, 139° 1'53"E

Earthquake: Jan. 14, 1978, Off-Izu Oshima Earthquake, Japan, M=7

A fault appeared in the 1970 Off Izu Oshima Earthquake (M7.0) across Inatori railway tunnel (906 m long) of the Izukyu line (**Fig. 3.4**). The northeastern half of the tunnel was pushed seaside, and an 85 cm lateral displacement was reached at the east mouth of the tunnel, while its western mouth was pushed about 20 cm up. The tunnel was the most seriously deformed at around the point where the tunnel was cut by the fault. **Figs. 3.4(a), (b)** and **(c)** show cross-sections at 31.055km, 31.035 km and 31.010 km points from Ito (North starting station of the Izukyu line) respectively. These cross sections were all pushed slightly out of shape exactly like those of a kinked water hose. As the consequence, crowns were bent up against soils, and some parts of their inner surfaces broke up into flakes. Some sidewall blocks were thrust forward lying between two less deformed blocks. Some invert concrete blocks were pushed up. Though cracked, the lining fortunately held the soil pressure probably because the surrounding soils had been softened by solfataric and/or hydrothermal activities.

Rails were buckled at several points (**Fig. 3.5(a)**). The biggest buckling was found at **Point A**, near the southwestern mouth of the tunnel where the tunnel goes through a debris deposit. Assuming that the shape of the buckled rail is expressed as:

$$f(x) = \begin{cases} A \sin \frac{\pi x}{L_0} \sin \frac{\pi x}{L_1} & \dots\dots 0 \leq x \leq L_0 \\ 0 & \dots x < 0, \quad L_0 < x \end{cases} \quad (3.1)$$

with

$$\sin \frac{2\pi L_0}{L_1} = 0 \quad (3.2)$$

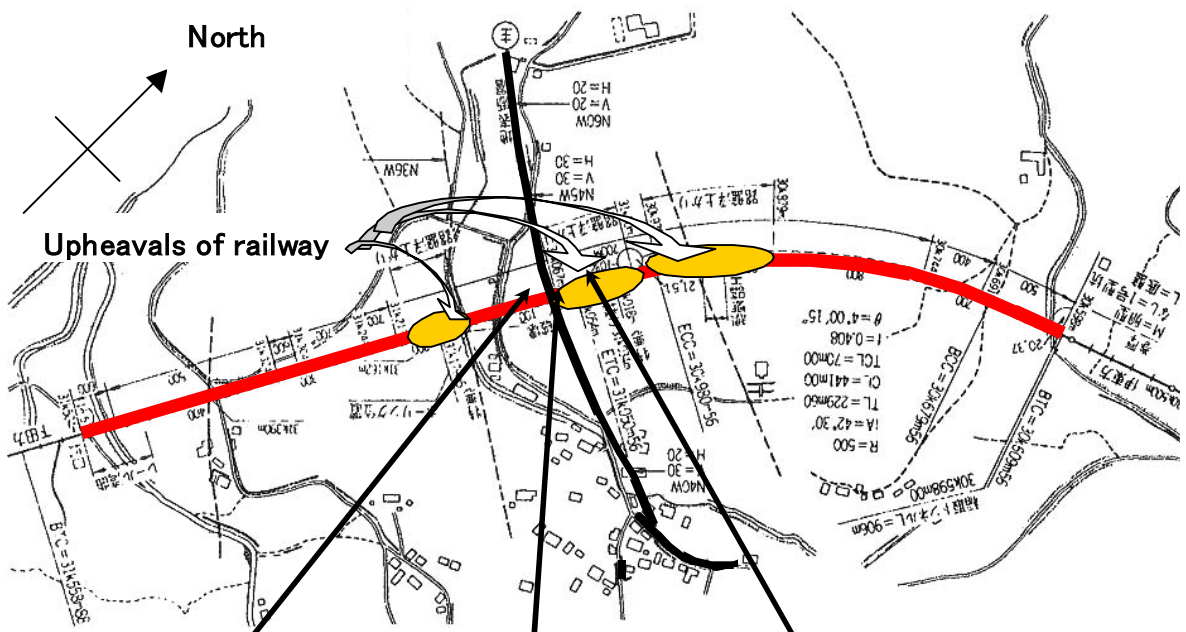
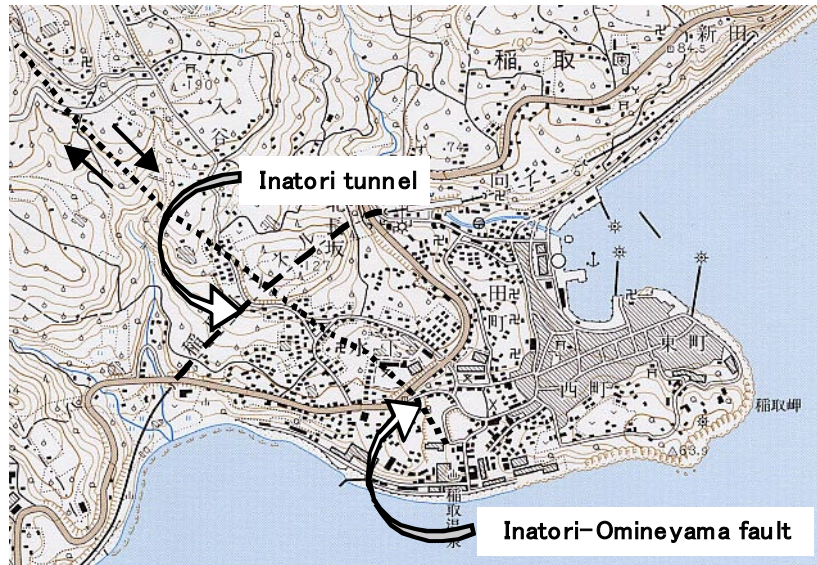
The average strain ε induced over the L_0 distance is obtained by

$$\begin{aligned} \varepsilon &= \frac{1}{L_0} \int_0^{L_0} \left(\sqrt{1 + \left(\frac{df}{dx} \right)^2} - 1 \right) dx \\ &\cong \frac{1}{2L_0} \int_0^{L_0} \left(\frac{df}{dx} \right)^2 dx \end{aligned} \quad (3.3)$$

Substituting Equation (3.1) in Equation (3.3), one obtains:

$$\varepsilon \cong \frac{\pi^2}{4} \left(\frac{A}{L_0} \right)^2 \left\{ 1 + \left(\frac{L_0}{L_1} \right)^2 \right\} \quad (3.4)$$

Overall strain of about 0.00114% was calculated for the total 50m buckling at Point A (**Fig. 3.6**). This overall strain, however, may not reflect the strain of the soil supporting the rail. A rail buckling often takes place where ties are exposed and the rail loses its lateral support. **Fig. 3.5(b)** shows that rails were buckled where they were pushed up. The overall strain thus depends greatly on the distance where rails were lifted off their subsoils. As for **Point A**, one can say that there was about 5.7 cm shortening of the subsoil.



(a) Inatori tunnel

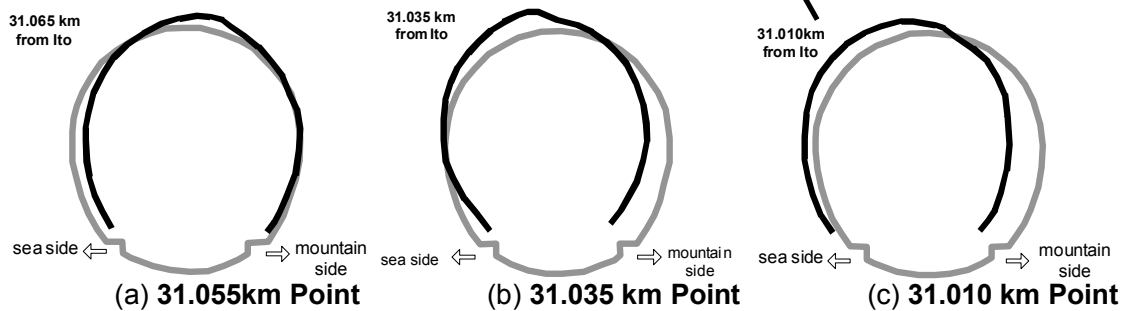
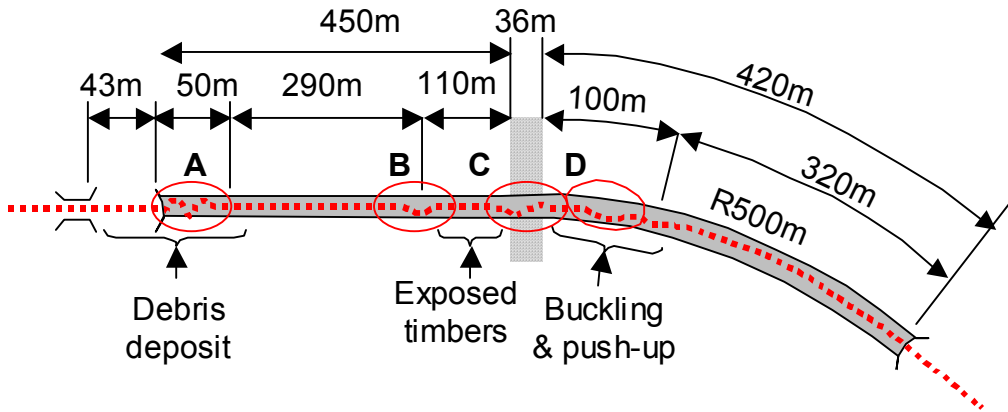
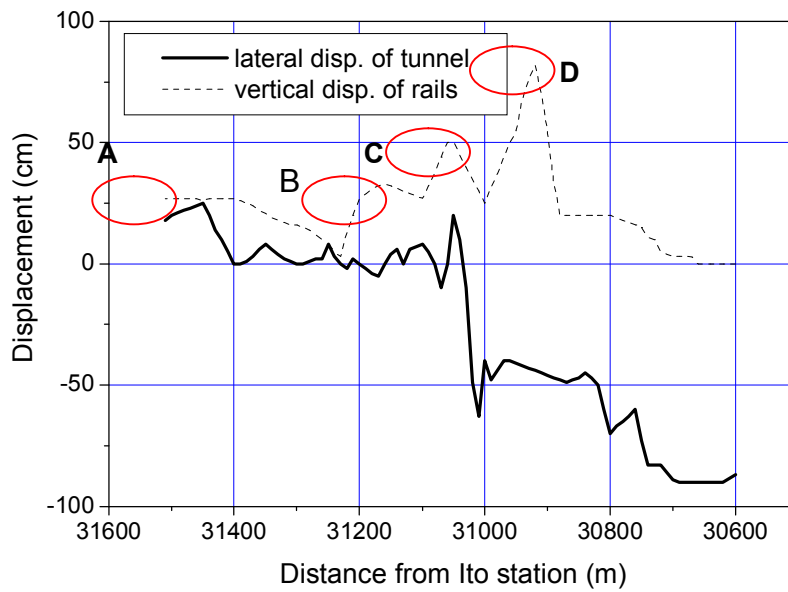


Fig. 3.4. Deformed cross sections of Inatori tunnel



(a) Locations of bucked rails



(b) Pushup of rails and lateral displacements of Inatori tunnel

Fig. 3.5: Buckled rails and tunnel deformation

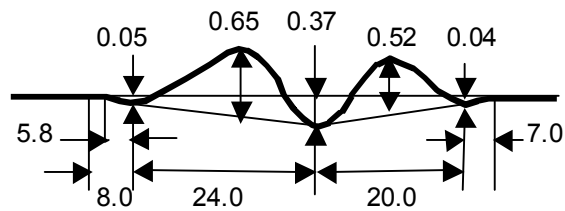


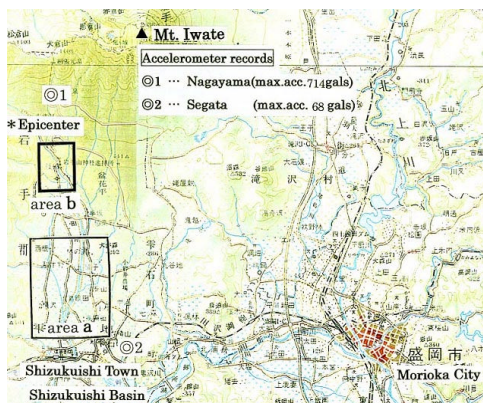
Fig. 3.6. Rail buckling at Point A in Fig. 3.4.

3.3. OUTLET TUNNEL OF 2nd KAKKONDA HYDROPOWER STATION

Location: 39° 46'49"N, 140° 56'48"E

Earthquake: Sept. 3, 1998, Mid-North Iwate Earthquake, Japan, M=6.1

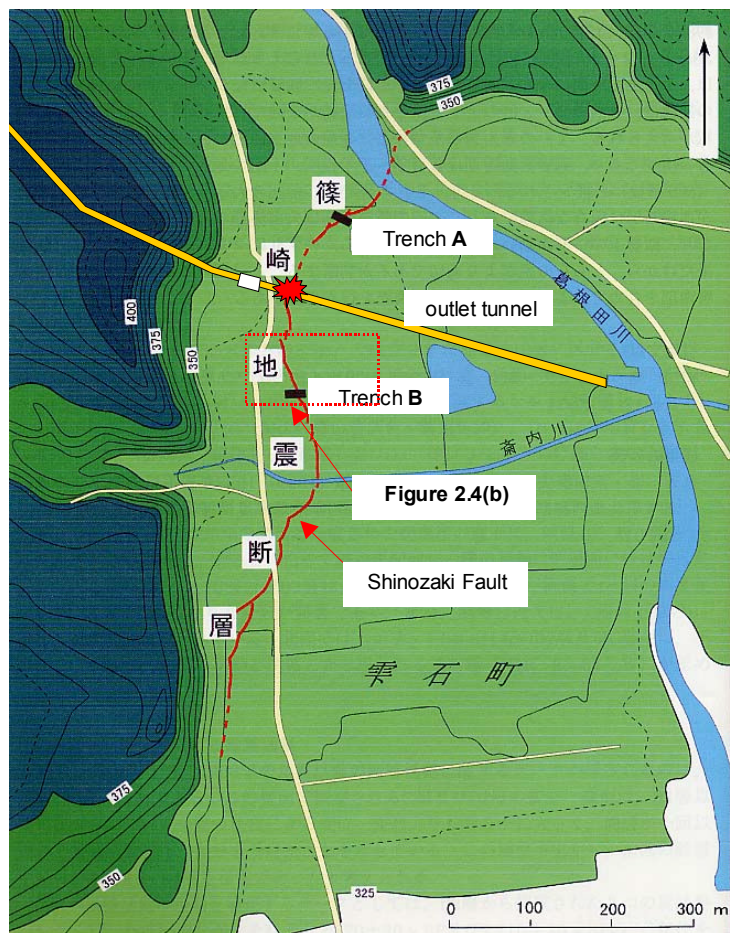
Shizukuishi, Iwate Prefecture, is located in the middle of the Shizukuishi Basin surrounded by peaks of northern Oou mountains and Mt. Iwate, mostly volcanoes rising to elevations of more than 1,000 meters. The volcanoes were quite active during the Quaternary Period, and this area has been covered deep with their products. Rivers from these mountains have carried over centuries volcanic ashes and other suspended matters in their waters, and have formed the basin (Konagai et al, 1999). An intense earthquake shook Shizukuishi area at 16:58, September 3, 1998, injuring 10 people. An intensity 6-weak on the Japan-Meteorological Agency (JMA) scale of 7 was registered in Shizukuishi (**Fig. 3.7(a)**). The hypocenter of the earthquake (39.8N, 140.9E, focal depth = 10 km, origin time 16:58, JMA) was located about 20 km north-west of Morioka city. The magnitude of the main shock was 6.1 on JMA scale.



(a) Shizukuishi Area



(b) Fault mark appeared in paddy field



(c) Area a in Fig. 3.7(a) (right)

Fig. 3.7: Shinozaki Fault appeared in the 1998 Mid-north Iwate Earthquake

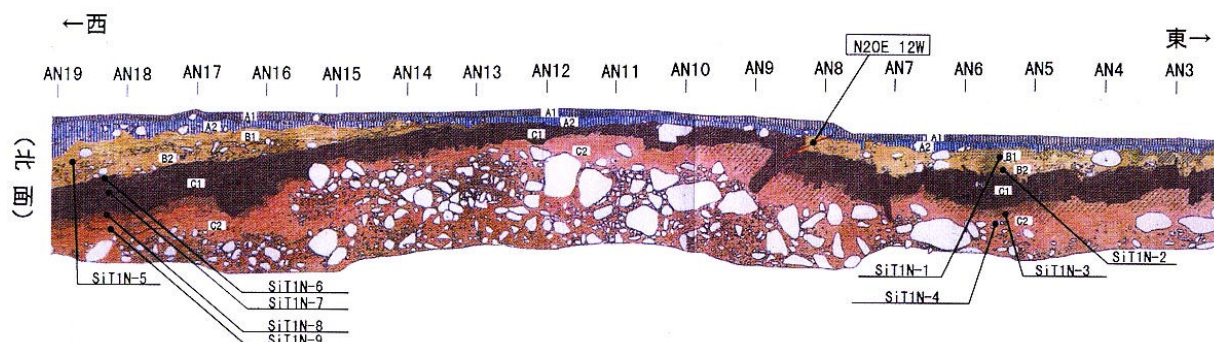


Fig. 3.8: North wall of Trench A across the Shinozaki Fault (Azuma et al., 1999)

The area was on strict guard against a possible eruption of Mt. Iwate, because frequent volcanism-related tremors had been observed for a month. Though this symptom did not lead to any actual eruption after all, JMA had taken a quick action of spreading a dense observation network over the area. The earthquake that followed this symptom was, thus, eventually recorded by these seismometers. After this earthquake, it was first suspected that the earthquake might have some link with this volcanic activity. But fault rupture planes, which appeared in this earthquake, evidenced that the dip-slip movement of this fault caused this earthquake.

The focal depth of this earthquake was quite shallow enough for its fault rupture planes to appear on the ground surface; the fact is quite unusual for earthquakes of this magnitude. The fault rupture planes were found roughly lined up at irregular intervals near a scarp formed along the Kakkonda glen. One of the rupture planes which appeared in a paddy field had a straight raised mark extending 880 m distance, clearly showing a compressive dip-slip movement of this fault (**Fig. 3.7**). The average upward movement of the hanging wall of this fault reached or exceeded 10 cm in this paddy field. An investigation team from the Active Fault Research Center, National Research Institute of Advanced Industrial Science and Technology (AIST), excavated two trenches (Trench A and Trench B) across this fault mark (Azuma et al., 2000). **Fig. 3.8** shows a sketch of the north walls of Trench A. There were seven layers (A1, A2, A3, B1, B2, C1 and C2) observed on the exposed wall, which fall into four broad categories: (1) A1-A3: Surface cultivated soils, (2) B1 and B2: fine and coarse sands including gravels, respectively, and (3) C1: old volcanic products of about 2500 years ago, and (4) C2: the layer including large boulders. A west-dipping fault rupture trace was found on the exposed wall forcing its way up through Layers C1, B2 and B1. The strike and dip of this plane were N20°E and 12°W, respectively. The seven Layers on the hanging wall side were slightly bent upward. 700 meter to the north of the power station a hot spring well intersecting the fault was damaged at 180 meters depth by the fault motion

These rupture planes that appeared on the ground surface form a part of Shizukuishi-Seien fault belt whose presence has been suggested by many geologists¹⁾. Continual movement of this fault belt has formed the scarp along the Kakkonda river, and by virtue of this configuration, some hydroelectric power stations were constructed along the Kakkonda river. A concrete outlet tunnel of the second Kakkonda hydroelectric power station runs across the fault rupture plane exactly beneath the paddy field. As an inevitable consequence, the circular tunnel wall was cracked up into several large pieces and smaller fragments (**Figs. 3.9** and **3.10**). Some pieces of the cracked wall were pushed in the tunnel reducing the tunnel's cross-section. One cracked piece of about 2 m high and 2 m wide completely fell down onto the invert allowing the soil with big boulders (30 ~ 50 cm) to fall into the tunnel. This movement of the fault was also responsible for the damage to a concrete drain (Sainai river) crossing the paddy field. Another fault plane branching east off the major fault crossed the Kakkonda river and buckled the pavement of the prefectural route 100 (Konagai, et al. 1999). An open aqueduct leading to the second Kakkonda hydroelectric power station was also damaged. Diagonal cracks found on its concrete walls are suggestive that the aqueduct might have experienced compressive force in its axial

direction. No clear evidence of fault dislocation was found there.

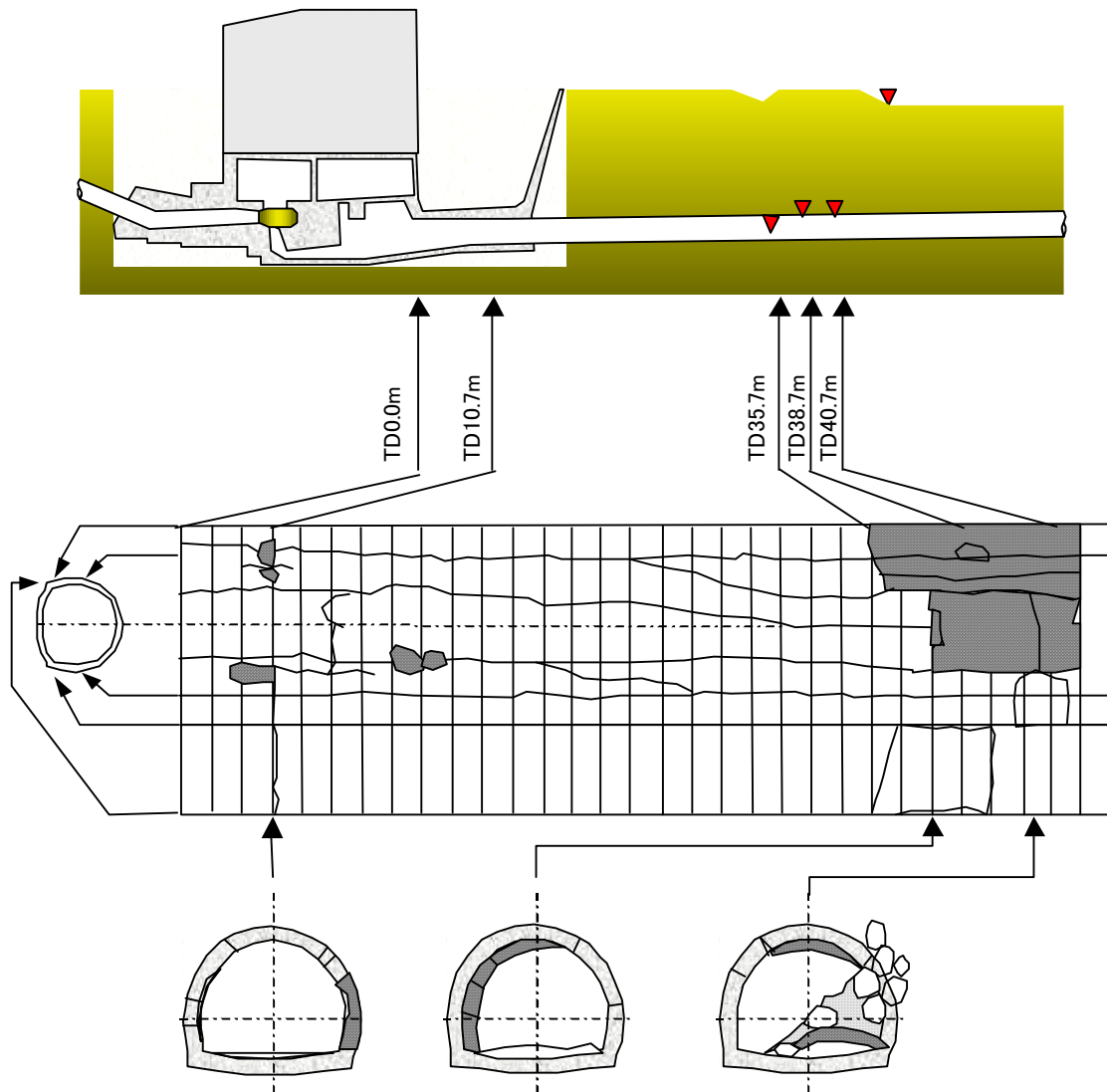


Fig. 3.9: Development and cross-sections of cracked tunnel (after Hashimoto, 1998)



(a) Boulders squeezed into tunnel



(b) Cracked tunnel

Fig. 3.10: Outlet tunnel of 2nd Kakkonda Hydropower station
(Photo: Tohoku Electric Power Co. Ltd.)

3.4 INTAKE TUNNEL OF SHIHKANG DAM

Location: 24° 16'42"N, 120° 46'14"E

Earthquake: Sept. 23, 1999, ChiChi Earthquake, Taiwan, M=7.6

The ground rupture in the 1999 ChiChi earthquake propagated north along the recognized CherLungPu fault trace, and suddenly turned east off at Feng-Yuan city shooting many branches that crossed ShihKang area (see **Chapter 4**). One of these branches crossed the intake tunnel of the ShihKang dam, and dislocated it about 3.5 m vertically and about 3 m horizontally (**Fig. 3.11**). The tunnel has an oval cross-section, 4.1 m and 3.8 m in upright and transverse diameters. Large and small pieces of concrete came off the tunnel lining, and the slacks of the roof cable show that the tunnel experienced a large axial force. This large axial force seems to have punched out the intake gate wall by about 20 cm (**Fig. 3.11 (b)**).

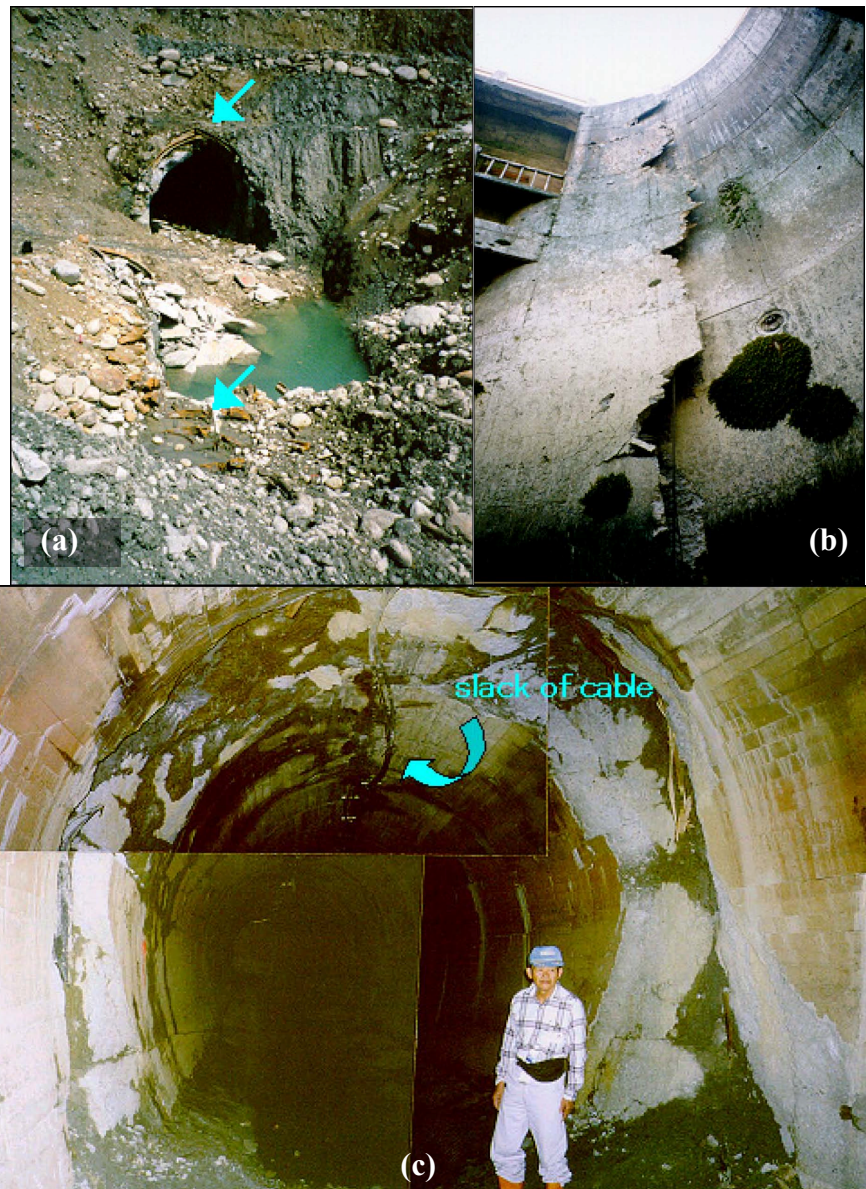


Fig. 3.11: (a) Intake tunnel of the Shih-Kang dam was cut off by the fault. (b) The intake gate sheared off due to large horizontal load from the axially compressed tunnel. (c) This photo shows the cracked up interior of the tunnel.

3.5. INTAKE TUNNEL OF OMIYA DAM

Location: 35° 13'46"N, 133° 22'39"E

Earthquake: Oct. 6, 2000, West Tottori Earthquake, Japan, M=7.3

On October 6 at 1:30 in the afternoon, a large earthquake hit the western part of Tottori prefecture, Japan. It was the largest earthquake to hit Japan since the devastating Kobe earthquake in 1995. It had a moment magnitude of 6.6 (M_w , JMA), which is about 40% of the Kobe earthquake. The epicenter was located some 30 km south of Yonago, a port city on the Japan Sea-coast. The focal depth was about 11 km. The right lateral strike-slip fault has caused some slight signs of surface rupture (**Fig. 3.12**).

The intake tunnel of the Omiya dam leads to Unoike Reservoir across NNW-SSE trending cluster of geological lineaments, among which several surface ruptures were observed (**Fig. 3.12**). It often happens that a fault shoots its branches wide in an echelon manner near the end of its rupturing path though there is no un-cemented soil deposit covering thick rock formations. This tunnel was eventually cracked at two locations A and B, and this example shows difficulty in foreseeing risks at these points among many others with similar features, while strains were distributed wide yielding less serious localization of strain.

At Point A, some fragments of concrete lining came off, and a left lateral dislocation of about 2 cm was observed on the exposed rock surface (**Fig. 3.13**). Cracks were found over 7m distance as shown in **Fig. 3.14**, and the tunnel was bent over this distance by about 10 to 20 cm (**Fig. 3.15**). Cracks on the lining show conjugate features with respect to the dislocation observed on the rock. Point B located about 365m west of Point A was less seriously cracked over 4m distance.

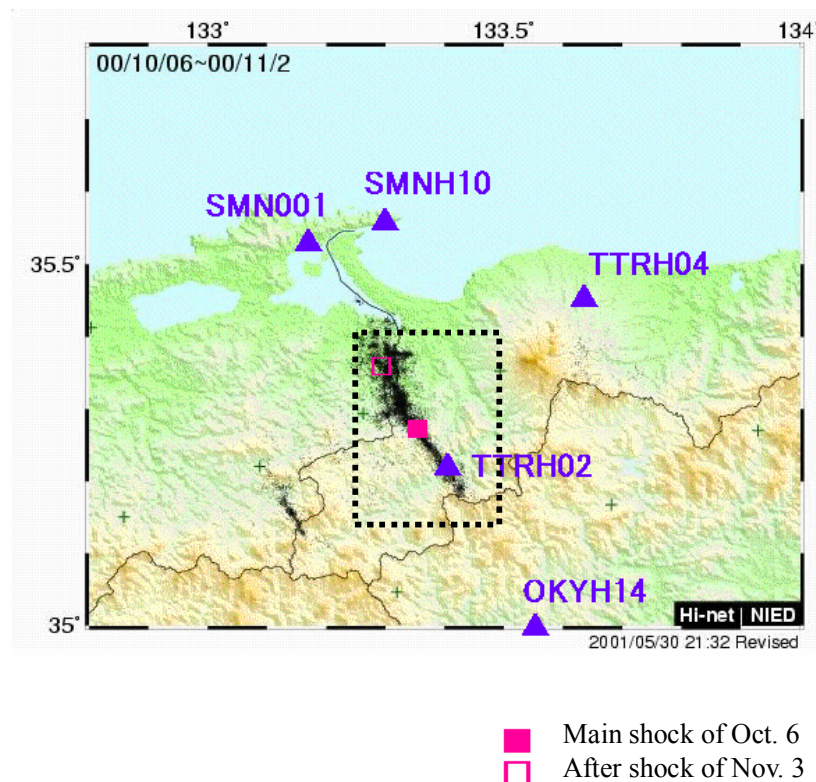


Fig. 3.12 (a): Aftershocks distribution of the 2000 West Tottori earthquake: Rectangular area is zoomed in to show the location of the tunnel (see Fig. 3.12(b)).

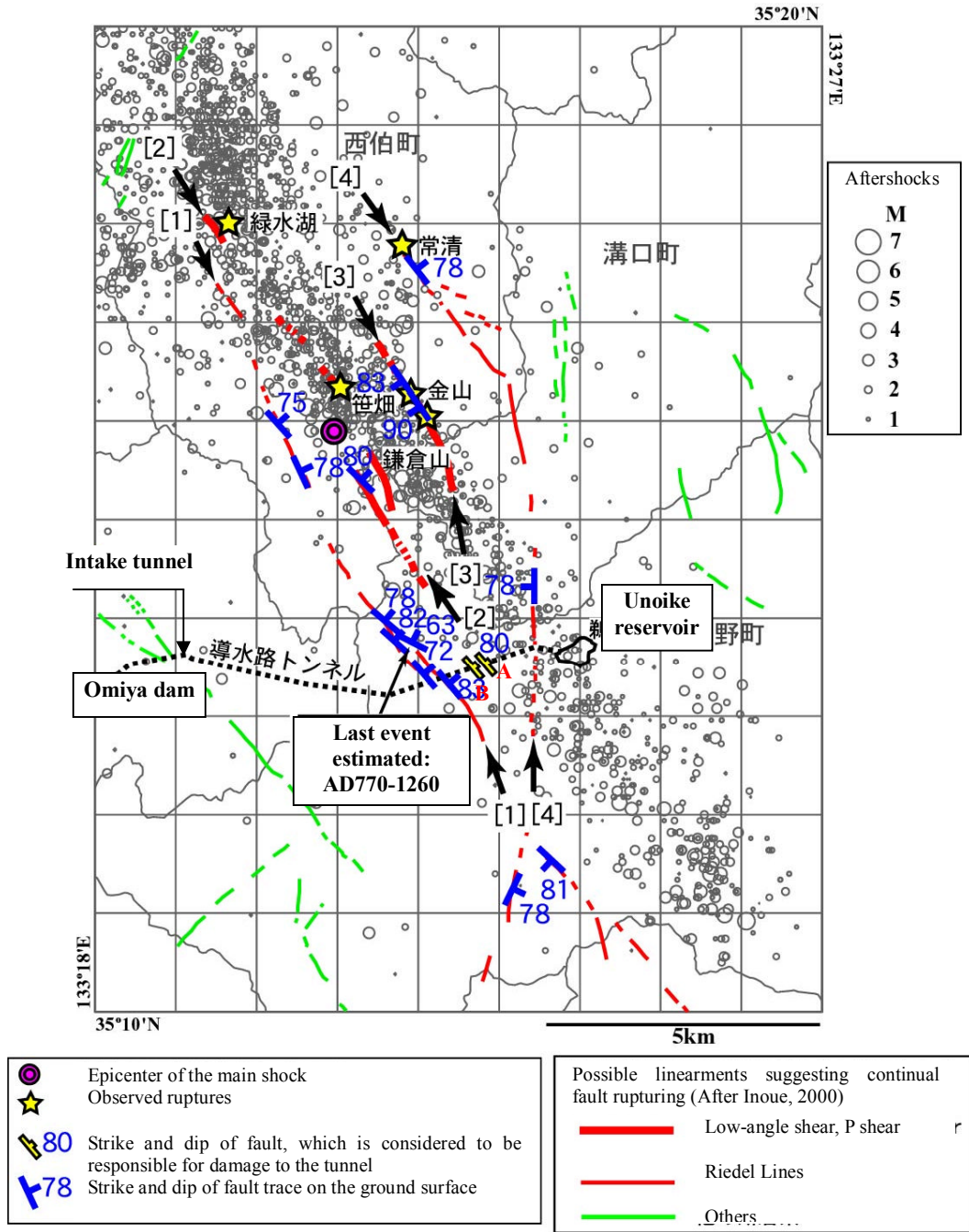


Fig. 3.12 (b): Aftershocks, surface ruptures and lineament distribution in the 2000 West Tottori earthquake (after Ueta 2002)

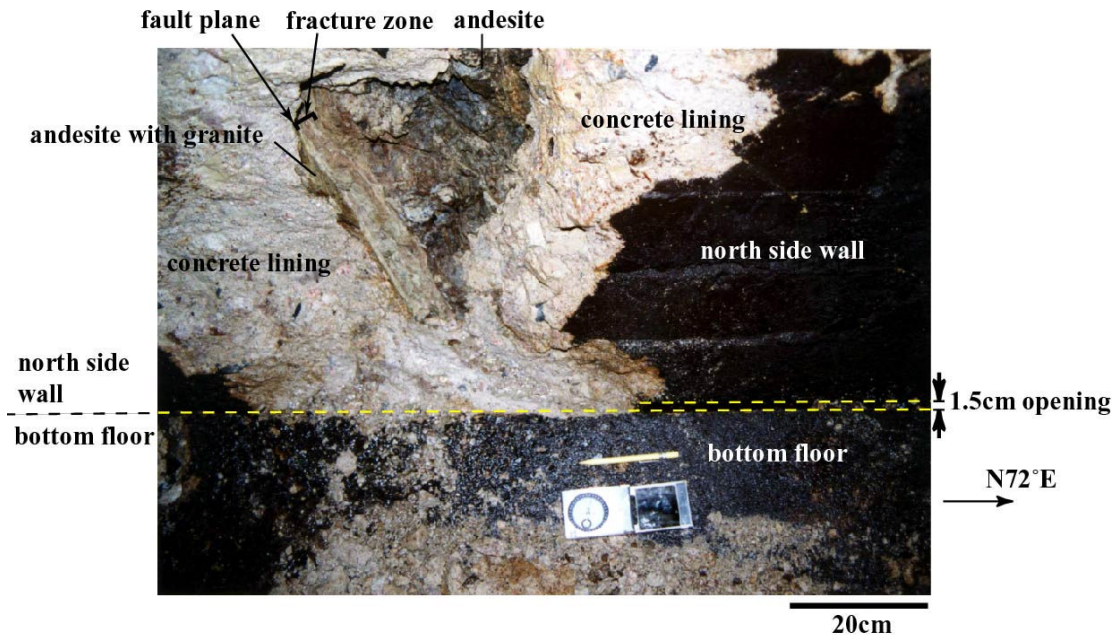


Fig. 3.13: Dislocation found on exposed rock in Intake Tunnel of Omiya dam in the 2000 West Tottori earthquake, (Ueta 2002)

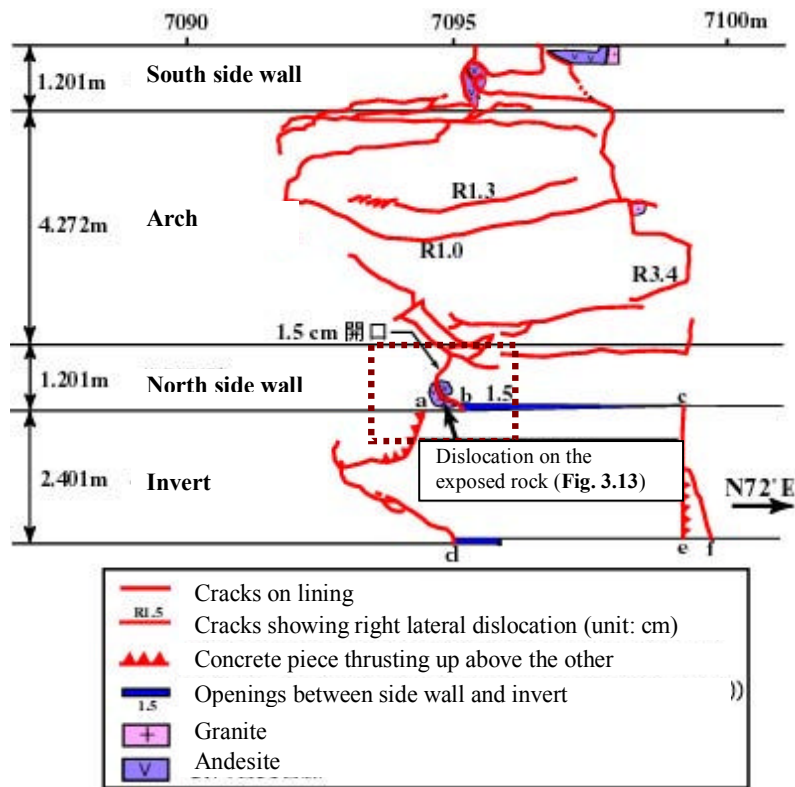


Fig. 3.14: Cracks that appeared on concrete lining, Intake Tunnel of Omiya dam in the 2000 West Tottori earthquake (Ueta 2002).

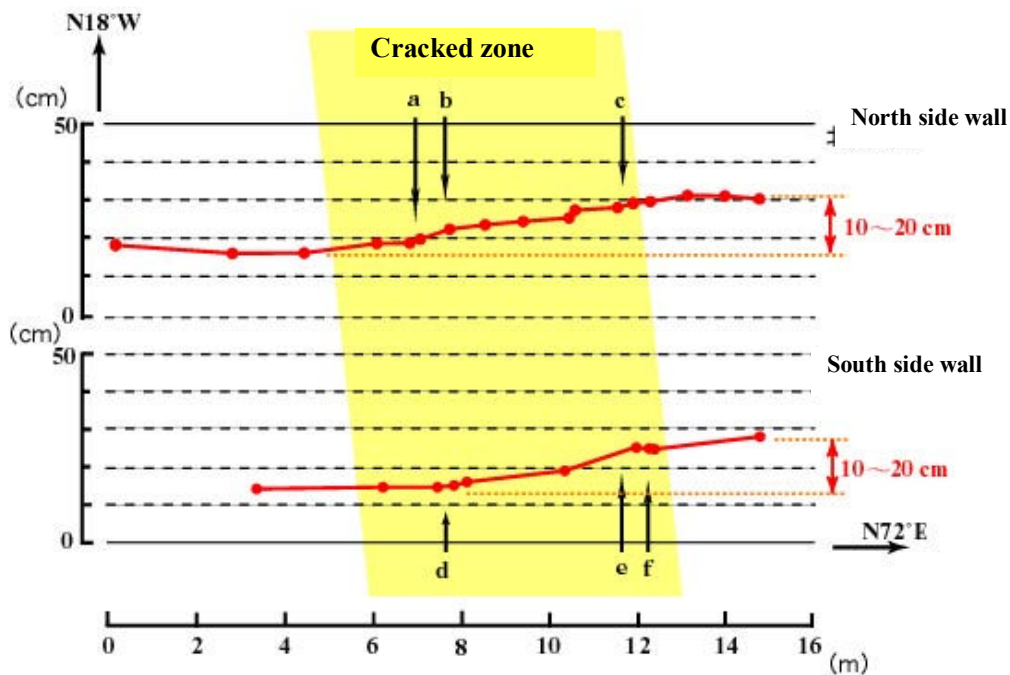


Fig. 3.15: Alignment of the Intake Tunnel of Omiya Dam deformed in the 2000 West Tottori Earthquake (Ueta, 2002)

3.6. UONUMA TUNNEL OF JOETSU SHINKANSEN RAILWAY

Location: 37° 17' 19"N, 138° 51' 43"E

Earthquake: Oct. 23, 2004, Chuetsu (Mid-Niigata) Earthquake, Japan, M=6.8

A sequence of powerful earthquakes struck Mid Niigata Prefecture, central Japan. The hypo-center of the main shock is located at 37.3 N; 138.8E with depth of 13 km and magnitude of 6.8 determined by Japan Meteorological Agency occurred at 17:56 JST on October 23, 2004. The intensity is registered 6+ on the 7-grade Japanese intensity scale. Many aftershocks including some M6 class events have been following.

Focal mechanisms of those major earthquakes are the reverse fault type with the compression axis oriented to NW/SE that is consistent to the historical solutions of major earthquakes in this area. Aftershocks are distributed along the northeast and southwest direction with a length of about 30km. The maximum acceleration of 1500 gal is recorded at station Ojiya that is the nearest K-NET site from the hypo-center. The recorded maximum acceleration for this earthquake is much greater than that for the 1995 Kobe earthquake.

Higashiyama mountain zone (**Fig. 3.16**), which was the most seriously affected by the 2004 Mid Niigata earthquake, is well known as one of the most landslide-prone zones in Japan. The prevalence of NNE-SSW-trending folds characterizes this zone. Stratified Pliocene rocks are found everywhere inclined or curved upward or downward. Since the up-folded rocks along anticlines were expanded and weakened, anticlines frequently have their crests eroded deep. As the consequence, asymmetric

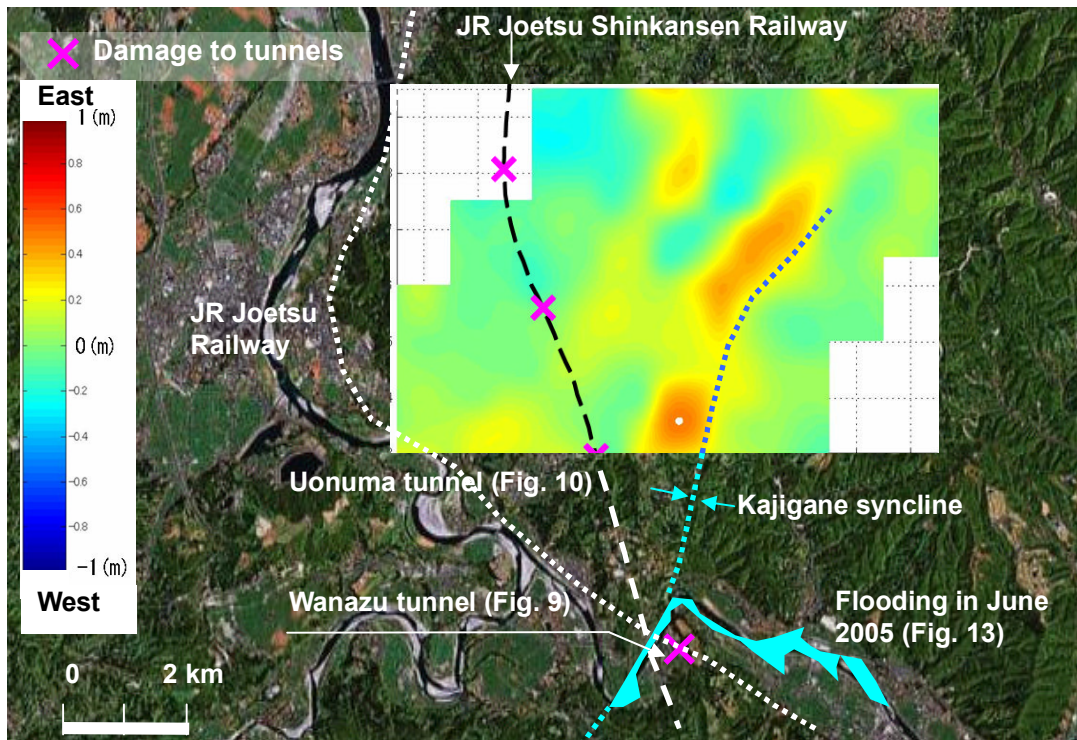


Fig. 3.18 (a) East-west component of subsoil deformation (East: positive)

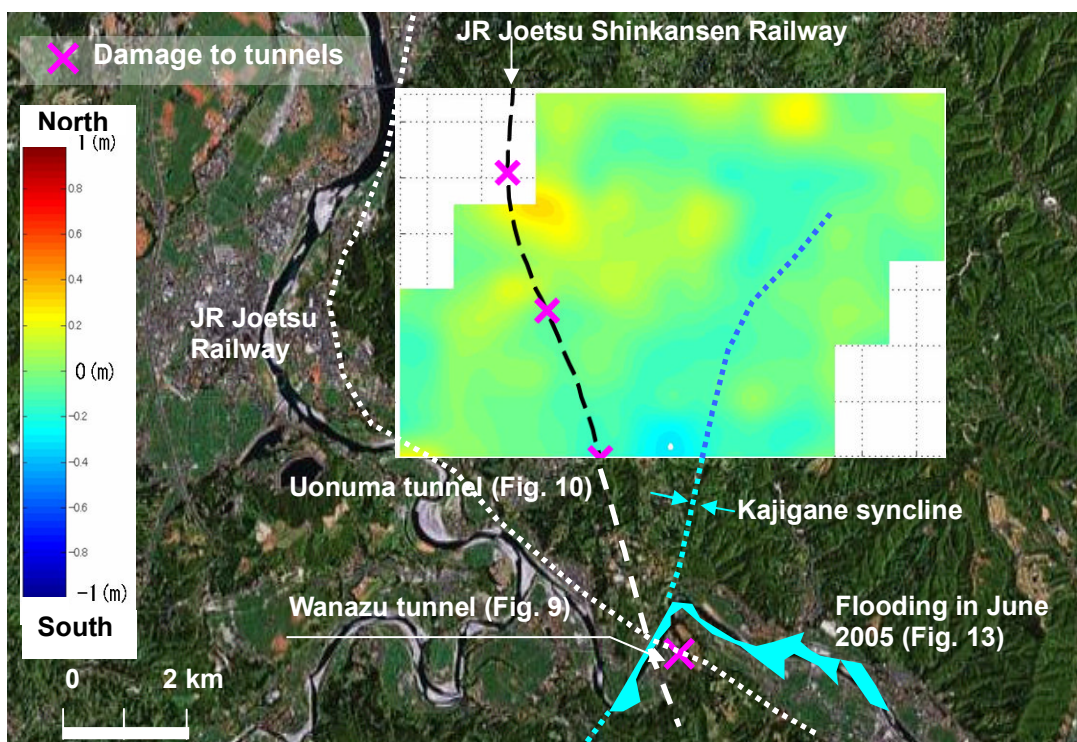


Fig. 3.18 (b) North-south component of subsoil deformation (North: positive)

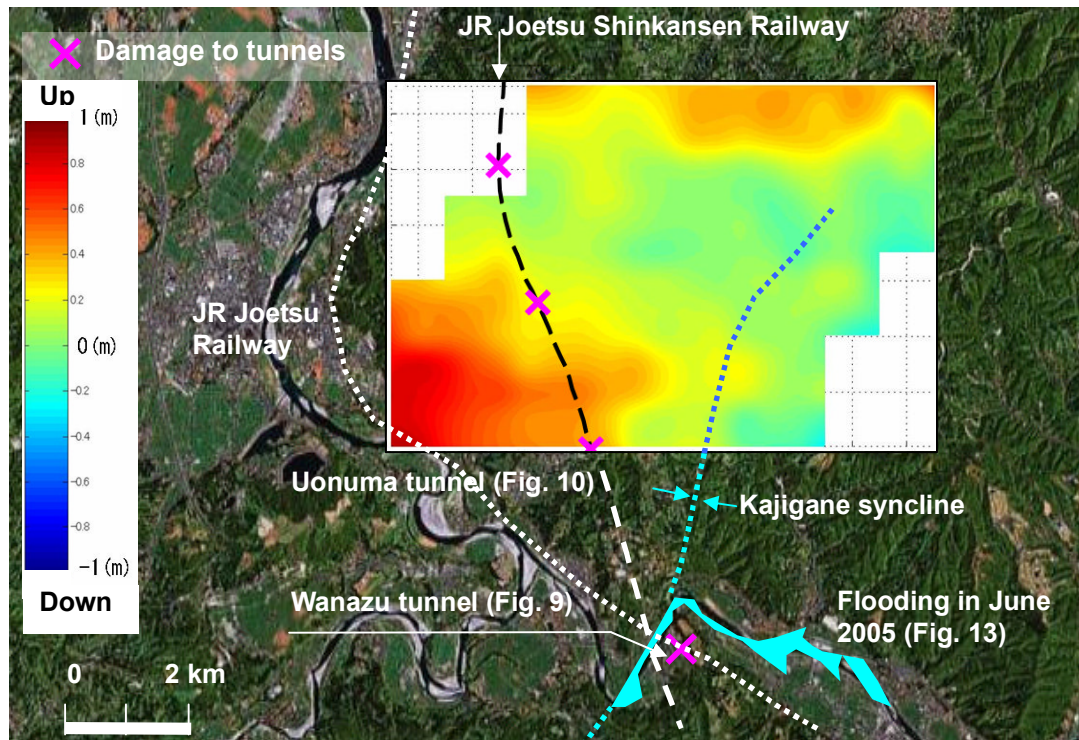


Fig. 3.18 (c) Vertical component of subsoil deformation (Up: positive)

Konagai and Fujita, et al. (2007) have prepared several digital elevation models (DEMs) for the affected area at different times to obtain subsurface soil deformations by comparing these DEMs (see **Chapter 5**). This study was a part of a three-years (2005-2007) Research and Development program for Resolving Critical Issues, “Earthquake damage in active-folding areas: creation of a comprehensive data archive and suggestions for its application to remedial measures for civil-infrastructure systems,” Special Coordination Funds for Promoting Science and Technology, Ministry of Education, Culture, Sports, Science and Technology. One can find detail procedures for obtaining three orthogonal soil displacement components in their report of 2006.

East-West components of tectonic deformation are plotted on a satellite image of the Mid Niigata area (**Fig. 3.18(a)**). In **Fig. 3.18(a)**, the Uono river after flowing straight west through a flat wide spread valley of Horinouchi, hits the sedimentary silty sand rock ridge of Cenozoic Era, and changes abruptly its direction, from SE-NW to NE-SW, along this rock ridge making a sharp down-folded bend. The Uono river then forces its way through the narrow and lowest points among the mountains making a sharp up-folded bend there. The about 2 km-long stretch of the Uono river between these two bends and Kodaka syncline are found on the direct extension of Kajigane syncline, which dies out on the geological map (Yanagisawa et al, 1986) immediately before reaching them. It is noted that there is a NNE-SSW trending belt of large eastward tectonic movements west along this Kajigane syncline, and Uonuma Tunnel crosses this Kajigane syncline.

North-South components of the soil displacements shown in **Fig. 3.18(b)** were in general much smaller than the East-West components, which fact is consistent with the general trend of the tectonic movement: the movement has been responsible for the active folding structure in the target zone.

It is remarkable there are two areas in the target zone, which have been risen up by 0.5 to 1.5 meters (**Fig. 3.18(c)**). The presence of these two humps in the target area is also suggested by the records from GPS stations arranged in a regular 40km×40km sparse square net. The most remarkable hump spreads wide across Kawaguchi town and Budokubo area where the Uono river flows in the Shinano river. It is noted that some areas along the upper reach of the Uono river was flooded in a heavy rain of

June 27-28, 2005, about 8 months after the earthquake (**Fig. 3.18(c)**). The Cause-and-effect relation between the earthquake-induced tectonic deformation and the flooding of June, 2005, is now being discussed among the authors taskforce, and will appear in future publications.

Tunnel and damage description

The 8625 meter long concrete tunnel was constructed with the New Austrian Tunnelling Method passing through the damaged location at a depth of 60-100 meter as interpreted from **Fig. 3.19**. **Fig. 3.19** indicates an extreme amount of leakage (200 liter/min) during the construction time. **Fig. 3.20 (a)** and **3.20(b)** show an original tunnel section and the damage location. A diagonal crack running from the south part to the central of the damaged area is marked with an orange line. The spalling of concrete block is seen in the background. A close up of the cracks are given in **Fig. 3.20(c)** and **20(d)**. With the help of tripod a crack development photos was also taken; the result is shown in **Fig. 21**. The south part of the damaged area is to the right in the figure and the central part to the left. The northern part of the damaged area has lighter damage and the rail foundation is not deformed as much as in the south part (see **Fig. 3.22**).

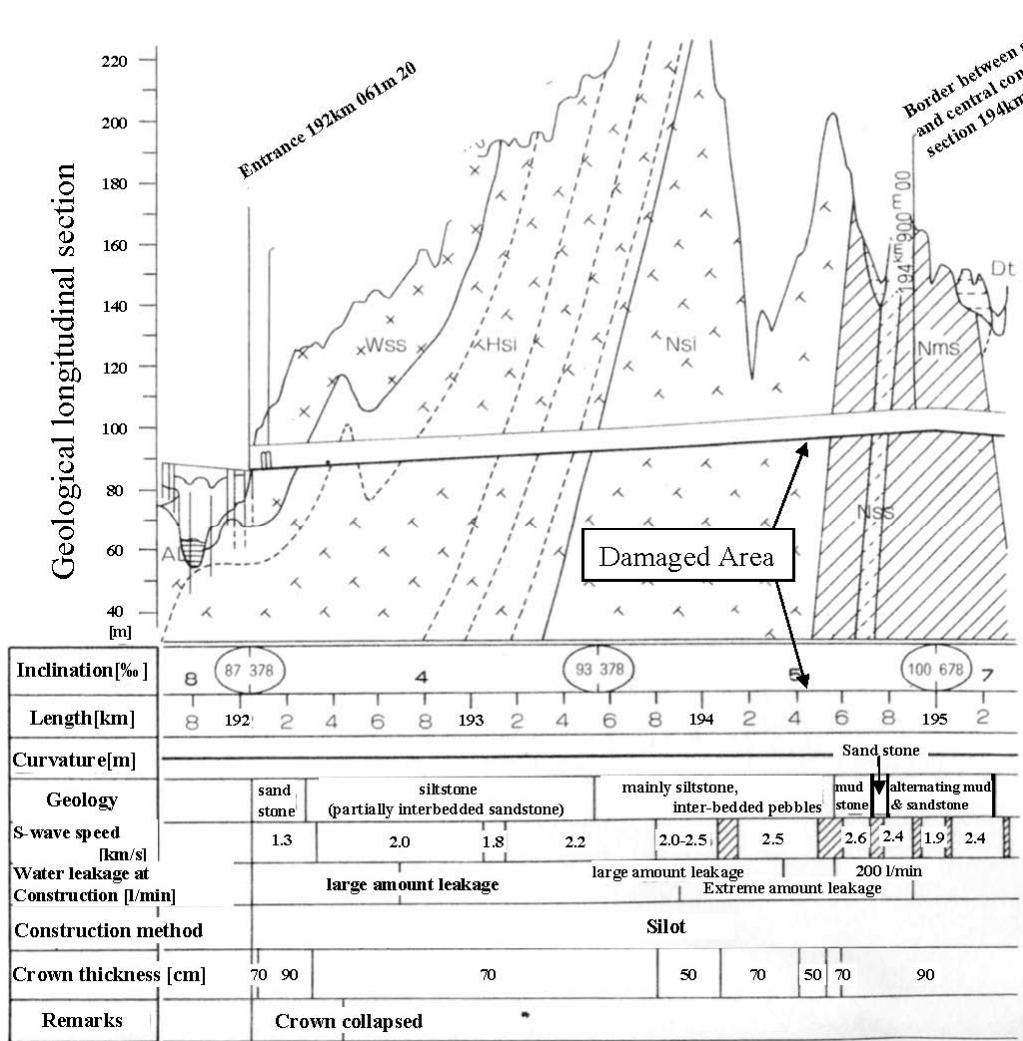


Fig. 3.19: Geological longitudinal section for the southern construction section



Fig. 3.20: a) Original section. b) Crack crossing the tunnel: white colored line. Top of rail is indicated by white arrows c) and d) Close up of cracks.

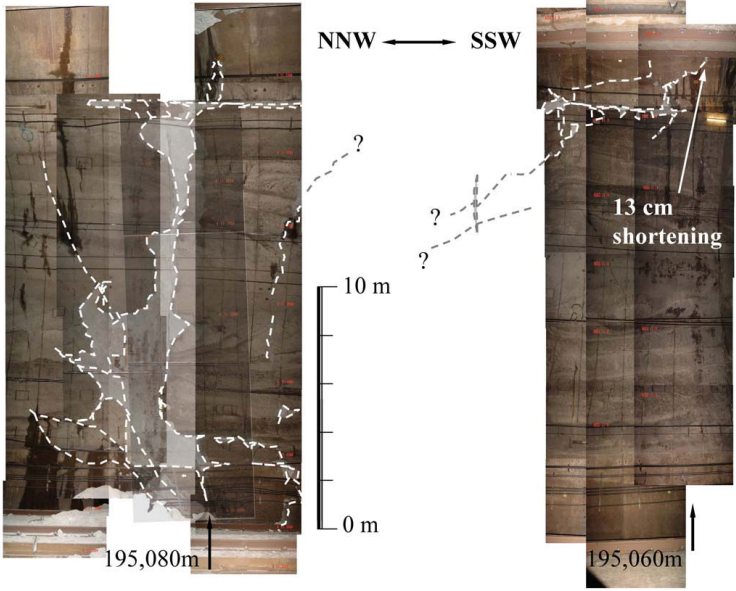


Fig. 3.21: Lining crack development of Uonuma tunnel. White dashed lines indicates crack location and shaded areas show spalling.

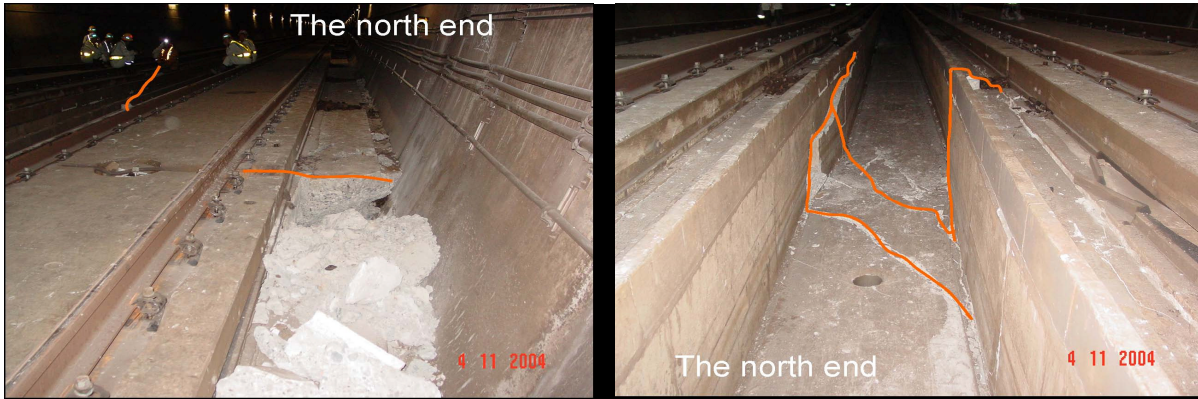


Figure 3.22: a) Cracks in the northern end of the damage area. b) close up of crack between rails (upper left corner of figure a).

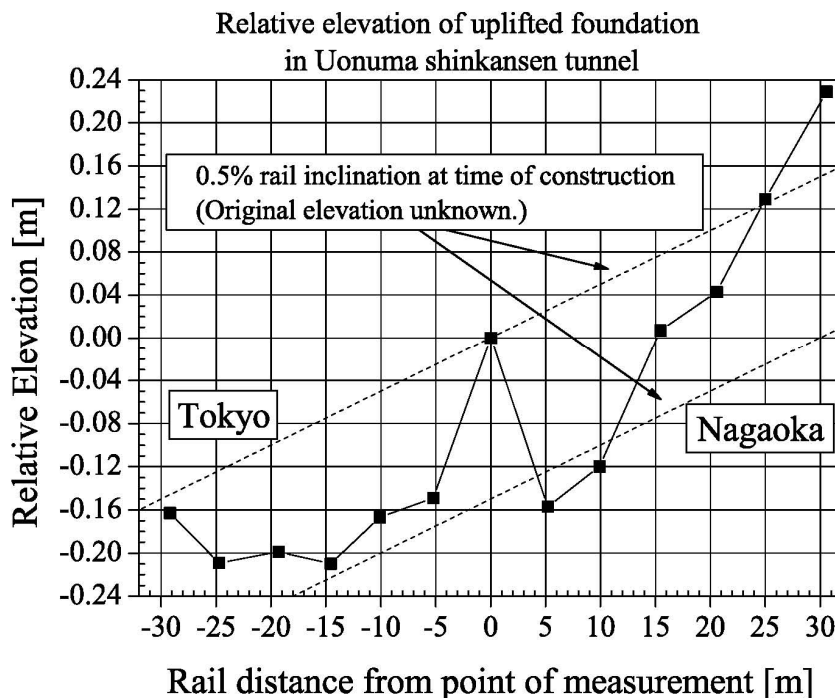
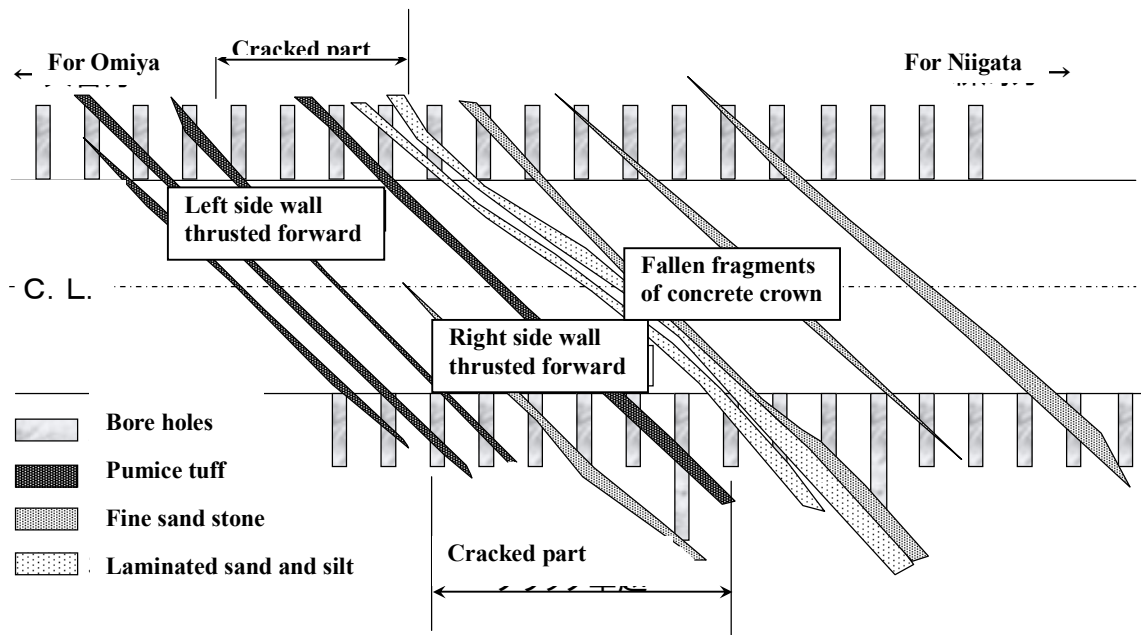


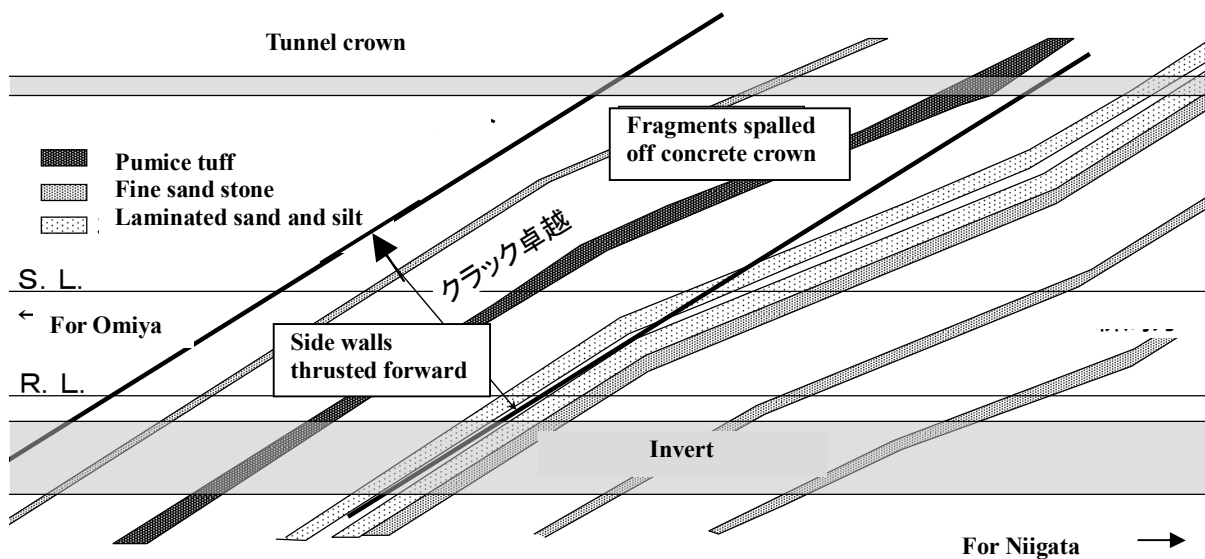
Fig. 3.23: Relative elevation of left rail (facing Nagaoka) before and after earthquake some 15-20 meters south of downfallen concrete block.

Fig. 3.23 shows the relative elevation of the rail measured with the help of laser range meter, which was put on the highest point in the southern end of the damage area some 15-20 meters south of downfallen concrete block (approximately in the middle of **Fig. 3.21**) (The original elevation is unknown.) The buckling deformation of the rail foundation is clear from the graph. Between 0 and 5 meters there is a maximum vertical difference of 18cm compared to the 2 cm difference due to the 5% inclination at the time of construction.

Due to the tunnel depth at the damage location the shallow landslides above the tunnel could not have caused the damage. Most likely the tunnel was damaged due to a combination of minor slips on laminated sedimentary rocks crossing the tunnel (See **Fig. 3.24**) and the overall axial compression due to movements on other nearby hidden faults within a belt along Kajigane syncline, which belt was shifted east as shown in **Fig. 3.18(a)**.



(a) Plan of the damaged section



(a) Elevation of the damaged section

Fig. 3.24: Estimated rock profile behind tunnel lining (JR East, 2006)

Similar damage has also been reported in the Myouken tunnel (1459 meter long). Another railway tunnel to the south of the Uonuma tunnel, the Wanazu tunnel suffered severe damage as well with diagonal cracks, collapsed crown and buckling of its rail at the north mouth.

3.7 BERKELEY-HILL BART TUNNEL*

Location: 37° 51'04"N, 127° 14'16"W

Earthquake: Cracking is due to continuous creeping movement of the Hayward fault.

BART Contra Costa line (C line) leading to Pittsburg bores through the rock of "Barkeley-hill" east of Berkeley (**Fig. 3.25**). The Hayward fault bisects this BART tunnel about 300 m inside from the west entrance. There was a debate erupted when USGS issued a press release indicating potential for damage to structures along the Hayward fault. BART has carried out careful alignment surveys of the tunnels since their completion in 1968. The extensometer measurements were continued in the fault zones and eventually, it was found that the total 80 mm dislocation due to the right-lateral strike slip had been built up over 10 years (1971-1980) in the north tunnel; There are 2 bores, each about 22 feet in diameter, spaced 50 feet apart and linked with pedestrian cross-tunnels at a regular interval of 1000 feet for emergency evacuation. By that time (1979) low angle cracks were visible on the lining of the tunnels, suggesting the compressional force along the tunnel axis (**Fig. 3.27**).

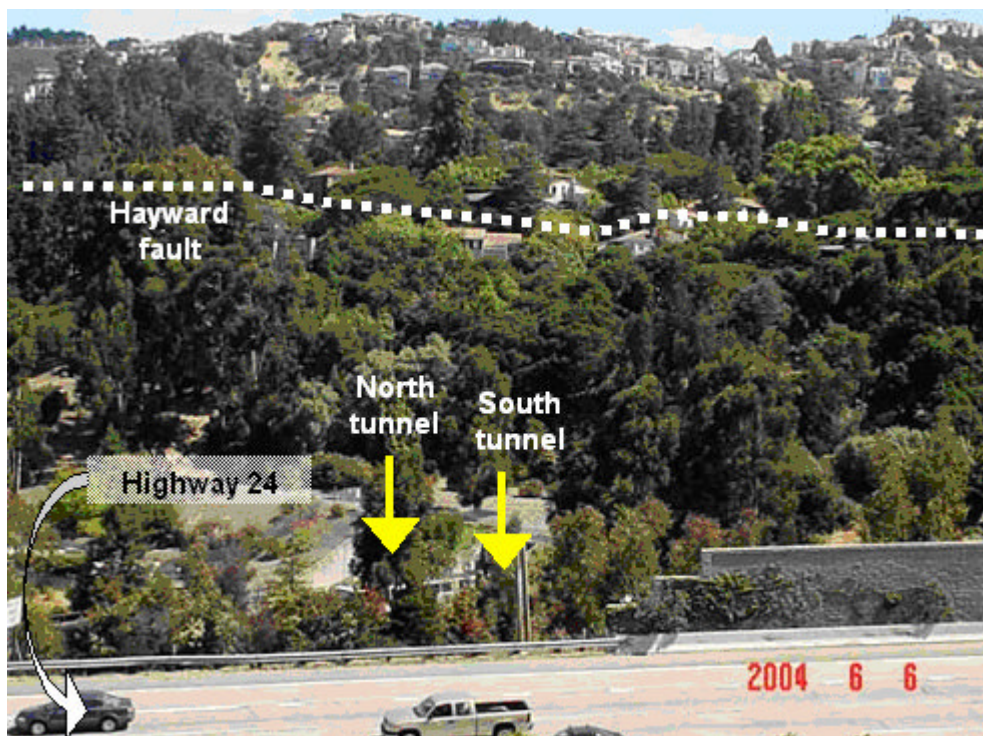


Fig. 3.25: West tunnel mouths of Barkeley-hill BART Tunnel

* The greater part of the following description is based on "BART TUNNEL" by David Rogers in "Engineering for surface ground rupture on the Hayward fault" by Glenn Borchardt et al, AEG/GRA 2000 Field Trip Guidebook.

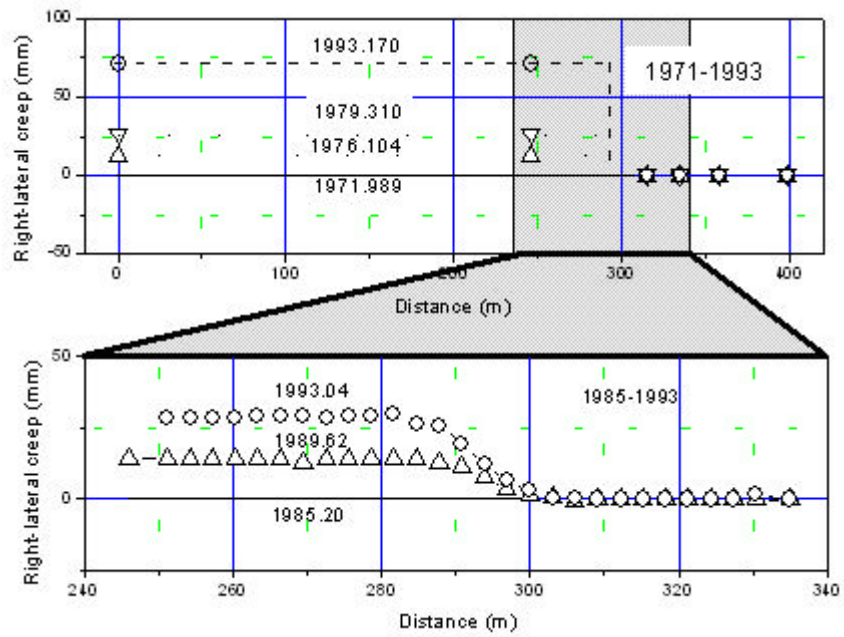


Fig. 3.26: Steady change in tunnel alignment

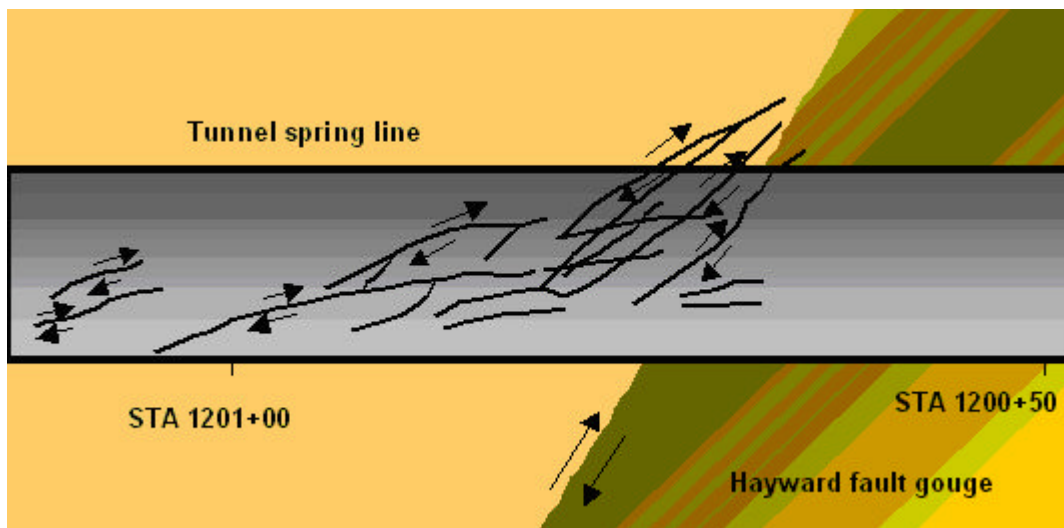


Fig. 3.27: Low angle cracks appearing on the tunnel lining.

3.8 BOLU TUNNEL CONSTRUCTION, after Atlas Copco (2003)

Location: 40°45'18"N, 31°27'04"E

Earthquake: August 17, 1999, Izmit Earthquake, Turkey, M=7.4

The uncompleted part of the Bolu tunnel in Turkey was heavily damaged during the Duzce earthquake in 1999. Reconstruction included the crossing of two active faults the Bakacak (40° dip-angle) and the Zekidagi (90° dip-angle.) Future possible displacement along the faults 0.15-0.25m for the Zekidagi fault in an earthquake of magnitude 6 to 6.25 and 0.5 m for the Bakacak fault which is identified as a secondary fault in the step-over region between the two major North Anatolian fault branches in the Bolu region. Two likely traces of the Bakacak fault crosses the tunnel over a width of about 100 m which is the zone where excavation was proceeding when the earthquake occurred.

Two construction strategies were considered for crossing the Bakacak

- Over-excavation: A double lining filled with porous material such as foam concrete is installed in an enlarged cross section. This technique is believed to be most effective when the rupture is concentrated a few meter wide zone.
- Articulated design: The width of the lining segments are reduced leaving independent sections over zone wider than the expected rupture zone. The movement is concentrated at the segment joints restricting the damage to a few elements. The maximum length of any single element depends on several factors, such as width of the cross section, expected movement of the fault, compressibility of the surrounding soil, and element kinematics.

For the Bolu tunnel the second strategy was selected. In case of fault movement the tunnel acts longitudinally as an embedded beam whose ends are displaced laterally. Justified by the geologists it is assumed that a rupture will be uniformly distributed across the fault boundaries and thus the shear strain is assumed as the ratio between offset and width of the fault at tunnel level. The tunnel is sheared and bent by the soil as a beam until the 50 cm wide joint's shear resistance is reached, after which the 4.4 meter long and 60 cm thick segments moves freely and independently following the external loads by surrounding soil. At the fault zone and 30 meters outside it extra reinforcement has been installed in the inner lining to increase the ductility.

Dalgic (2002}, Brox and Hagedorn (999) provide more detailed descriptions this case history.

REFERENCES

- Atlas Copco (2003), Seismic tunnelling at bolu.
<http://www.tunnelbuilder.com/rockreinforcement/edition2pdf/page91.pdf>
- Azuma, T. Awata, Y., Yoshioka, T. and Fushimi, Y. (1999). "Trench excavation across Shinizaki Fault dislocated in the September 3, 1998, Mid-North Iwate Earthquake," Annual Report of Active Fault Research Center, AIST, 19-27.
- Brown, I.R., Brekke, T.R., (1981). "Behavior of the Bay Area Rapid Transit tunnels through the Hayward fault," Final Report: Washington, DC, U.S. department of Transportation, Urban Mass Transportation Administration, 208p.
- Dalgic, S. (2002): "Tunneling in squeezing rock, the Bolu tunnel, Anatolian Motorway, Turkey," *Engineering Geology*, **67**, 73–96
- Hashimoto, S., Miwa, K., Ohashi, M. and Fuse, K. (1999). "Surface Soil Deformation and Tunnel Deformation caused by the September 3, 1998, Mid-North Iwate Earthquake," 7th Tohoku Regional Convention, Japan Society of Engineering Geology.
- Konagai, K., Mikami, A., Katagiri, T., Ahsan, R. and Maruyama, D. (1999). "Report of damage caused by the Mid-North Iwate Earthquake of September 3, 1998," *Bull., Earthquake Resistant Structure Research Center, IIS, University of Tokyo*, **32**, 3-13.
- Konagai, K., Numada, M., Zafeirakos, A., Johansson, J. Sadr, A. and Katagiri, T. (2005a). "An example of landslide-inflicted damage to tunnel in the 2004 Mid-Niigata Prefecture earthquake," *Landslides* **2(2)**, pp. 159-163.
- Konagai, K., Johansson, J., Zafeirakos, A., Numada, A. and Sadr, A. (2005b). "Damage to tunnels in the October 23, 2004 CHUETSU earthquake," *JSCE Journal of Earthquake Engineering*, **28**, 75-127.
- Konagai, K., Johansson, J., Zafeirakos, A., Numada, A. and Sadr, A. and Katagiri, T. (2005c) "Geotechnical hazard for civil-infrastructures in the October 23, 2004, Niigata Chuetsu Earthquake, Japan," *Bull., ERS*, **38**, 3-18.
- Konagai, K. et al. (2007). "Annual Report of the Research and Development program for Resolving Critical Issues, "Earthquake damage in active-folding areas: creation of a comprehensive data archive and suggestions for its application to remedial measures for civil-infrastructure systems," Special Coordination Funds for Promoting Science and Technology, Ministry of Education, Culture, Sports, Science and Technology."
- Rogers, D., BART Tunnel, in "Engineering for surface ground rupture on the Hayward fault" by Glenn Borchardt et al., AEG/GRA 2000 Field Trip Guidebook.
- Ueta, K., Miyakoshi, K. and Inoue, D. (2001): "Left-lateral deformation of head-race tunnel associated with the 2000 western tottori earthquake," *Journal of the Seismological Society of Japan*, **54(2)**, 547–556.
- Yanagisawa, Y., Kobayashi, I., Takeuchi, K., Takeishi, M., Chihara K. and Kato H. (1986). "Geology of the Ojiya District, Quadrangle Series Scale 1:50,000." Niigata (7), No. 50, Geological Survey of Japan.
- Yoshikawa, K. (1979). "Examples of damage to railway tunnels," *RTRI Report*, **1123 (497)**.

Chapter 4

DAMAGE TO DAMS

4.1 SHIHKANG DAM

Location: 23° 54'02"N, 120° 42'21"E

Earthquake: Sept. 23, 1999, ChiChi Earthquake, Taiwan, M=7.6

A large earthquake of local magnitude 7.3 (moment magnitude 7.6) struck the west-central Taiwan September 21, 1999. The epicenter was located close to the city Chi-Chi at latitude 23.85°N and longitude 120.81°E with a very shallow hypo center at about 7 km depth. **Fig. 4.1** shows the main shock and aftershocks distribution. It is the largest in-land earthquake and the most destructive to hit Taiwan in over hundred years. In this devastating earthquake, a total of 2,450 lives were lost, some 10,000 people were injured, more than 100,000 buildings suffered various levels of damages, and numerous infrastructures, lifelines and facilities were severely damaged. Among the most extraordinary phenomena during this earthquake were the extremely large displacement of the fault ruptures along the 105-km long activated fault. The earthquake that originated at a shallow focus produced spectacular reverse faulting. The fault seems to have appeared exactly along the CheLungPu Fault, whose presence had been already recognized. Hence, the activated fault, in this chapter hereafter, will be referred to as the CheLungPu Fault. The activated fault, however, appeared branching east off the recognized trace of the CheLungPu in the vicinity of Feng-Yuan City, and crossed the Shih-Kang area. Zooming in on this area, it is found that this branch also shoots out further thinner separate branches. Some details of this area will be given later on. **Fig. 4.2** shows dislocation vectors along the CheLungPu Fault (Otsuki, 1999). The different diameters of gray circles show the extent of vertical offsets, and arrows represent net slips. The offsets, in general, increase as we go north, and the maximum net offset of 13.5m is reached at Point 10, the second largest net offset of 11.1m at Point 12. **Fig. 4.3** shows elevation increments measured over 7 km distance in ChunShinHin town across the fault. The eastern side of the fault seems to have been continuously pushed up, which might be interpreted as an early sign of the event.

The mechanical properties of the soil overlying uplifted bedrock due to a fault offset greatly affects how the deformations are distributed and thus changes the width of the affected zone. **Fig. 4.5** shows how a sharp offset was induced in the stiff soil/rock next to the Bei-Fong bridge and the smooth distribution of the soil deformation at a cemetery west of the Shih-Kang town. A more ductile soil distributes the soil deformation; Chen et. al. (2001) measured vertical and horizontal deformations along the freeway route 3.

Chia et. al. (2001) reported changes in water levels in different locations on the foot wall side of the Chelungpu fault. In a 5 to 7 km wide area next to the fault co-seismic water level fell and at a greater distance 10 to 50 km water level rose. It seems that on a larger scale that the foot wall side underwent compression and next to the fault extension.

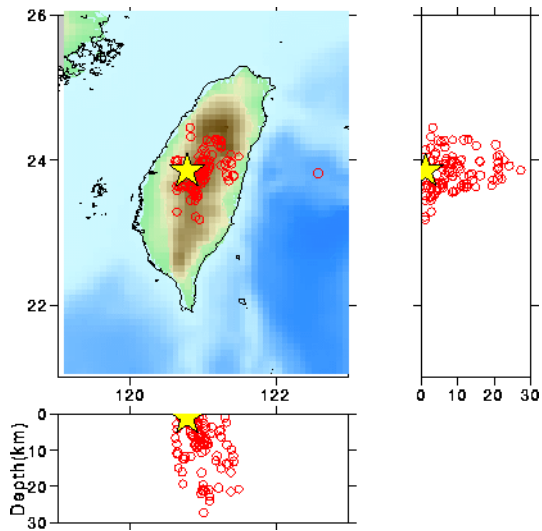


Fig. 4.1 Aftershocks distribution of the Sept. 23, 1999 ChiChi Earthquake, Taiwan
<http://www.eri.u-tokyo.ac.jp/topics/taiwan/yoshin2e.html>

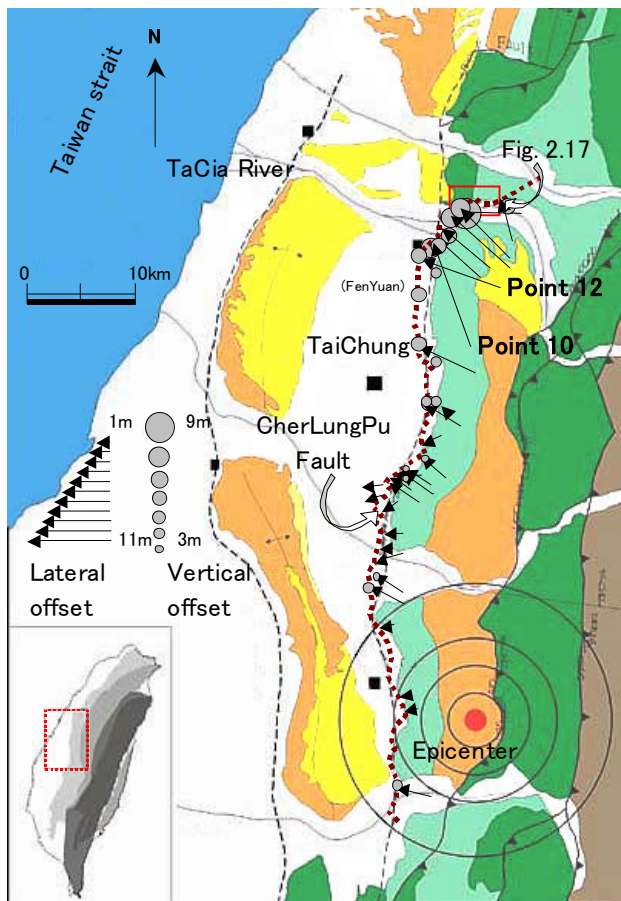


Fig. 4.2. Dislocations along Chelungpu fault (Otsuki and Yang, 2000)

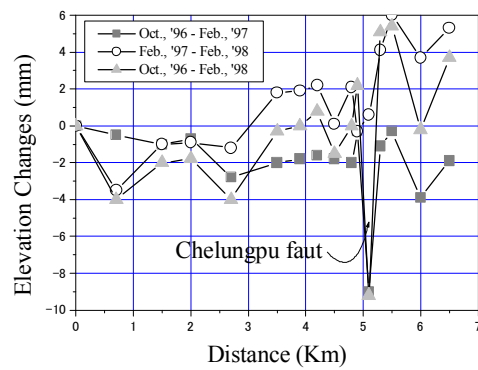


Fig. 4.3: Elevation increments measured over 7 km distance in Chunshinhin town

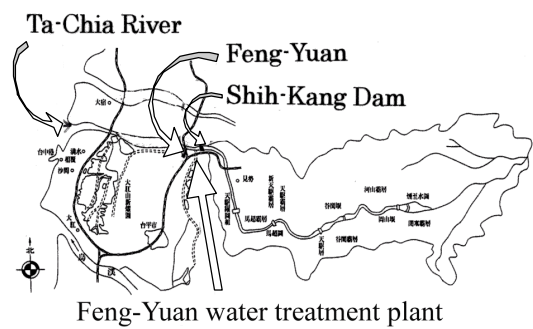


Fig. 4.4: Ta-Chia River

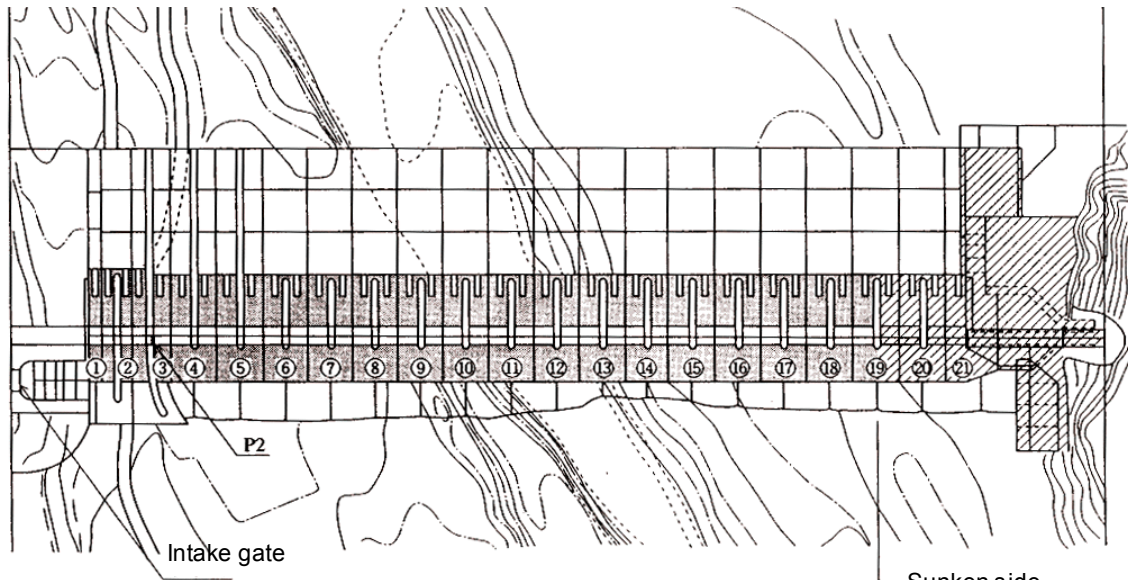


Fig. 4.5: (a) stiff soil/rock next to Bei-Fong bridge, and (b) cemetery west of Shih-Kang with soft soil deposit.

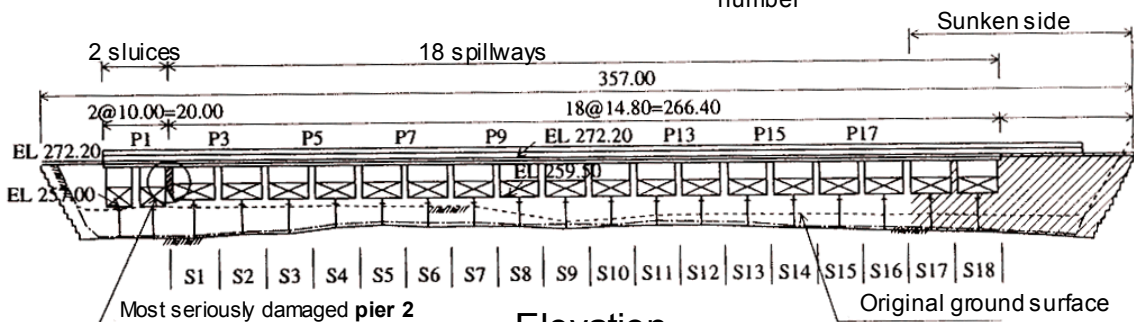
Shih-Kang Dam was built across the Ta-Chia river where the river's fan-shaped plain begins to spread gradually towards the East China Sea (**Fig. 4.4**). The dam site lies over a shallow sandy and gravelly soil deposit spreading over a laminated mass of mud stone, silt stone and sand stone of the Pliocene Epoch, Tertiary Period. The construction of the dam began with the excavation of this shallow sandy and gravelly soil deposit down to the underlying rock surface, and was completed in 1977.

The Shih-Kang Dam, 25 m tall and 357 m long with 18 gates lined up, has a total concrete bulk of 141,300 m³ (**Fig. 4.6**). The reservoir with a capacity of 3.38 million m³ collects water from a catchment area of 1,061 km² in the Chung-Yang Mountains, and provides a steady supply of water for irrigation, etc. An intake tunnel on the left abutment of the dam leads the water through a diluvial terrace down to the Feng-Yuan water-treatment plant.

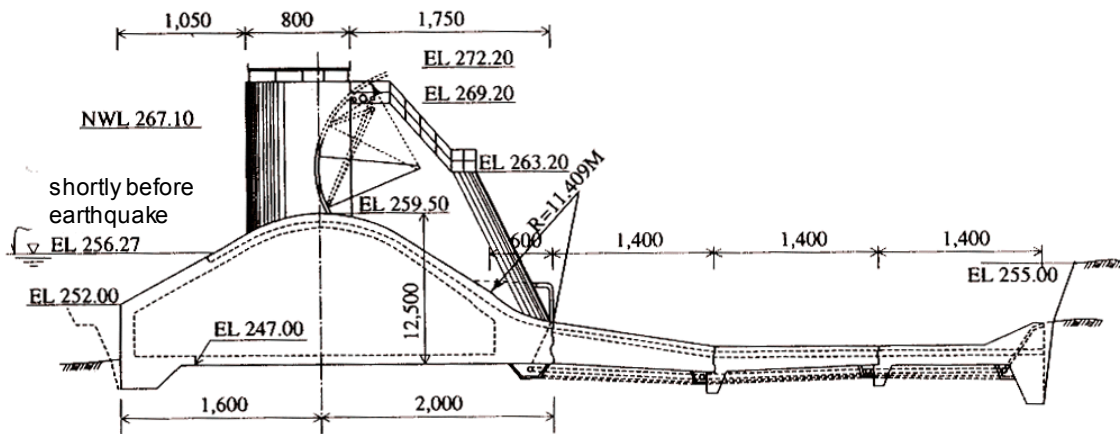
The construction of the dam was preceded by some necessary geological investigations. The contours in **Fig. 4.6 (above)** describe the configuration of the base rock of the Tertiary period overlaid with sands, gravels and other suspended matters that the Ta-Chia river has carried over centuries. **Fig. 4.6 (middle)** shows that the base rock surface is quite shallow in the middle of the river bed, 3 to 4 m below the soil surface, and reaches 10 to 13 m depths on both sides. These sedimentary base rocks of the Tertiary period can be recognized from their stratified features. The strata of these rocks run, in general, in about N40°E-40°S direction, and meet the dam axis at an angle of 60 degrees. The strata planes have a dip of about 40 degrees down towards southwest. Hammer blows on these rocks do not create any sharp sounds, suggesting that the compressive strengths of the rocks are some 100 kgf/cm² or less. When the base rocks were exposed after the excavation for constructing this dam, no clear evidence of the presence of a fault was found (Water Resources Bureau, Ministry of Economic Affairs, Taiwan).



Plan ①~⑳:Block number



Elevation



Spillway

Fig. 4.6: Shih-Kang Dam

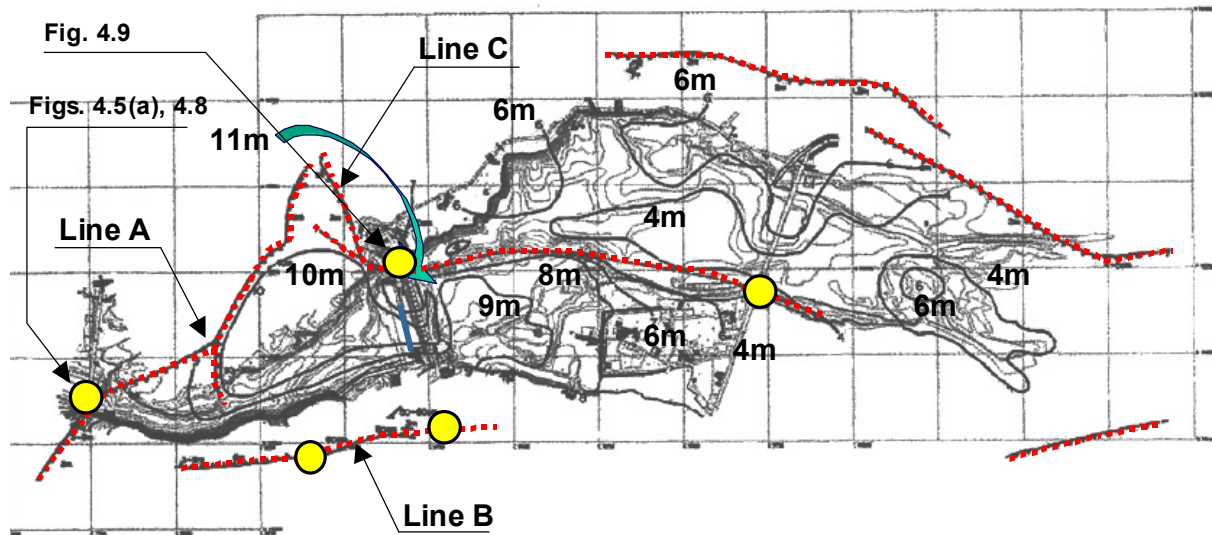


Fig. 4.7: Ground upheaval in ShihKang area (After Kung, C.S., 2001): Thin and thick contour lines show the original configuration and ground upheaval caused by faulting.



Fig. 4.8: Bei-Fong bridge and fault-created Waterfall



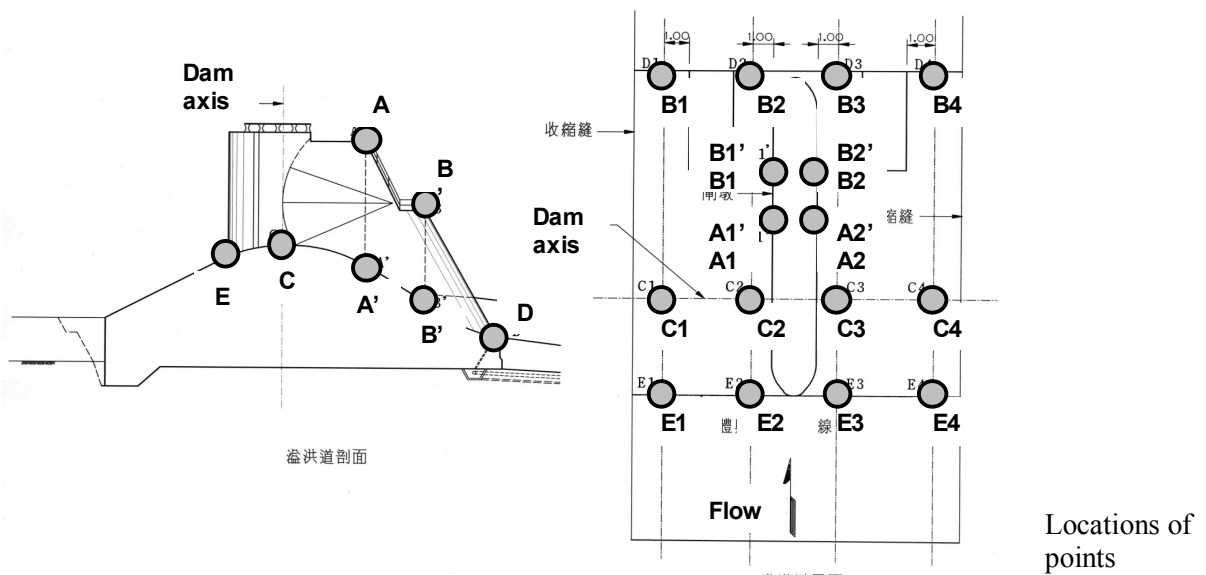
Fig. 4.9: Broken spillways of ShihKang dam

As has been mentioned, the fault rupture planes appeared branching east off the recognized trace of the CheLungPu fault in the vicinity of Feng-Yuan City, and crossed the Shih-Kang area. The complicated features of this fault rupture emerge as one zooms in on the Shih-Kang area. Thick contour lines in **Fig. 4.7** show the ground upheaval in ShihKang. In this figure, line *A* forms a part of the northeast extension of the CheLungPu Fault. Line *A* crossed the Ta-Chia river near the Bei-Fon bridge, where the southeast side of the fault rose up by about 6 m with respect to the other side, causing a water fall to appear (**Fig. 4.8**). This line, however, dies out as it climbs the north hillside, and another line, *C*, appears abruptly several of hundred meters east off Line *A*. Line *C* crossed the northern end of the Shih-Kang dam causing three spillways of the Shih-Kang dam (No. 16-18) to be destroyed (**Fig. 4.9**). The vertical offset of 10-11 m was reached at this point.

As was shown in **Fig. 4.6**, the dam is made up of 21 blocks whose numbers are put in circles in **Fig. 4.6 (top)**. A pier sticks upright in the middle of a block, and a pair of blocks put side by side forms a spillway or a sluice. As is illustrated in **Fig. 4.6 (bottom)**, all 18 spillways are equal in their cross-sections; 12.5m high and 36m wide of bulk concrete. There are two sluices on the left side of the dam.

Table 4.1: Elevations of points on dam body (unit: m)

No.	EL of SL2	EL of SP1	EL of SP2	EL of SP3	EL of SP4	EL of SP5	EL of SP6	EL of SP7	EL of SP8	EL of SP9	EL of SP10	EL of SP11	EL of SP12	EL of SP13	EL of SP14	EL of SP15
A1	280.74	280.83	280.98	281.13	281.25	281.34	281.45	281.57	281.63	281.67	281.7	281.76	281.71	281.68	281.69	281.64
A1'	266.08	268.44	268.46	268.44	268.29	268.96	268.91	269.07	269.15	269.08	269.2	269.07	269.11	269.21	269.08	269.1
A2	280.4	280.45	280.6	280.73	280.88	281	280.1	281.22	281.34	281.4	281.45	281.45	281.51	281.47	281.44	281.41
A2'	268.29	268.45	268.46	268.55	268.82	268.94	268.99	269.1	269.08	269.23	269.25	269.17	269.09	269.13	269.25	269.14
B1	273.65	273.83	273.94	274.08	274.18	274.34	274.48	274.57	274.71	274.74	274.77	274.78	274.76	274.78	274.75	274.73
B1'	263.61	265.47	265.81	265.97	266.06	266.14	266.33	266.19	266.39	266.7	266.66	266.63	266.69	266.79	266.81	266.63
B2	273.67	273.82	273.94	274.07	274.2	274.34	274.5	274.6	274.72	274.76	274.76	274.77	274.79	274.78	274.75	274.79
B2'	265.77	265.77	265.84	265.98	266.09	266.27	266.13	266.43	266.86	266.62	266.77	266.73	266.26	266.74	266.93	266.68
C1	267.47	270.06	270.25	270.39	270.47	270.6	270.73	270.54	270.61	270.63	270.64	270.65	270.61	270.6	270.59	270.81
C2	267.54	270.07	270.3	270.43	270.49	270.64	270.75	270.56	270.62	270.63	270.65	270.66	270.6	270.59	270.59	270.84
C3		270.21	270.29	270.44	270.55	270.67	270.75	270.61	270.61	270.62	270.66	270.66	270.62	270.59	270.58	271
C4		270.23	270.34	270.45	270.57	270.7	270.78	270.61	270.63	270.66	270.65	270.63	270.6	270.57	270.55	271.43
D1	259.9	260.71	260.91	261.11	261.17	261.35	261.43	261.66	261.71	261.55	261.65	261.7	261.72	261.72	261.7	261.68
D2	259.64	260.74	260.97	261.06	261.19	261.36	261.53	261.69	261.73	261.59	261.7	261.68	261.75	261.73	261.72	261.67
D3		260.81	261.06	261.14	261.25	261.42	261.6	261.69	261.76	261.61	261.65	261.7	261.71	261.75	261.67	261.67
D4		260.91	261.11	261.14	261.32	261.42	261.56	261.76	261.82	261.65	261.65	261.7	261.73	261.72	261.7	261.7
E1		268.73	268.94	268.95	269.25	269.28	269.29	269.44	269.52	269.47	269.43	269.48	269.4	269.42	269.38	269.37
E2		268.68	268.94	269.04	269.08	269.28	269.29	269.54	269.52	269.49	269.46	269.44	269.37	269.39	269.37	269.36
E3		268.79	268.95	269.08	269.1	269.22	269.32	269.51	269.45	269.5	269.47	269.41	269.4	269.37	269.39	269.25
E4		268.84	268.81	269.01	269.14	269.18	269.24	269.49	269.49	269.48	269.46	269.43	269.41	269.39	269.36	269.25



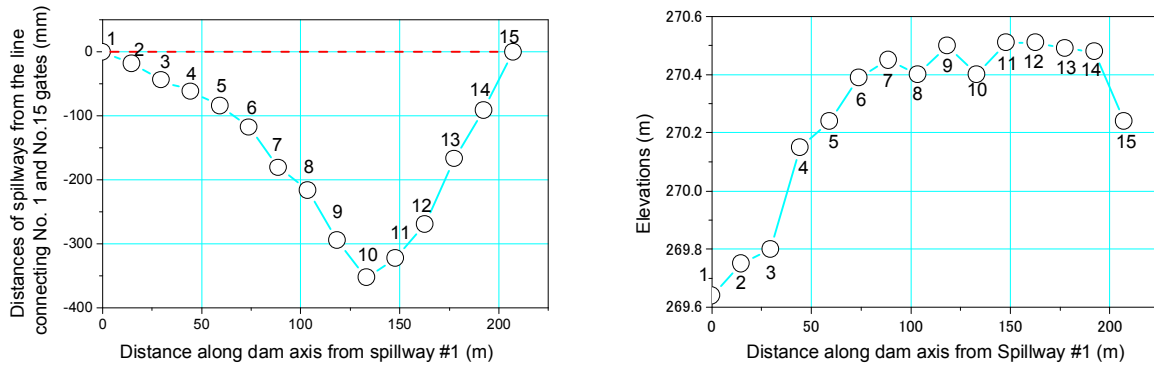


Fig. 4.10: Deformation of dam body along its axis

Kung (2001) measured elevations of total 312 points on the dam body (**Table 4.1**). **Fig. 4.10** shows the deformation of dam body along its axis measured shortly after the earthquake. Horizontal distances of spillways were measured from the line connecting Spillways #1 and #15. Though the vertical elevations are not completely identical with those (C points) listed in Table 2.2, the deformation pattern in **Fig. 4.10** and that from Table 2.2 (Kung, 2002) are about the same in shape and size. The entire dam body thus seems to have been warped both upward and towards upstream side.

Sugimura, Y. and Jyh, (Sugimura, 1999, Konagai et al., 2000) mapped cracks that appeared on the dam body (**Fig. 4.11**). Cracks excluded from the figure include those lying under water, the upstream slopes of spillways behind gates, and spillways with their gates open. The seriously and/or completely destroyed spillways #16-18 were also excluded from this mapping. Major cracks on spillways were found between spillways #6 and #16, namely on blocks ⑧-⑱. In general, diagonal cracks were found on most damaged spillways, and transverse joints between blocks were opened in such a way that the openings on the upstream side were wider than those on the downstream side.

Diagonal cracks on blocks ⑨, ⑩, ⑪, ⑫, ⑭, ⑯, ⑰ and ⑱ reach the piers, and the crack on Block ⑪ further extends diagonally up through Pier 10 (see **Fig. 4.12(e)**). The largest crack openings of 20 mm, 8mm and 40 mm are reached on Block ⑪, Pier 10 and the block joint between ⑩ and ⑪, respectively (see **Fig. 4.12(e)**).

Cracks along horizontal construction joints were found on four piers #9, #10, #15, #16 and #17. No major cracks were found on blocks more than 200 m away from fault C. In this less-damaged part also, Piers #1-#5 were found to be cracked. The cracks on Piers #1-#5, however, have some different features from those found on the piers closer to fault C. Some small fragments of concrete came off a jagged horizontal crack on the sluice-side wall of Pier #2 (**Fig. 4.12(b)**), and the rupture surface inferred from the cracks seems to run diagonally down through this pier to the other (spillway-side) wall of the pier. It is noted here that the concrete bulk of the sluice is 2.5m higher than the next spill way.

Upper construction joints of Piers #3 and #4 were cracked as illustrated in **Fig. 4.12(c)**. A crack that developed diagonally up through Pier #1 is illustrated in **Fig. 4.12(d)**, whereas the crack found on Pier #5 seems to have developed upright from a similar position.

Simply supported RC bridges span all spillways and sluices. They all came off their bearings. The cracks on the dam body caused 6 gates (5 for spillways and one for sluice) to be inoperable.

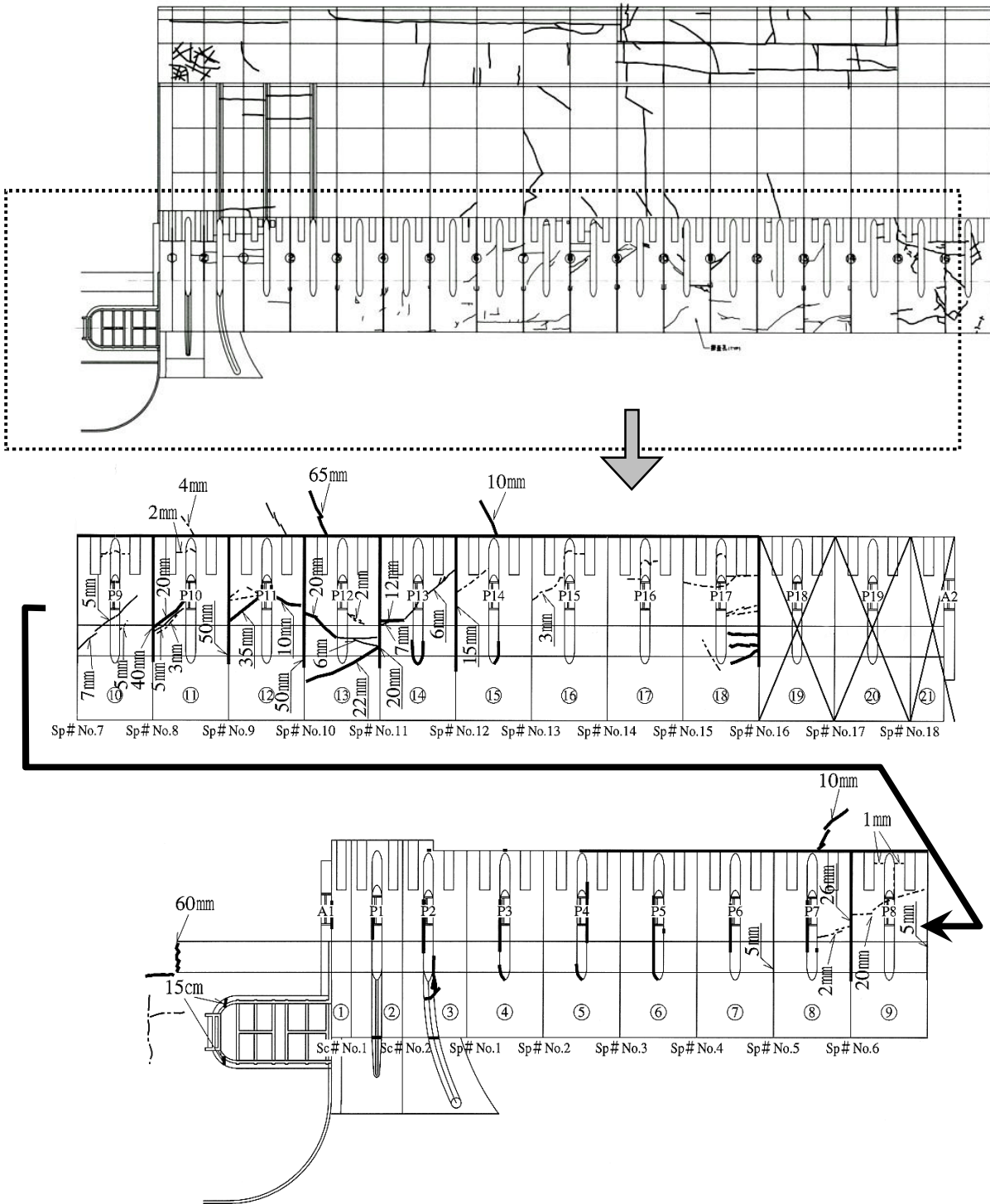
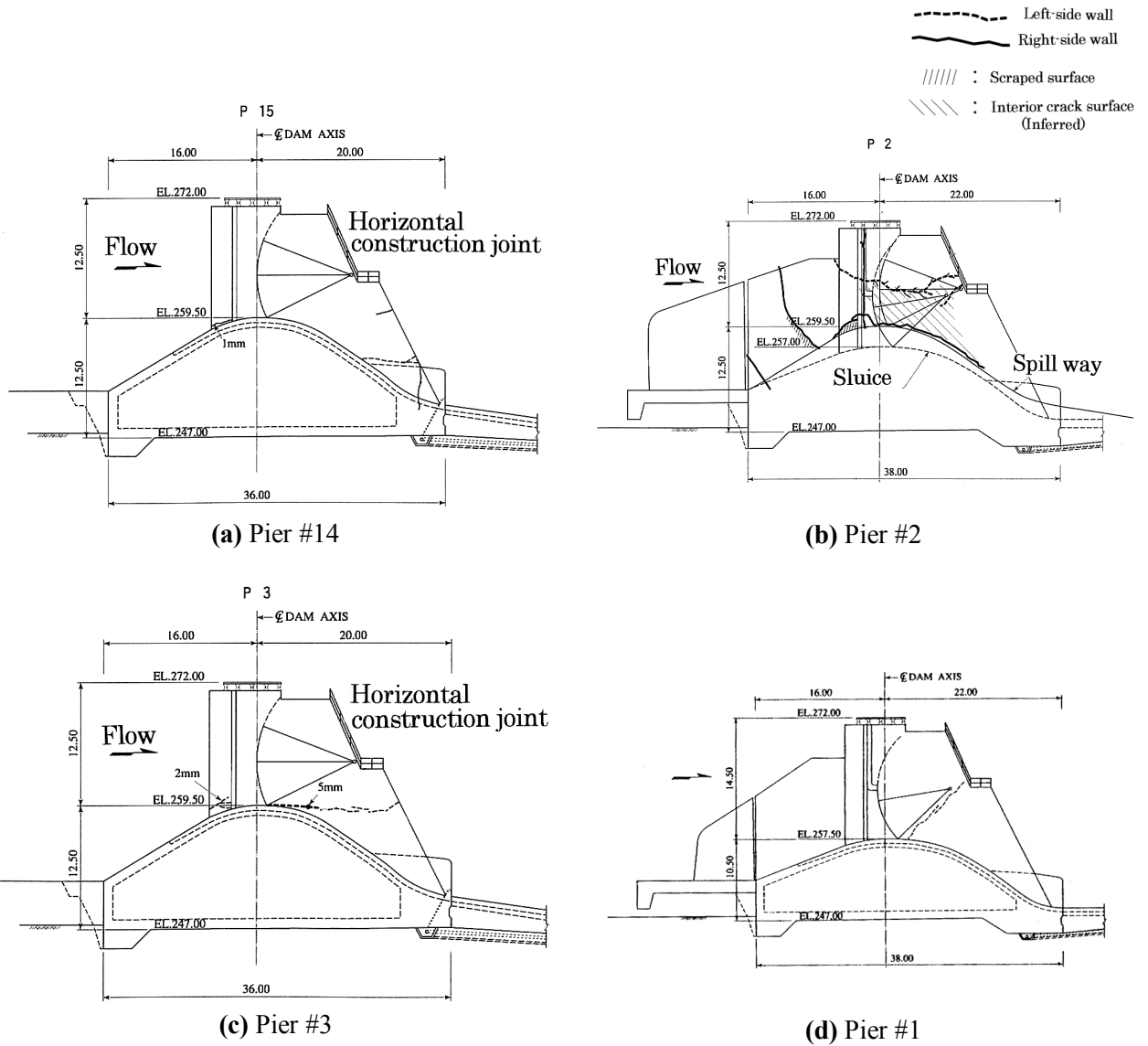


Fig. 4.11: Crack map of ShihKang dam (Sugimura et al, 1999)



(e) Cracks extending diagonally up through Pier #10



(f) Pier #2

Fig. 4.12: Cracks on dam piers

It is noted that the structure on the hanging wall side of the fault had suffered more serious cracking than the footwall side. Since the dam was constructed directly upon the base sedimentary rock mass, the pattern of cracks on the dam body might indicate how the base rock was deformed during the earthquake. Ground upheaval in Fig. 4.7 shows that the peak value (+11 m) of upheaval was reached near Line C on the hanging wall side, and this fact is consistent with both the deformation pattern shown in Fig. 4.10 and the crack pattern in Fig. 4.11.

However, the base rock deformation may not be the sole cause of the dam body deformation. It was an urgent task to restore the water supply function and to provide necessary flood control for the coming flood season. Therefore, grout injection was carried out for the remaining gates, preserving the completely damaged gates as a memorial park. Fig. 4.13 shows the variation with the axial distance of the volume of grout injected. A noticeable amount of grout was poured into hidden cracks in the right side of the dam body; this suggests that this part of the dam body may have come off the base sedimentary rock due to a large axial force induced in it. This may have made the upheaval of the dam body even more remarkable.

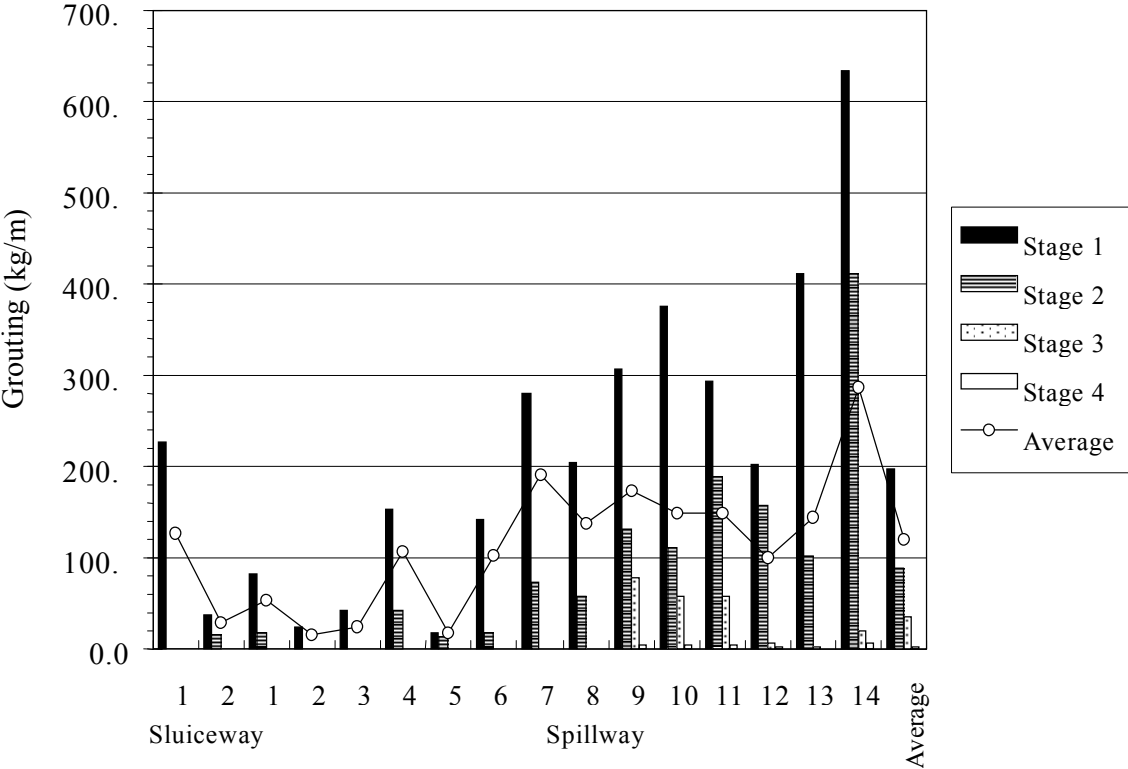


Fig. 4.13: Variation with the axial distance of the volume of grout injected (Kung, C.S., 2000)

REFERENCES

- Chia, Y., Yuan-Shian, Chiu, J. J. and Liu, C.-W. (2001): "Changes of groundwater level due to the 1999 chi-chi earthquake in the choshui river alluvial fan in taiwan," *Bulletin of the Seismological Society of America*, vol. 91, no. 5, pp. 1062–1068.
- Chen, Cheng-Hsing, Chow Hung-Sheng, Yang Chin-Yuan, Shieh Baih-Jung, and Kao Yao-Hung (2003) "Chelungpu fault inflicted damages of pile foundations on FWY Route 3 and fault zoning regulations in Taiwan," 2nd JSCE/EqTAP/JSPS Workshop on Seismic Fault-induced Failures, -- Possible Remedies for Damage to Urban Facilities --, Konagai, K. Hori, M. and Meguro. K. eds., Feb. 22, 2003, Inst. Of Industrial Science, University of Tokyo.
- Kung, C. S. (2001): "Damage andrehabilitation work of Shih-Kang Dam," *Seismic Fault-induced Failures; Possible Remedies for Damage to Urban Facilities*, Konagai, K., Hori, M. and Meguro, K. eds., JSPS Research Project 2000, Grant-in-Aid for Scientific Research (No. 12355020), 33-48.
- Otsuki, K. and Yang, C.N. (1999): <http://www.eprc.eri.u-tokyo.ac.jp/HANSHA/>
- Sugimura, Y., Miura, S. and Konagai, K. (2001): "Damage to Shih-Kang dam inflicted by faulting in the Sept. 1999, Chi-Chi Earthquake," *Seismic Fault-induced Failures; Possible Remedies for Damage to Urban Facilities*, Konagai, K., Hori, M. and Meguro, K. eds., JSPS Research Project 2000, Grant-in-Aid for Scientific Research (No. 12355020), 143-154.

Chapter 5

LANDSLIDES / LANDFORM CHANGES

5.1 TIGER HEAD HILL SLIDE, after Kamae, S. and Shuzui, H., 2002

Location: 24° 07'52"N, 120° 44'18"E

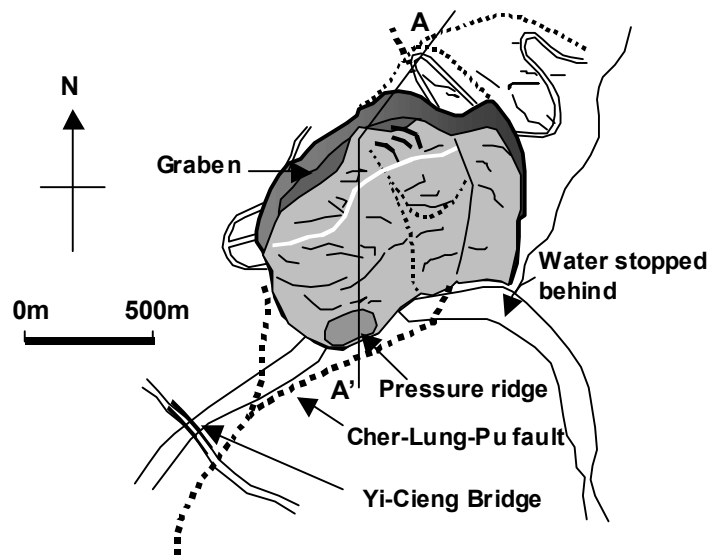
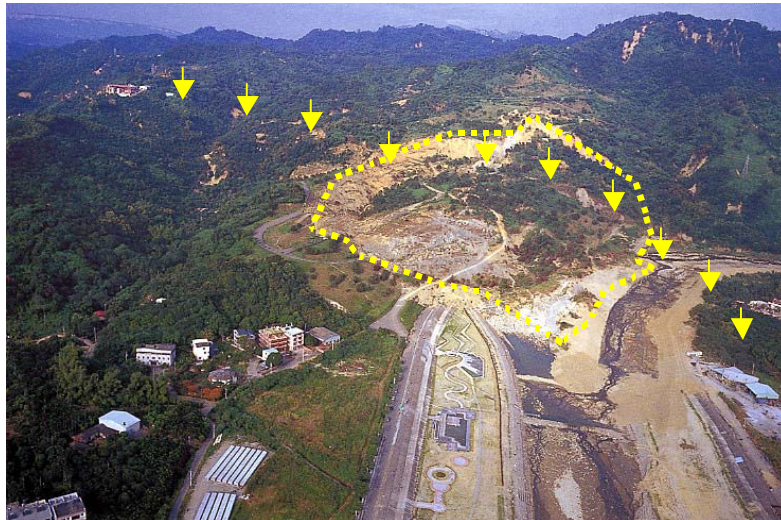
Earthquake: Sept. 23, 1999, ChiChi Earthquake, Taiwan, M=7.6

Landslides occur on a regular basis throughout the world as part of the ongoing evolution of surface configurations (Kramer S., 1994). They are mostly due to heavy precipitations, and about 1000 landslides are triggered every year in Japan. However, when landslide-prone zones were superimposed on a seismic fault map, one can recognize that many landslides are found scattered along active fault traces. Intense ground shakes must have been responsible for these landslides, but we should not forget that fault dislocations could cause landslides. An example follows.

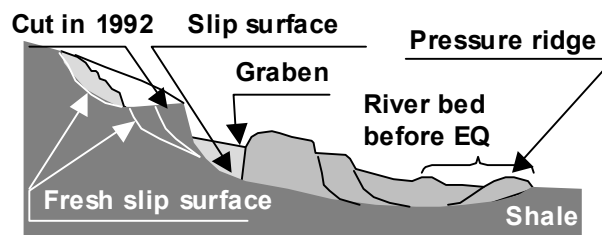
Cher-Lung-Pu fault winds along eastern hillsides in Tai-Chung County, and shoots branches where it reaches Tou-Bien Creek (**Fig. 5.1**). Some of these branches crossed Yi-Chiang Bridge causing collapse of its western spans. The main fault rupture, after going another 700 m along the east bank of Tou-Bien-Kun Creek, crossed the river and hit the slope of Tiger Head Hill. A slow and steady motion of the soil has been observed since 1992, the time when the top part of the hillside was cut flat for developing a residential area. Tiger Head Hill is geologically made up of Jin-Shui Shale bedrock dipping southeast. Debris of about 10m thick slipped down the slope and surged 200m across Tou-Bien-Kun Creek, and dammed it. The slid soil mass is estimated to be about 1.5 million cubic meters. Extension of the soil has created a graben, a 50m-deep and 100m-wide down-dropped soil block 400m along the top scar.



Fig. 5.1: Tiger Head Hill Slide and Yi-Chiang Bridge



(a) Plan of Tiger Head Hill Slide



(b) Cross-section A-A'

Fig. 5.2: Plan and cross-section of Tiger Head Hill Slide (after Kamae, S. and Shuzui, H., 2002)

5.2 LANDFORM CHANGES IN MID-NIIGATA REGION, after Konagai, Fujita et al, 2007.

Location: 7 km (North-South) × 11 km (East-West) area in Mid-Niigata with its center at 37°18'41"N, 138°53'03"E

Earthquake: Oct. 23, 2004, Chuetsu (Mid-Niigata) Earthquake, Japan, M=6.8

An intense earthquake of magnitude 6.8 jolted central Japan at 17:56 JST on October 23, 2004. The hypocenter of the main shock was located at 37°17'18" N; 138°52'12"E, mid Niigata Prefecture, with depth of 13 km. Higashiyama mountain zone (**Fig. 5.3**), which was the most seriously affected by the 2004 Mid Niigata earthquake, is well known as one of the most landslide-prone zones in Japan. The prevalence of NNE-SSW-trending folds characterizes this zone. Stratified Pliocene rocks are found everywhere inclined or curved upward or downward. Since the up-folded rocks along anticlines were expanded and weakened, anticlines frequently have their crests eroded deep. As the consequence, asymmetric ridges called *cuesta*, characterized by a steep cliff or escarpment on one side, and a gentle, dip slope on the other, have been formed (**Fig. 5.4**, Yanagisawa et al. 1983). Yamakoshi village, where all the inhabitants were forced to evacuate, spreads over old landslide masses along the deeply eroded Higashiyama anticline. Some large landslides are also found on long, gentle slopes of these *cuestas*.

Digital Elevation Models (DEMs) representing ground surface topography of terrain at different times as raster graphic images are essential in this study to detect landform changes. After the 2004 Mid Niigata Earthquake, affected areas have been laser-scanned by different aerial survey companies, private and public institutions including the authors' project's research group etc. Considering the seriousness of geological damage in overlapped areas surveyed at different times, a target zone of 11×7 km² was determined. Before the earthquake however, no precise DEM had ever covered the entire target zone. Therefore a series of aerial photographs on a scale of 1/8000 to 1/10000 respectively taken in 1975-1976 together with triangulation data in 1985 were used to prepare a precise DEM before the earthquake.

Two DEMs for the target zone (**Fig. 5.5**) from the 1975-1976 survey and from the Oct. 24, 2004 survey were compared. **Fig. 5.6** shows elevation changes that have been built up in the target zone during the 29-30 years interval including the changes due to the Oct. 23, Mid Niigata earthquake. Numerous amounts of pixels with their elevation changes displayed with different colors are all arranged in a 2m by 2m square grid. It is remarkable there are two areas in the target zone, which have been risen up by 0.5 to 1.5 meters (**Fig. 12**). The presence of these two humps in the target area is also suggested by the records from GPS stations arranged in a regular 40km×40km sparse square net. The most remarkable hump spreads wide across Kawaguchi town and Budokubo area where the Uono river flows in the Shinano river. It is noted that some areas along the upper reach of the Uono river was flooded in a heavy rain of June 27-28, 2005, about 8 months after the earthquake (**Fig. 5.7**). The Cause-and-effect relation between the earthquake-induced tectonic deformation and the flooding of June, 2005, is now being discussed among the project's taskforce, and will appear in future publications.

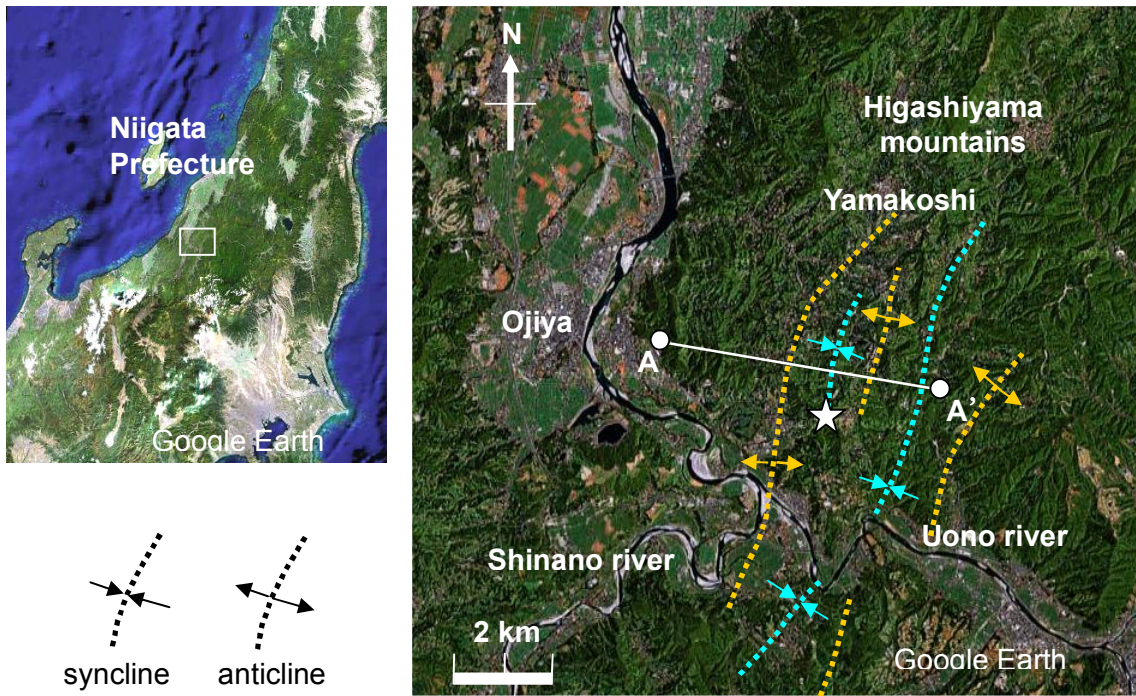


Fig. 5.3: Mid Niigata Prefecture affected by the Oct. 23, 2004 Mid Niigata Earthquake

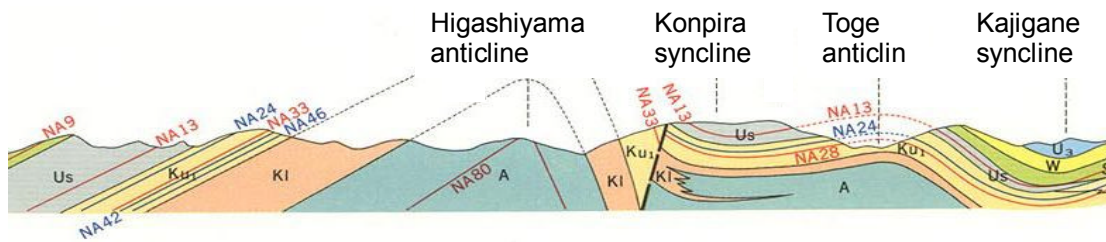


Fig. 5.4: Geological cross-section AA' in Fig. 5.3 (Yanagisawa et al., 1986)



Fig. 5.5: Target zone

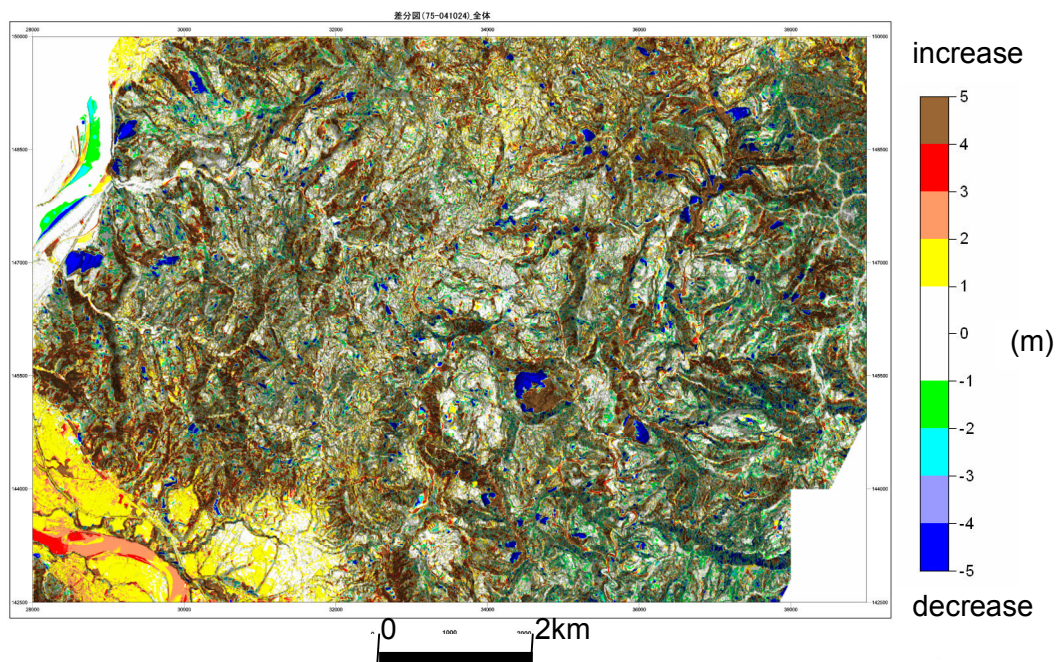


Fig. 5.6: Elevation changes in the target zone on Eularian coordinate system

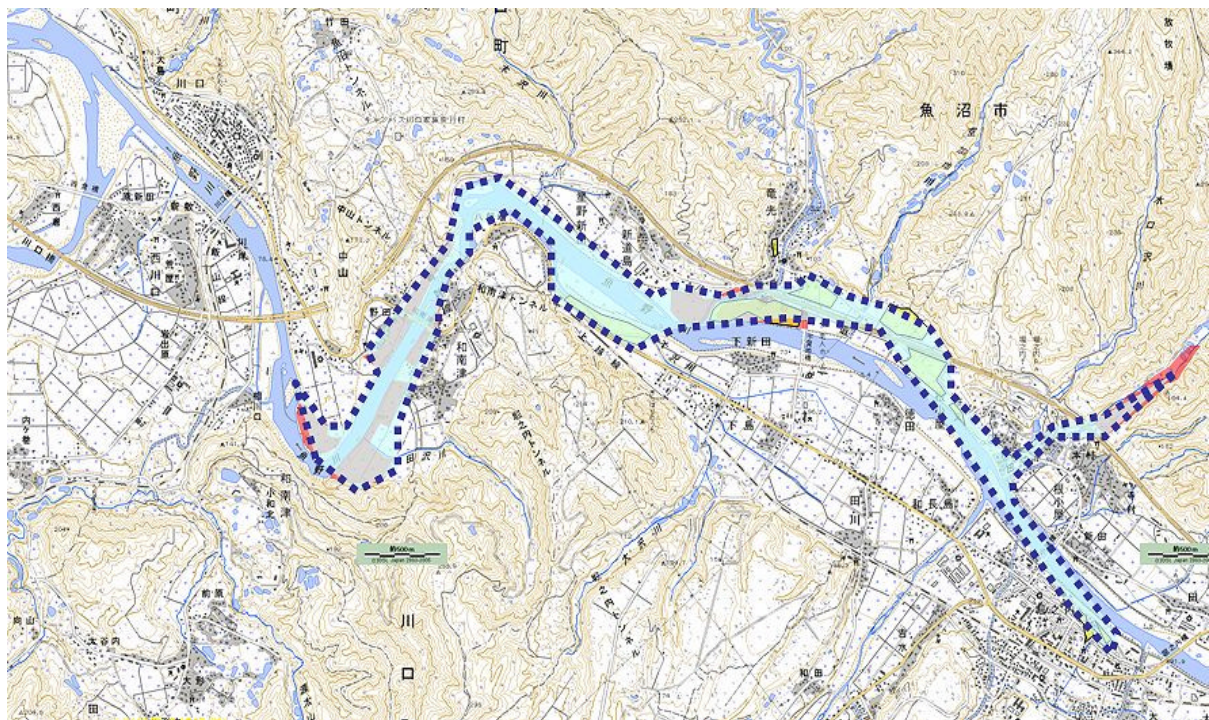


Fig. 5.7: Flooded zone in the heavy rain of June 27-28, 2005 (Yellow area in Fig. 5.5)

5.3 STRAINS INDUCED WITHIN SOILS NEAR FAULT RUPTURE PLANES

Location: 40°43'32"N, 29°49'02"E for **Fig. 5.8(b)** and
40°43'21"N, 29°50'55"E for **Fig. 5.8(c)**

Earthquake: August 17, 1999, Izmit Earthquake, Turkey, M=7.4

Izmit earthquake occurred along the western portion of the North Anatolian Fault. The activated fault had a surface rupture length of 150 km extending from the city of Düzce all the way into the Sea of Marmara along the Gulf of İzmit. Offsets along the rupture were as large as 5.7 meters. As contrasted with thrust faults in general, strains are localized just along the activated fault. However several photos from the affected areas show that strains can be distributed over some distance from rupture planes. In Golcuk, the east-west trending major fault line under the sea shoots at least two conjugate rupture planes. One branch (N55°W) appeared across the Gölcük Atatürk Stadium (**Fig. 5.8(c)**). The bend in the line of curb blocks evidences that the soil on this side of the rupture plane, which has settled about 1.7m down with respect to the other side, is deformed over a several-10m distance from the rupture plane. A manhole embedded 40 to 50 meters north off another branch (**Fig. 5.8(b)**) has been deformed oval, causing its lid not to fit in; the fact seemingly evidences that the surrounding soil experienced a noticeable shear strain near the fault.

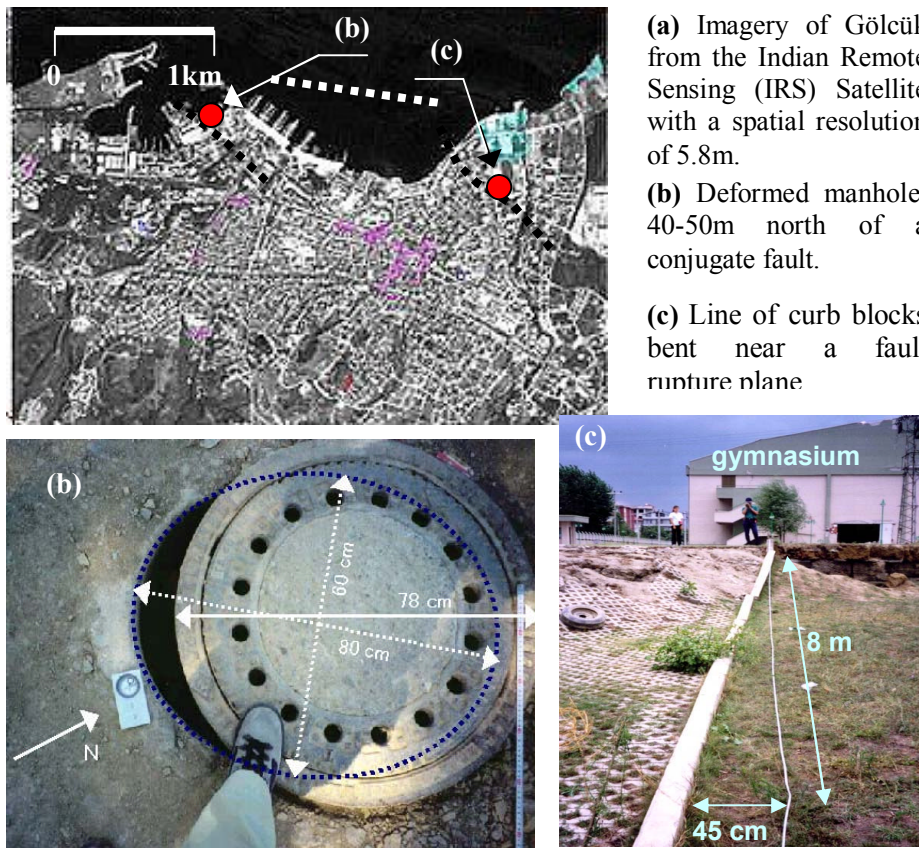


Fig. 5.8: Some evidences showing strain buildup near in soils near activated fault (Gölcük city in the August 17, 1999, Izmit Earthquake, Turkey, M=7.4)

5.4 LONG LASTING LANDFORM CHANGES IN PAKISTAN

Location: 23° 54'02"N, 120° 42'21"E

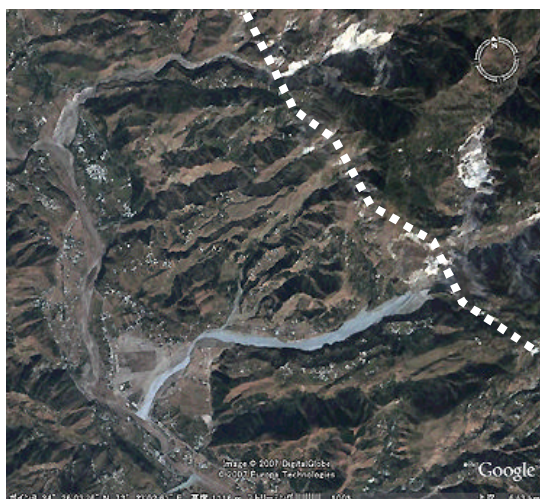
Earthquake: Oct. 8, 2005, Kashmir Earthquake, Pakistan, M=7.6

Rehabilitation issues often attract less attention than those in the immediate aftermaths of earthquakes, and have never given to prominent coverage by news media. However, both, the 1999 ChiChi earthquake, Taiwan, and the 2005 Kashmir earthquake, Pakistan, formed a great number of debris sources along their activated faults. Heavy rains in the monsoon of 2006 that followed the Kashmir earthquake of 2005, Pakistan, were responsible for raising river beds. At Ghari Habibullah village, 4 to 5 kilo meters west of the northern segment of the Muzaffarabad fault, about 4 to 6 meters thick debris sediment was formed at the exit of a canyon onto a flat plain along Kunhar river (**Fig. 5.9**). This example tells that an earthquake can cause long lasting geotechnical hazards.

Among options for rehabilitating Muzaffarabad, local capital in the affected areas, one feasible idea will be to lay out satellite towns outside the municipal boundary as described in the JICA master plan. Staying a little off unstable rims of terraces, terraces will be appropriate locations for developing satellite towns.

One difficulty will be the maintenance of roads, which will have to cross deep gorges from the mountains with seismic faults (such as Tanda and Jelum faults). During the earthquake slope failures created debris deposits (sources) along the activated fault, and during heavy rains, further debris flows can occur. These flows will most likely follow the gorges, namely branches of the Jehlum and Nihlum rivers crossing roads and suspending traffic. Clearing debris remaining on the roads will be just a stopgap. Connecting existing roads point-wise by constructing new bridges etc, a cost-effective bypass can be constructed allowing bi-directional traffic to be realized.

Steady and continuous efforts for rational rehabilitation based on scientific knowledge will certainly lead to developing nation-wide capacity for coping with disasters, and for better rehabilitation tactics, monitoring changes of landforms will be one of important keys to this success.



(a) Sattelite imagery (Google earth)



(b) Debris deposit

Fig. 5.9: Debris deposit from activated fault in Kashmir (Ghari Habibullah village): White broken lines show the activated fault in the Oct. 8, 2005, Kashmir Earthquake, Pakistan. (Konagai, et al. 2007)

REFERENCES

- Kamai, T. and Shuzui, H. (2002). "Landslides in urban region," *Riko-Tosho Press*.
- Konagai, K. et al. (2007). "Annual Report of the Research and Development program for Resolving Critical Issues, "Earthquake damage in active-folding areas: creation of a comprehensive data archive and suggestions for its application to remedial measures for civil-infrastructure systems," Special Coordination Funds for Promoting Science and Technology, Ministry of Education, Culture, Sports, Science and Technology."
- Konagai, K., et al. (2006). "Quick Report of the JSCE Mission for Geotechnical Survey along Jehlum and Kunhar Valleys (Ver. 1.2)," JSCE, http://www.jsce.or.jp/report/41/ss-JSCE-IDI_Pakistan.pdf.
- Yanagisawa, Y., Kobayashi, I., Takeuchi, K., Takeishi, M., Chihara K. and Kato H. (1986). "Geology of the Ojiya District, Quadrangle Series Scale 1:50,000." Niigata (7), No. 50, Geological Survey of Japan.

Chapter 6

INTENSE SHAKES

6.1 VELOCITY PULSES

There are two important features of near-fault ground motions, *i.e.*, the forward directivity effect and permanent displacement effect. Seismic records in recent earthquakes have provided evidence that ground motions in vicinities of rupturing faults can contain large energies, or “directivity” pulses (**Fig. 6.1**). A directivity pulse occurs when the propagation of the fault proceeds at near the same rate as the shear wave velocity. This pulse is seen in the forward direction of the rupture, and can cause considerable damage during an earthquake. The first two examples given herein are from presentation by Nozu, A. (member of “Technical Committee for Fault-related Geotechnical Issues about Civil-infrastructures, Japan Geotechnical Society,” see PREFACE) regarding the “Handbook for designing port facilities reflecting seismic directivity”, Port and Airport Research Institute.

For discussing directivity features in real earthquakes, acceleration records are really important. The records of the 1999 Chi-Chi earthquake from sites on the hanging wall, for example, exhibited larger values than those from the footwall (Chang T.Y., et al. 2004). However reflecting local site effects, damage can differ from street block to street block. In countries such as Japan, Taiwan and Iran ranked as the most seismic hazard prone zones in the world, strong ground motion networks are very dense to describe seismological features of earthquakes, and yet can be very sparse to describe detail features of damage. Thinner seismometer networks frustrate many attempts for learning lessons from tragedies. Among possible breakthroughs, measuring traces of intense shake remaining in structures, which are seen everywhere and have common features, can be very effective. Two examples in the latter half of this chapter are both from recent massive earthquakes in Iran. Density of cracks on utility poles was used as the index for describing the seismic intensity distribution (**Fig. 6.2**).

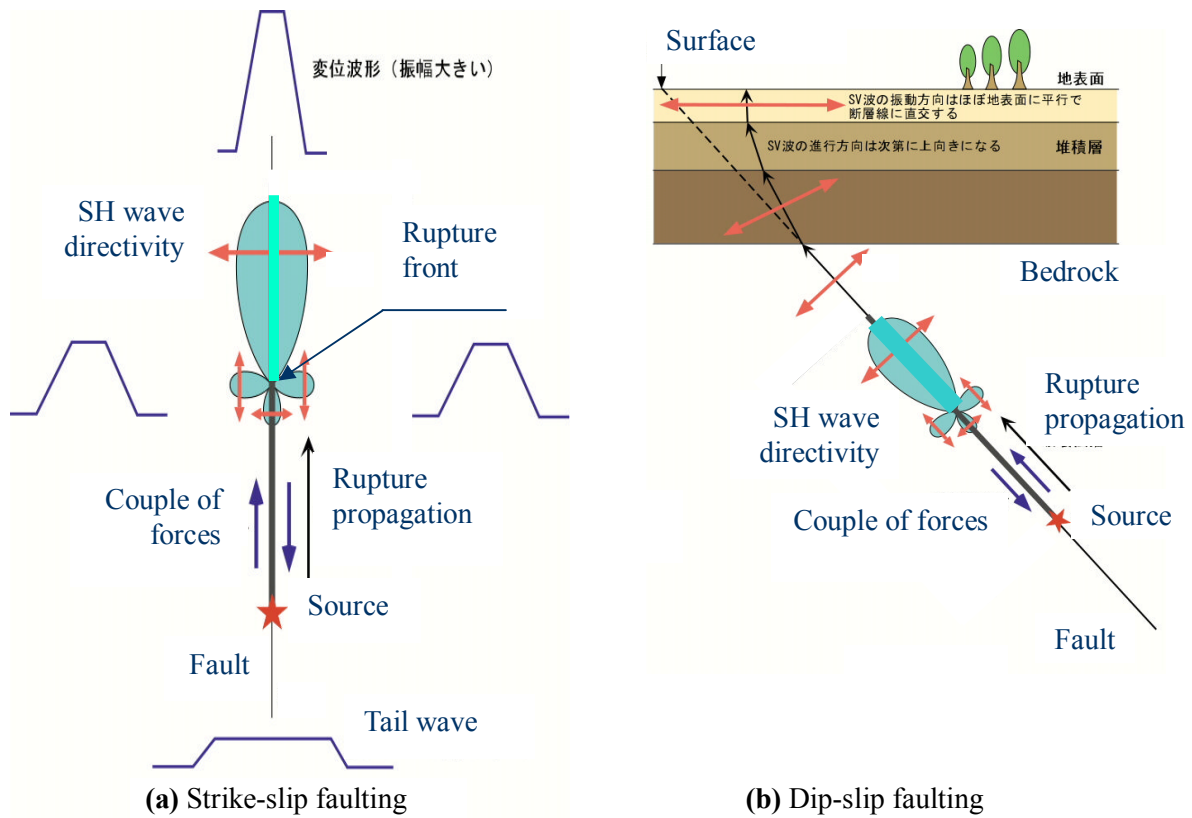


Fig. 6.1: Accumulation of directivity pulse as rupture propagates: Forward directivity effects can be felt for both strike-slip faults and dip-slip faults. The directivity effects are mostly concentrated at the rupture front because the energy builds up as the transverse motion of shear wave travels away from the point of dislocation toward the site.



Fig. 6.2: Poles remaining upright in debris (2003 Bam Earthquake, Iran)

6.2 DAMAGE TO QUAY WALLS, after Nozu, A., 2001, 2004

Kobe Port in the 1995 Great Hanshin Earthquake

Location: Port island 34° 39'33"N, 135° 13'22"E and
Rokko island 34° 40'37"N, 135° 16'19"E

Earthquake: Jan. 17, 1995, Great Hanshin Earthquake, Japan, M=7.2, and

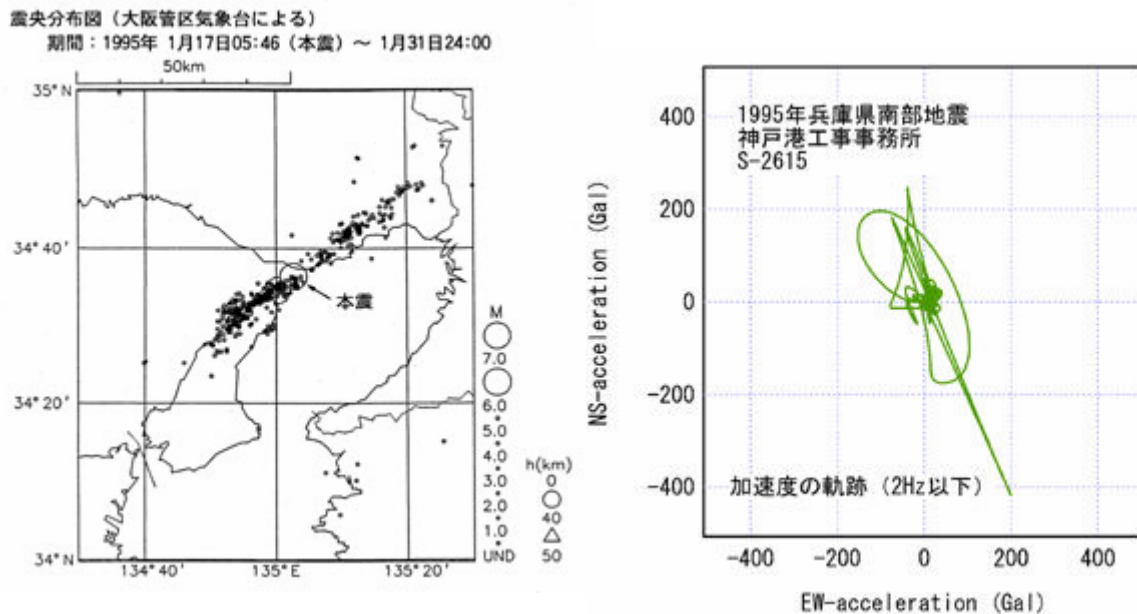
Sakai Port in the 2000 West Tottori Earthquake

Location: Port island N35° 32'41", E133° 14'55" for Station F-1493

Earthquake: Oct. 6, 2000, West Tottori Earthquake, Japan, M=7.3

The 1995 Great Hanshin Earthquake, commonly referred to as the Kobe earthquake, was one of the most devastating earthquakes ever to hit Japan; more than 5,500 were killed and over 26,000 injured. **Fig. 6.3** shows acceleration locus observed at the Kobe Port obtained after filtering out frequency components higher than 2Hz. The filtering reveals that there is an intense ground motion reaching 0.4G orthogonal to the direction of fault rupture propagation. **Fig. 6.4** shows displacements of quay walls of both Port and Rokko artificial islands pushed forward into the sea. In general, displacements in NS direction are larger than those in EW direction suggesting the effect of the intense velocity pulse. Another similar example is from Sakai Port in the 2000 West Tottori Earthquake (see **Fig. 6.5**).

Given all examples for quay walls including above, Port and Airport Research Institute has published the "Handbook for designing port facilities reflecting seismic directivity," recommending that all port facilities that fall within the near field of an active fault can be designed for a possible velocity pulse.



(a) Epicenters of main shock and aftershocks (05:46, Jan. 17 – 24:00, Jan. 30) (b) Locus of acceleration (< 2Hz) at S-2615

Fig. 6.3: Velocity pulse recorded at S-2615, Kobe Port ("Handbook for designing port facilities reflecting seismic directivity (CD ROM)," Port and Airport Research Institute, 2003.)

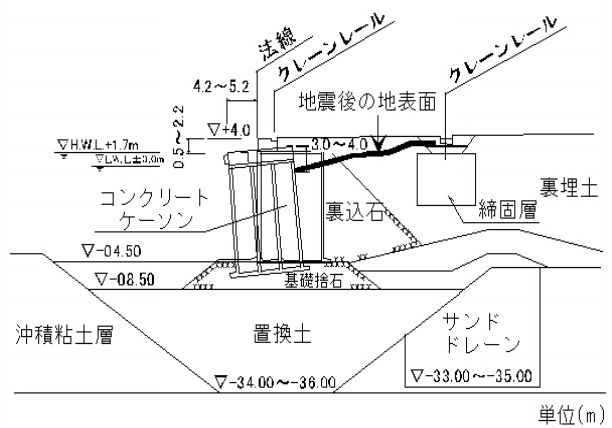
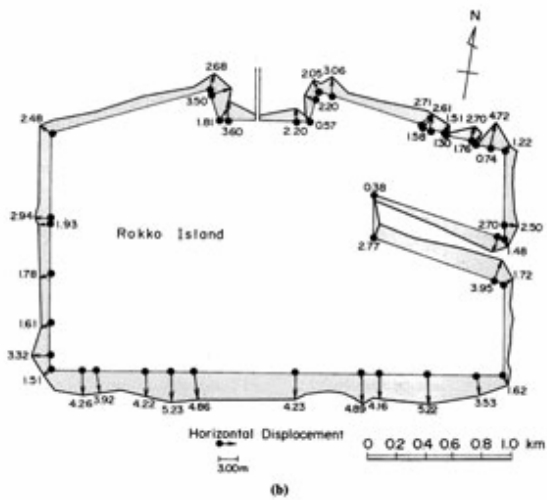
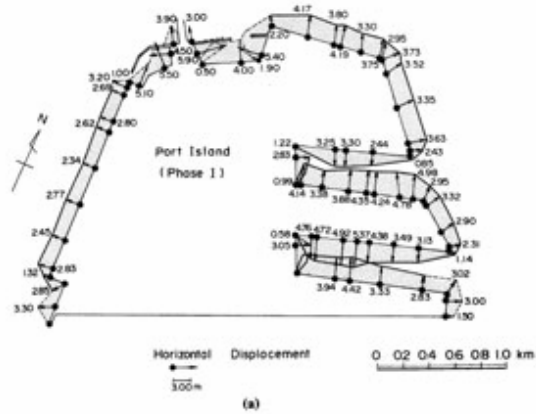
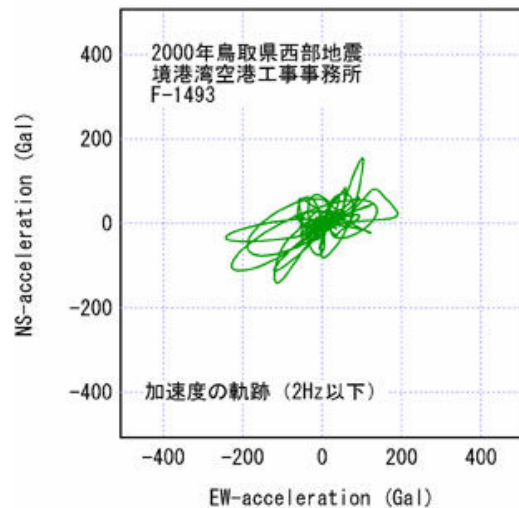
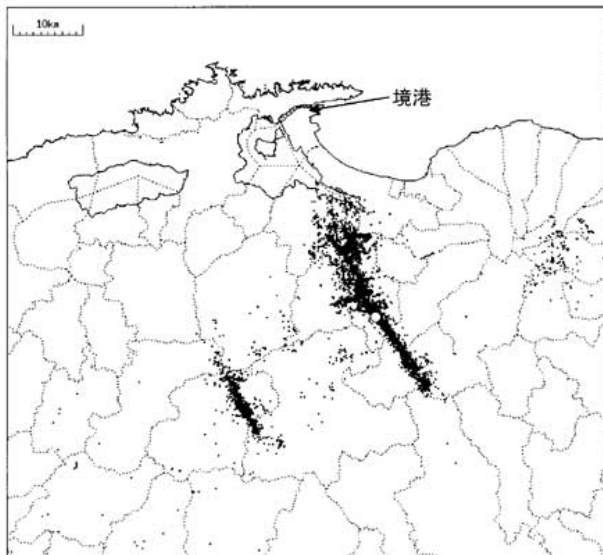


Fig. 6.4: Displacements of quay walls at Port and Rokko islands and typical damage example with settlement of backfill (Inagaki et al., 1996).



(a) Epicenters of main shock and aftershocks (b) Locus of acceleration ($< 2\text{Hz}$) at F-1493

Fig. 6.5: Velocity pulse recorded at F-1493, Sakai Port (“Handbook for designing port facilities reflecting seismic directivity (CD ROM),” Port and Airport Research Institute, 2003).

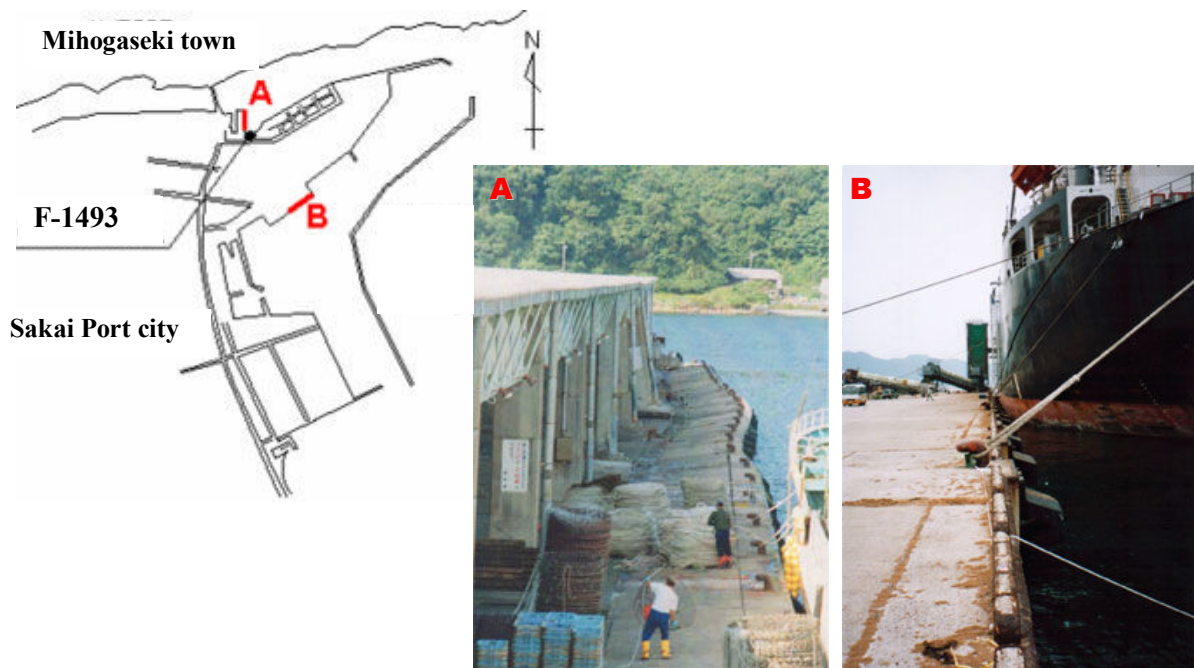


Fig. 6.6: Displacements of quay walls at Sakai Port: Displacement is larger at Point A than that at Point B. (“Handbook for designing port facilities reflecting seismic directivity (CD ROM),” Port and Airport Research Institute, 2003).

6.3 ABDARREH VILLAGE, IRAN, IN THE 2002 CHANGUREH EARTHQUAKE, after Konagai et al., 2003

Location: 35° 47'43"N, 49° 01'16"E

Earthquake: June 22, 2002, Changureh Earthquake, Iran, M=6.4-6.5

The dry and barren plateau dominates most of Iran that lies in southwestern Asia. The plateau, lying at height of 900 to 1,500 m above the sea level, has a continental climate, with cold winters and hot summers. An intense earthquake occurred in western Iran, about 225 km west of Tehran at 7:28 local time, June 22, 2002. Though the moderate moment magnitude of 6.4(ERI, University of Tokyo) – 6.5 (USGS) calculated for this earthquake was not particularly large compared with the major earthquakes that ever occurred in this country, seriously ravaged villages were found along east-west oriented valley in the west of Abegarm, and 261 people were reportedly killed and 1,300 injured.

The epicenter and the damaged area are located in a fold and thrust (low-angle reverse fault) belt in the north of Zagros tectonic boundary (**Fig. 6.7**). This belt trends NW-SE direction. Mountain ranges and valleys of about 30 km wide run along the belt. Reverse fault movements have been responsible for large earthquakes including 1962 Ipak (Buin-Zahra) earthquake.

In this barren area, its surface geology is easily observed. Hills are mainly composed of Miocene siltstones with their southern area covered with Quaternary fan deposits. Two deformation lines are recognized in the valley. The northern deformation line is near the main stream of the valley. Bedding of Miocene siltstone dips north, while on the southern deformation line near Abdarreh, siltstone layers dip south. The 1:200,000 scale tectonic map of this area shows these deformation lines as thrusts. The topographic feature is consistent with its geologic structure. The Quaternary terraces are deformed along the northern line, and a low land extends behind the hill near the south line.

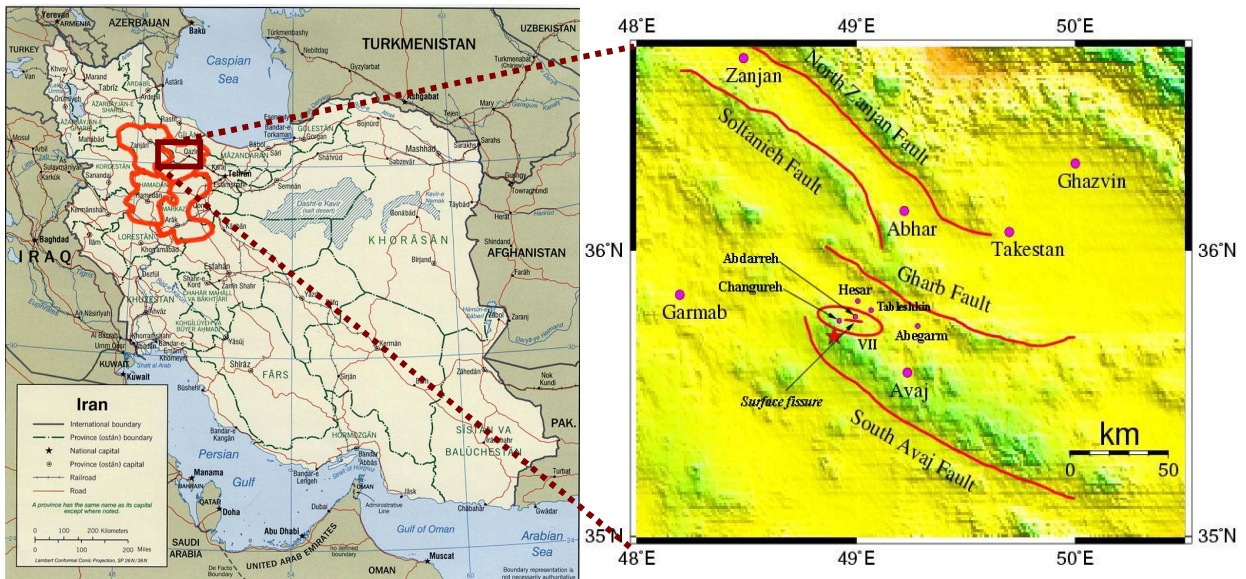


Fig. 6.7: Faults and seismicity of the zone:

★ Epicenter

Magnitude (M_W): 6.5
 Time: 07:28:21.61 (local)
 Location: 35.63N 48.95E
 Focal Depth: 10 km
 Fault Mechanism: reverse
 (Source: USGS, NEIC)

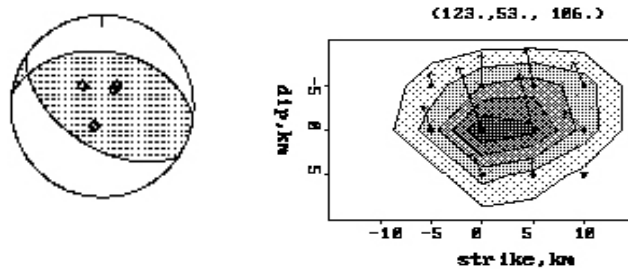


Fig. 6.8: Focal mechanism and slip distribution (Kikuchi and Yamanaka, 2002, ERI)

Kikuchi and Yamanaka, Earthquake Research Institute, University of Tokyo, put up their fault plane solution (Fig. 6.8, http://www.eic.eri.u-tokyo.ac.jp/EIC/EIC_News/020622.html) that indicates that the main shock occurred on a reverse fault of about NW-SE trend. That mechanism is consistent with the tectonic setting of this area. The Moment Magnitude M_W of 6.4 was calculated for the main shock, while 6.5 was calculated by USGS. The focal depth was about 7 km (ERI, 2002).

A surface fault related to this earthquake appeared across the epicenter area of the main shock. According to Sassan, Eshighi, Mehdi Zare and Mohammad R. Mahdaviyar, IIEES, surface fissures are continually lined up 3 km straight across the barren terraces between Changureh and Abdareh (Fig. 6.9).

An about 700m part of the surface fault extending east from Abdareh was traced. The rupture runs straight across the mountain ridges, and is related to the compressional mechanism. The southern hanging wall side has been pushed about 5-10 cm up. This trace of the fissures trends $N70^\circ W$, and is approximately orthogonal to the axis of the focal solution for this earthquake given by NEIC and Harvard University (2002).

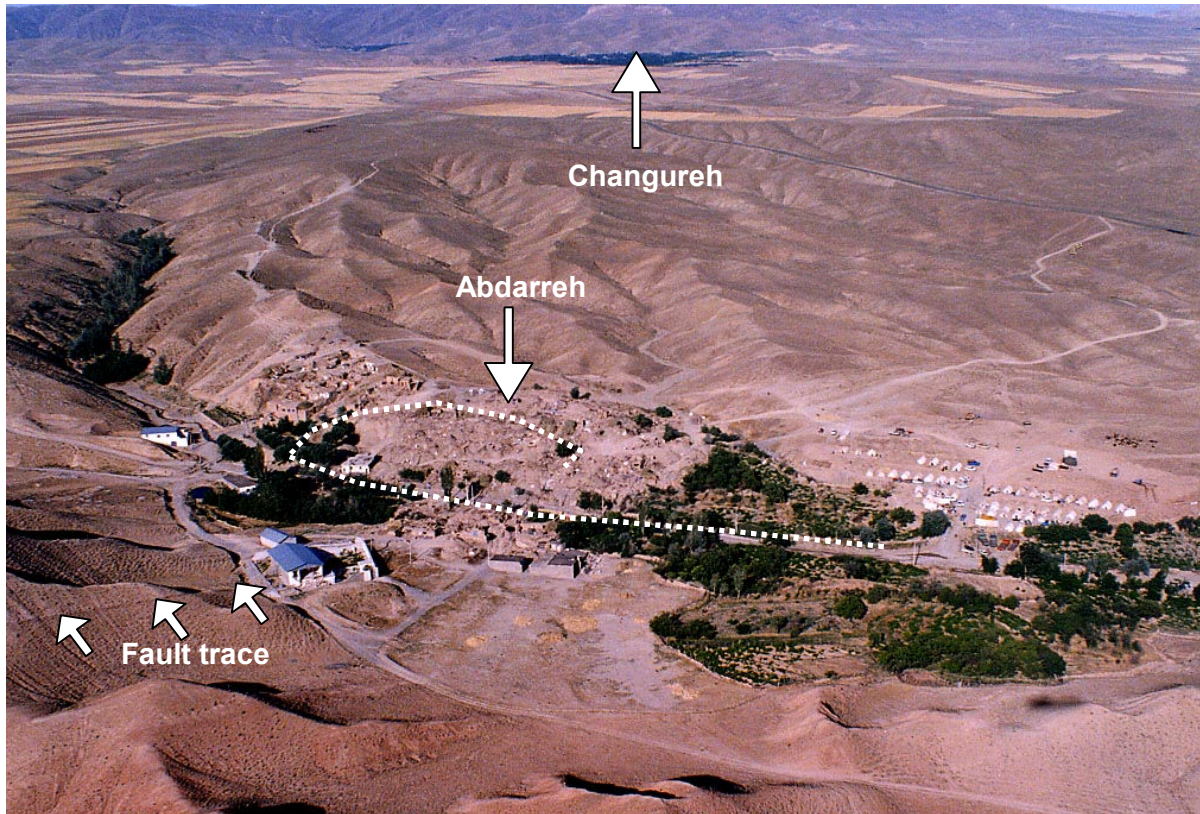


Fig. 6.9: Surface fault trace and affected areas

A trench was excavated at a narrow valley approximately 500 m east of Abdarreh (Fig. 6.10). The site was chosen in expectation of finding charcoals that would allow dating possible previous events. Since the location was inaccessible by any machines, the trench was dug by hand, and was 3 m wide, 5 m long and about 1.2 m deep with east and west side walls cutting straight in the middle of the valley and along the mountainside (Figs 6.11, 2.12).

Fig. 6.12 shows a sketch of the east and west walls of the trench. Layer A is the weathered soil covering thin both the mountainside and the valley. Layer B is composed of granule and less matrix. Layer C contains semi-angular pebbles. Layer D is a matrix rich bed. Maximum grain size of 2 cm is reached in this layer. Layer E is a clearly imbricated gravel bed. The average and maximum gravel sizes are about 1 cm and 5 cm, respectively. Layer F is a paleo-soil covering a gravel bed of layer G. Layer H is also a paleo-soil bed, but is overlain by gravels of layer G. Layer I is a gravel bed covered by layer H. Maximum gravel size of layer I is about 5 cm. Layer F, G, H are overlain by layer E with unconformity. The fault found clearly from surface to layer E. It is recognized as open rupture and there is no displacement along the fault. In the layers below layer F, the fault is hardly recognized.

On the west-side wall, layer H and I are considered to be extensions of those on the east wall. The uppermost bed of the valley sediment, layer J, is a sandy soil with much matrix. Layer K is a thin bed of silt or very fine sand. Layers L and M are sand and gravel beds. The matrix is rather rich in layer L than layer M. Layers N and O are paleo-soil and gravel beds overlain by layer I. Though the surface fissures lined up across the valley have clearly proven the presence of the fault at the slope foot, no clear fault dislocation was observed on the west-side wall probably because the strain caused by the faulting has spread over the uncemented soil. Nothing indicating previous fault dislocations was found in the trench.

On the east edge of Abdarreah, surface soil was scraped off to observe the fault trace on a silt rock (Figure 2.30). The silt rock dips to south. Tufficious fine sand and silt film is caught thin in the silt rock and faulting occurred on its bedding plane. Most southern part of the tufficious sand has developed into clay of 2-3 cm thick probably because of the continual fault dislocations. Siltstone among the thin tufficious sand film has been weakened.

A “bedding plane fault” can be considered as a by-product of folding, and causes a moderate earthquake of M6 class.

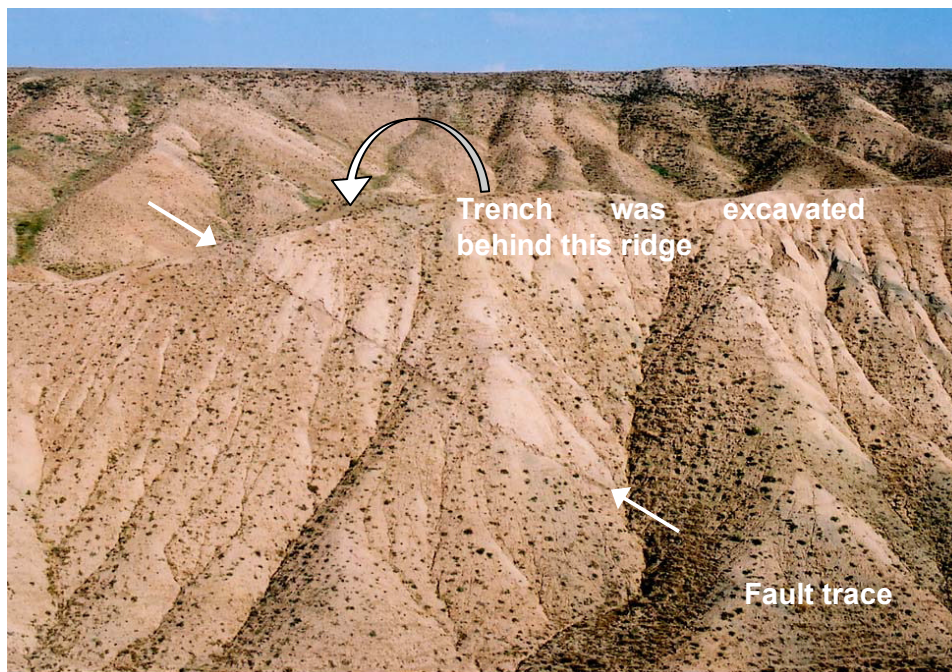


Fig. 6.10: Surface fault trace and location of trench



Fig. 6.11: Excavated trench

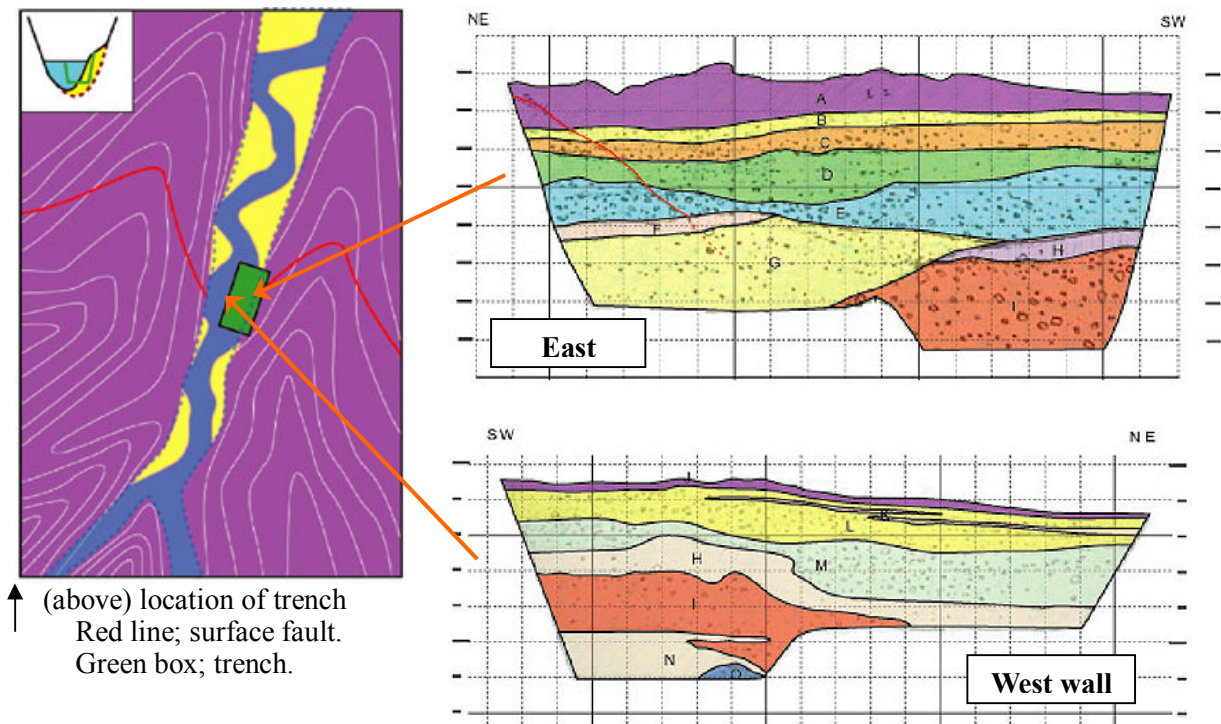


Fig. 6.12: Illustration of trench. (by Azuma, Goto, Konagai, Sadr 2002)

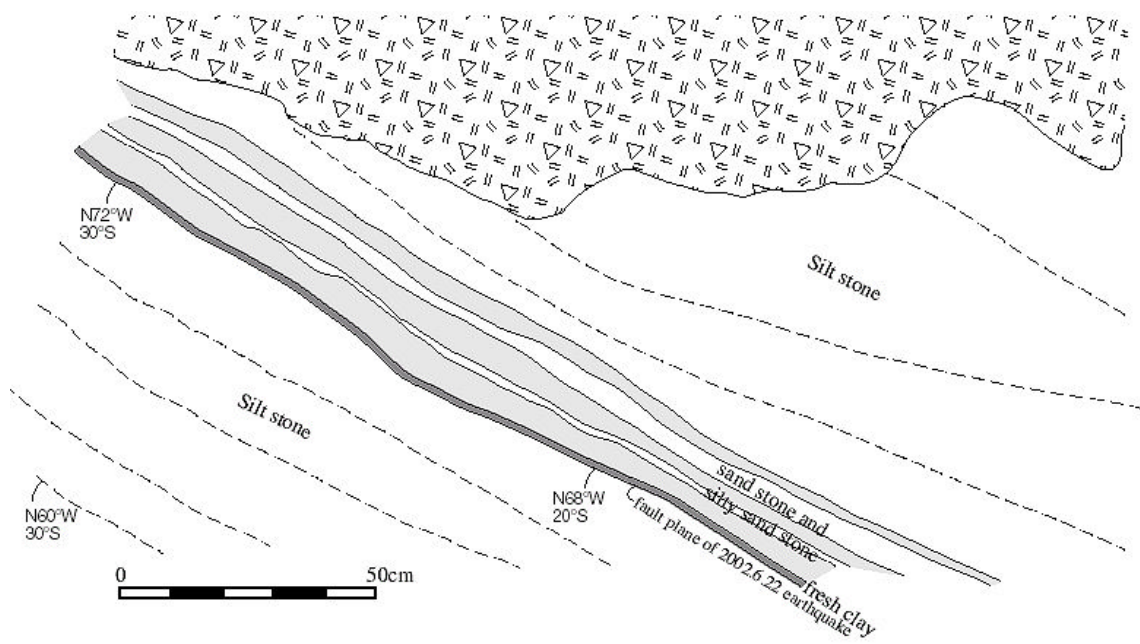


Fig. 6.13: Exposed surface of silt rock (photo by Goto)

Abdarreh was one of the hardest hit villages by this earthquake. A gentle ridge, the northeast extension of a sand rock terrace rising behind, dips gently towards its northeast lowland. This ridge is densely covered with adobe dwellings, and most of them were flattened in the earthquake.

Distribution of cracked utility poles is considered to be a good index for estimating possible spatial distribution of intense ground motions. Observed crack intensities on total 28 utility poles were roughly classified into the following 5 groups:

- Group 1:** no visible crack. (White)
- Group 2:** with hair cracks (>0.1 mm, Light yellow)
- Group 3:** with cracks (0.1-0.2 mm, Yellow)
- Group 4:** with cracks (0.2-0.3 mm, Dark yellow)
- Group 5:** with cracks (<0.3 mm, Brown) that can be seen at a distance of about 2m

Fig. 6.14 shows the observed distribution of crack intensities. In this figure, the route taken for the inspection is lined up with the utility poles (colored circles). The route goes straight from right to left along a valley, and turns sharply up towards the ridge when it reaches the southern edge of the village. Then it comes slightly back along the ridge. Several arrows near the bend of the route indicate the inferred directions of strong ground motions. The other line of dark sphere marks is the fault trace. It goes across another mountain ridge that rises east of the village, and meets the route. It is noted that the fault trace seemingly divides the utility poles into two groups; cracked poles on the hanging wall side and less damaged on the foot wall side. This clear contrast suggests that the shake on the hanging wall side must have been more intense than that on the foot wall, and thus must have been responsible for serious destruction of the village. The arrows show that the motion was intense in the normal direction to the fault trace.

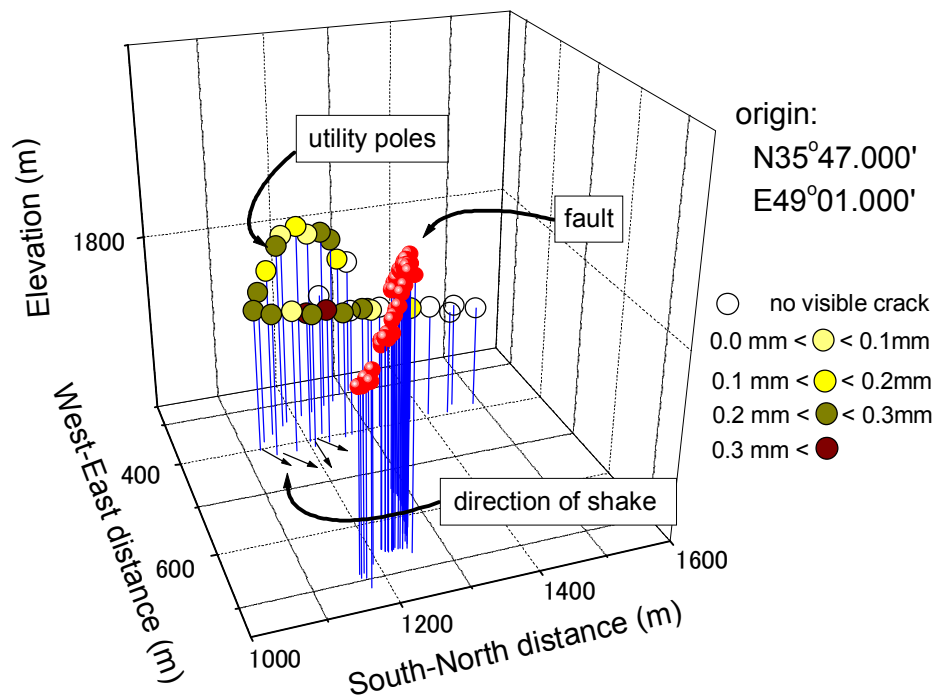


Fig. 6.14: Locations of cracked utility poles

6.4 BAM CITY, IRAN, IN THE 2003 BAM EARTHQUAKE, after Konagai et al., 2004.

Location: 29° 06'18"N, 58° 21'31"E

Earthquake: Dec. 26, 2003, Bam Earthquake, Iran, M=6.6-6.6

An intense earthquake occurred in southeastern Iran at 5:28 local time, December 26, 2003. Though the moderate moment magnitude of 6.5 (Building and Housing Research Center, Iran) – 6.6 (USGS) calculated for this earthquake was not surprisingly large as contrasted with those major earthquakes that ever occurred in this country, Bam, an oasis city in a desert, was seriously ravaged. About 43,100 people were reportedly killed and 1,300 injured making this earthquake the worst that Iran has ever had.

The city had about 100,000 residents according to official figures. Shortly after the earthquake, the officials announced that the possible deaths would be 28,000. The number was revised down to 26,500 on January 3, but as the rescue crews continued to pull out dead bodies from debris, the death toll increased. On Jan. 15 the official estimates put the number of casualties between 30,000 and 35,000, and up until now the death toll has been increased up to 43,100. Since the earthquake happened quite early in the morning, the majority of the casualties were killed in their dwellings, mostly adobe, un-reinforced and/or confined masonry structures.

Since the effect of the earthquake was seriously large in amount and broad in scope, it turned out that several organizations in Japan were dispatching their teams. They included the Japan Association for Earthquake Engineering (JAEE), Japan Society of Civil Engineers (JSCE) and the Ministry of Education, Culture, Sports, Science and Technology (MEX). The MEX team was made up of several sub-teams for a wide expertise. After some discussions, a joint engineering team was organized for an efficient reconnaissance survey. Although the major counterpart organization was the International Institute of Earthquake Engineering and Seismology (IIEES), the Building and Housing Research Institute (BHRC) and the University of Tehran (UT) also collaborated during the field survey. The joint team made the first and second reconnaissance trips on Feb. 16–25 and Feb. 23–March 5, respectively, stressing on the evaluation of damage to dwellings, description of the damage in terms of possible intensity distribution, which might have been affected by local and geological site conditions, and discussion with Iranian specialists about possible future collaborations beneficial for both Iranian and Japanese sides.

Source Parameters and Geological Structure

Southeastern Iran is a region of widespread active faults (**Fig. 6.15a**) that take up basically right-lateral shear in this area. The Bam Earthquake measuring 6.51 on the Richter scale occurred on December 26, 2003 at 05:28 local time, with its epicenter located at 29.004 N, 58.337 E, on a predominantly right-lateral strike-slip fault. The focal depth was located 7 to 12 km directly underneath Bam city spreading west behind a pressure ridge formed along Bam fault (**Fig. 6.15b**). The presence of a pressure ridge suggests that there are shortening (thrusting) components associated with the strike-slip movement of the fault.

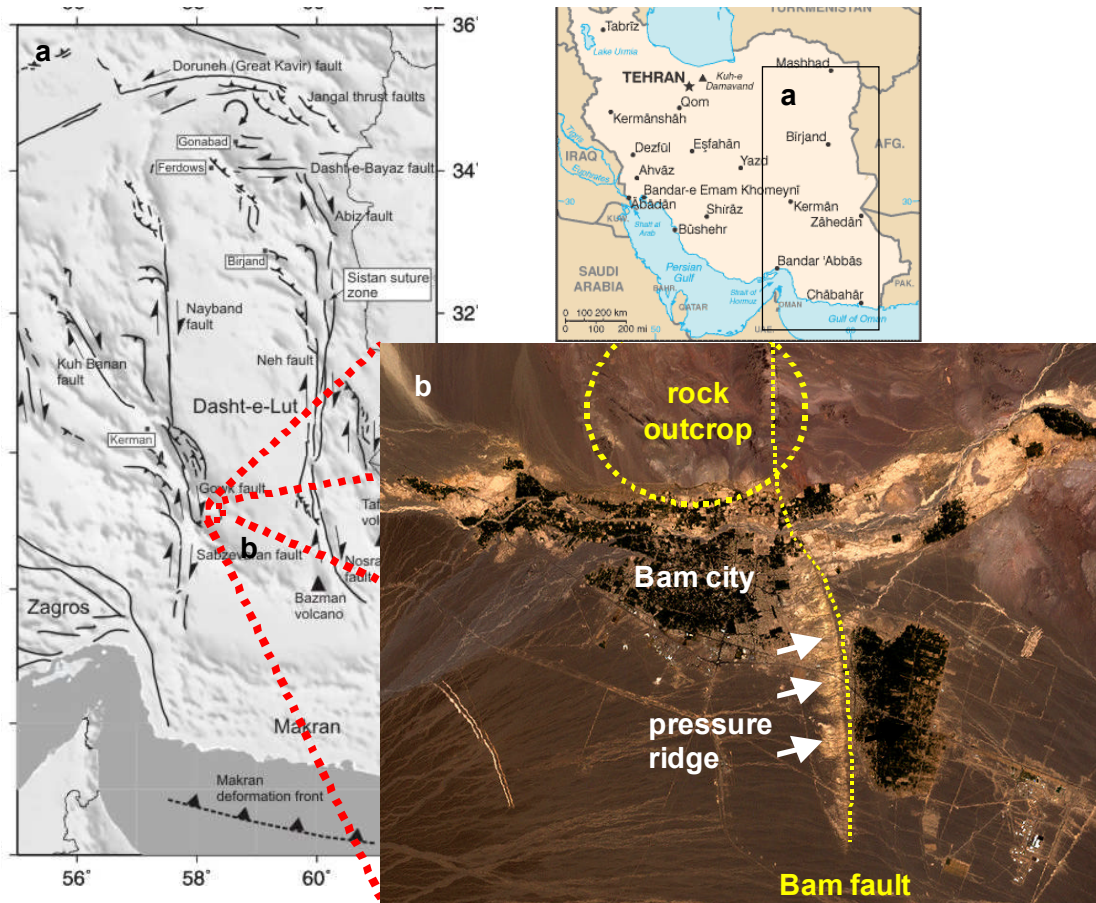


Fig. 6.15: Location of Bam and its satellite imagery: Bam fault take up basically right-lateral shear in this area. However some shortening component has been responsible for forming a pressure ridge along the fault. Bam city spreads behind the pressure ridge on the hanging wall side. (Satellite imagery from LANDSAT, (NASA, 2004), October 1, 1999, Fault map from Walker et al. (2003)).

Fig. 6.15b shows satellite imagery from LANDSAT (NASA, 2004) covering Bam. A volcanic rock outcrop can be seen just north of the city, which dips to the south. The rock is cut in half by Bam fault, which extends from north to south. The 2 km wide pressure ridge has stopped sand, soil and other suspended matters that rivers from mountains have carried over centuries. The area is thus rich of underground water. Taking this advantage, Bam, an old oasis city has been developed with no reported great historical earthquake before this event. The city spreads about 6 km from north to south and 8 km from east to west on the hanging wall side.

The International Institute of Earthquake Engineering and Seismology (IIEES) did seismic profiling along total 10 lines taken in the city after the earthquake (IIEES, 2003). Color bars in **Fig. 6.16** show average soil profiles at these lines. Alluvial soil covers thick the mid to southern part of the city area, while the soil becomes thinner as we go north. **Fig. 6.17** shows inferred layer boundaries of shear wave velocities 155 m/s and 900 m/s respectively, both showing rich variation of soil profile in Bam city.

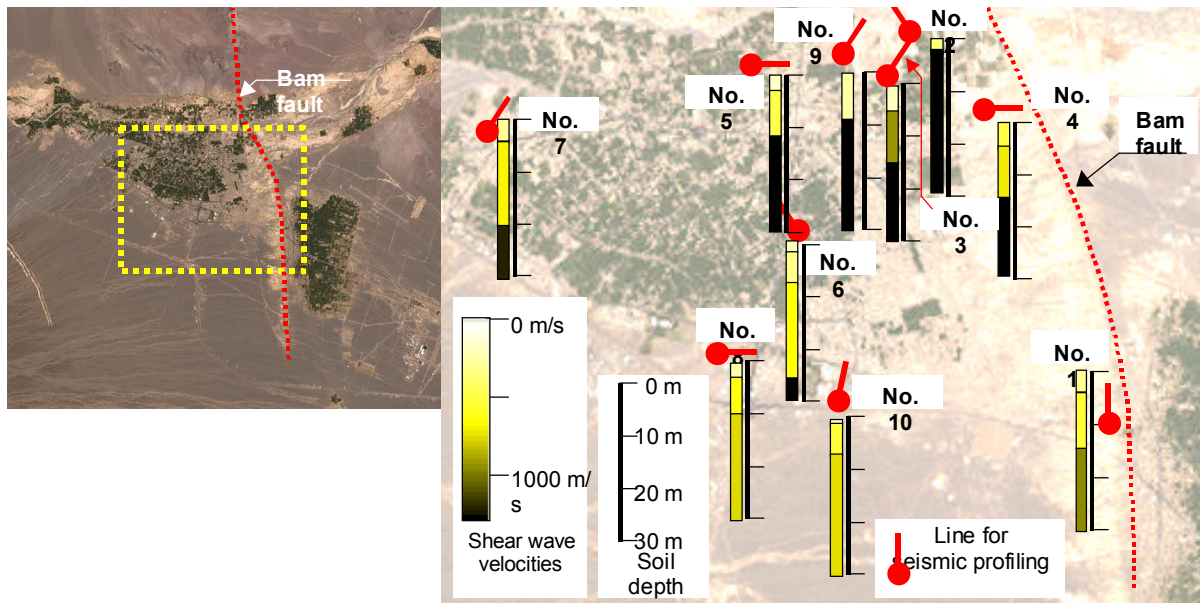


Fig. 6.16: Seismic soil profilings in Bam: Each marks with a circle on its one end show a line taken for seismic profiling. Circle denotes the point where a blow was given. (Original data from IIEES)

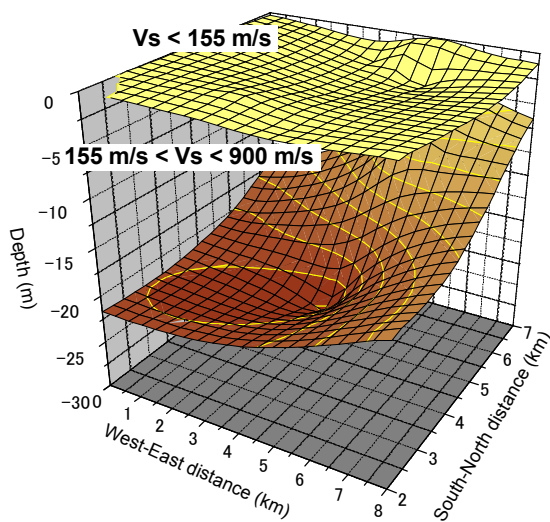


Fig. 6.17: Inferred layer boundaries of shear wave velocities 155 m/s and 900 m/s respectively.

Strains Remaining on Utility Poles

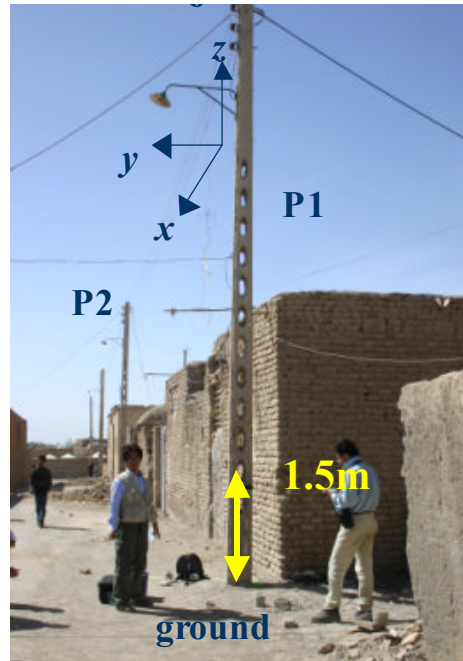
For oasis cities near active faults to be prepared for possible future earthquakes, damage caused by the Bam earthquake is to be discussed in terms of strong ground motion features that dwellings have experienced. However, as was often the case, damage differed from street block to street block, while only one seismometer was available in the city. In countries such as Japan and Iran ranked as the most seismic hazard prone zones in the world, strong ground motion networks are often very dense to describe seismological features of earthquakes, but yet very sparse to describe damage distribution frustrating many attempts for learning lessons from tragedies. Among possible breakthroughs, measuring traces of intense shake remaining in structures, which are seen everywhere and have common features, can be very effective. The authors used utility poles in Bam as this structure. Poles differ in their dimensions from area to area, but a thin pole type, with holes for climbing on, were the most widely used in the city (**Fig. 6.18(a)**) and, thus, chosen as the target.

Table 6.1: Characteristics of the surveyed poles

Name	Height (m)	Remarks
P-1	6.6	Pole with hexagonal holes
P-2	6.6	Pole with hexagonal holes filled with concrete



(a) 8m pole with holes and embedment depth of 2 m



(b) Poles P-1 and P-2

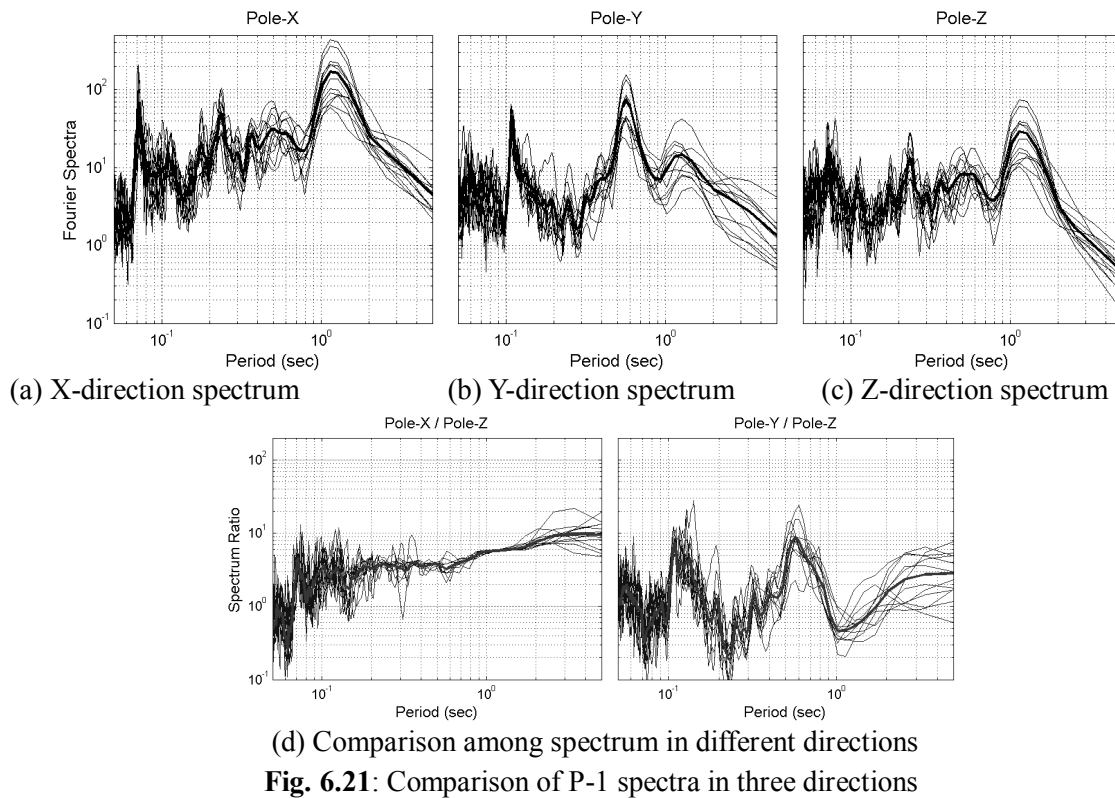
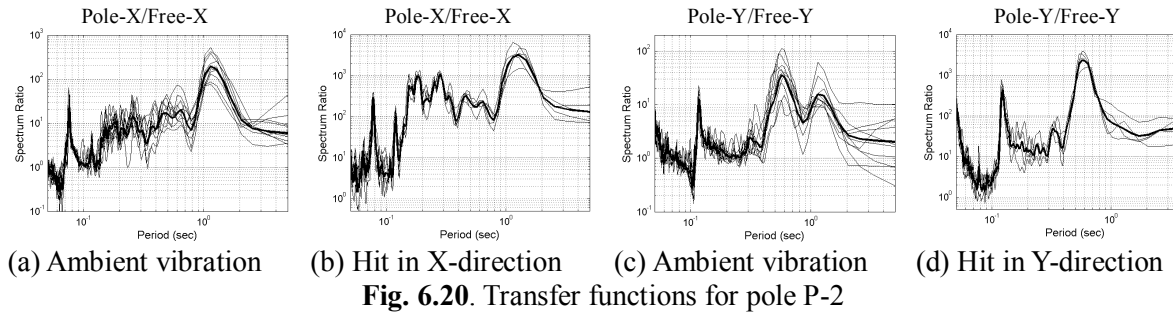
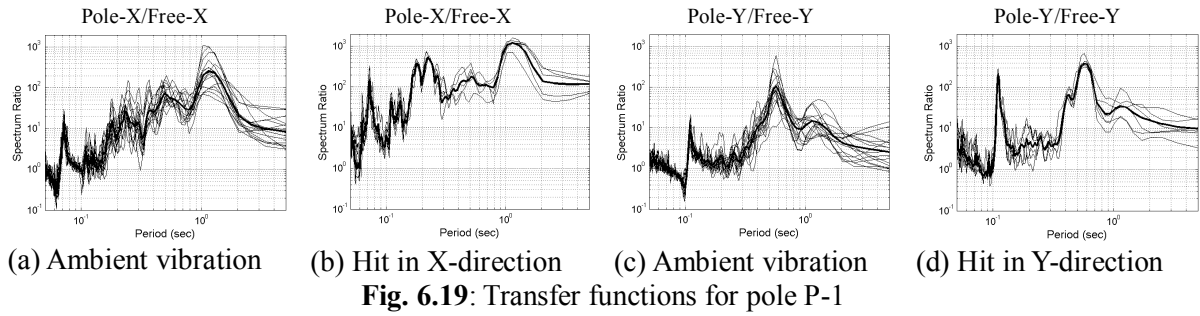
Fig. 6.18: Poles taken in Bam

In order to examine the dynamic features of this pole type, microtremors were measured at two poles (**Fig. 6.18(b)**). Their characteristics are summarized in Table 1. Bottom holes on P-2 pole were filled in to prevent theft.

A pair of 3-components velocity sensors was used for the measurement, one on the ground and the other strapped to each pole at the height about 1.0 to 1.5m above the ground. In each case, the X-axis was taken along the transmission line. Tremors were measured with poles a) subjected to ambient vibration, basically wind; b) hit in X-direction; and c) hit in Y-direction.

Each time history of the tremor was divided into several 10.24sec pieces. Fourier spectra of all pieces were then calculated and averaged for each time history. In order to obtain transfer functions in the frequency domain, spectra measured on the pole were divided by those on the ground.

Fig. 6.19 shows the transfer function for P-1. It is clear in Y-direction that there is little change of the predominant periods between the “ambient” and “hit” cases. In both cases, clear peaks are found at 0.105 and 0.57sec, with the main difference being the peak relative amplitudes. When the structure is hit, the lower period amplitude becomes higher.



Poles exhibits quite different vibration features in X-direction. As for ambient vibration cases, two peaks at 0.07 and 1.10 sec are distinguished among the others at 0.18, 0.21, and 0.6. When the structure is hit, two clear peaks appear at 0.18 and 0.21s in addition to 0.07 and 1.10s, but 0.6s peak is not clearly seen suggesting that this peak is the crosstalk from Y-component of the pole vibration.

Fig. 6.20 shows the transfer functions for P-2 pole. The functions have similar shapes as those for P-1 pole in all cases, suggesting that mortar filled in holes had little effect on the dynamic behavior of the pole. **Fig. 6.21(a), (b)** and **(c)** show X, Y and Z components of the pole vibration spectra. It is noted that the spectra for X and Z components are similar with each other, while Y component exhibits some different shape. **Fig. 6.21(d)** shows X/Z and Y/Z spectra ratios to highlight this feature. Assuming that the vertical vibrations of the pole were mainly induced by cable oscillations, it may be concluded that a cable has an important effect on the pole's motion along the cable.

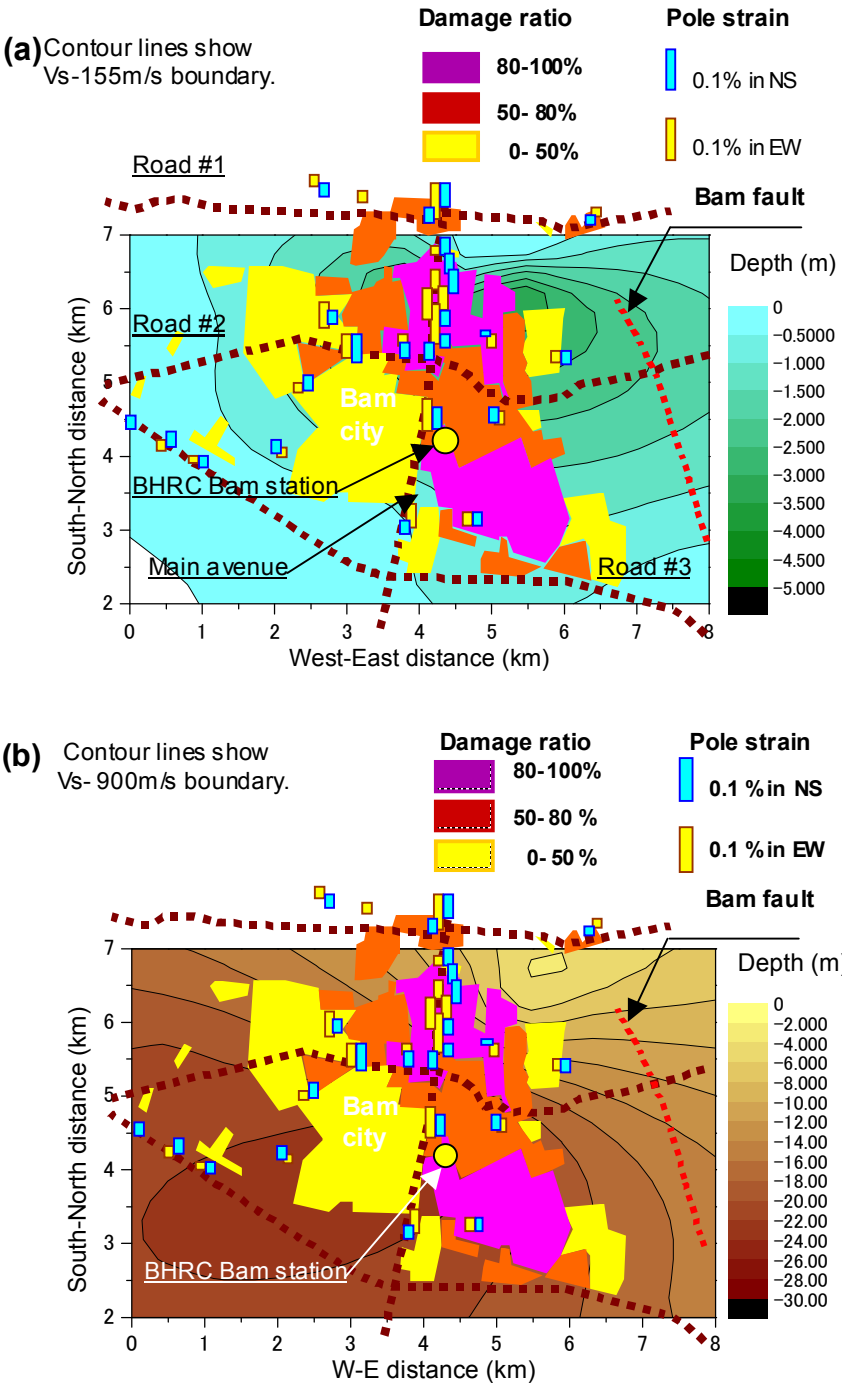


Fig. 6.22: Strains remaining in poles: (Damage distribution mapped by NCC, Iran)



(a) Near the main avenue
29°07'00.5"N 58°21'41.5"E



(b) East of the city
29°06'23.3"N 58°22'36.7"E



(c) Along the Street #2
29°06'24.6"N 58°21'13.1"E

Fig. 6.23: Damage to dwellings in Bam

For this reason, crack openings on pole sides without holes were taken to minimize the effect of transmission lines, the cracks caused by poles' motion in Y direction. For each pole, crack openings were added up over about 2m distance near the lower pole end, and then the total openings were divided by the distance to obtain average strain remaining on the pole. Total 270 poles were taken both in the city and its suburbs. The poles were then divided into several tens clusters in such a way that each cluster includes at least one crossing in it. Since the poles in one cluster line up at least two roads crossing each other, both north-south (NS) and east-west (EW) average strains were obtained cluster-wise. **Fig. 6.22(a)** and **(b)** show the distribution of remaining average strains in the city. Contour lines in **Figs. 6.22(a)** and **(b)** show inferred layer boundaries of shear wave velocities $V_s = 155m/s$ and $V_s = 900m/s$, respectively (see **Fig. 6.17**), and colored zones show percentages of damage mapped by the National Cartographic Center of Iran. In general, strains are large along the main avenue that runs through the city from north to south. Damage was also severe along this avenue (**Fig.6.23(a)**) and it faded out quickly as we go some street blocks away from the avenue (**Fig. 6.23(b)**). Some severe damage to dwellings was also found along Road #2, which used to be an old river trace, and goes through the city from East to West (**Fig. 6.23(c)**). The strain distribution thus seems to be consistent with the overall damage distribution pattern. However, a calibration is

necessary to interpret the strain distribution pattern in terms of intensity in spite of the fact that only one strong ground motion record was available in the city (see the location on the map **Fig. 6.22**). The further discussion will turn up in a future publication.

Summary

Measuring traces of strong ground motions remaining in structures, which are seen everywhere and have common features, may provide useful pieces of information for discussing spatial distribution of damage. Utility poles were taken as the target structures in Bam, the city flattened in the December 26, 2003 earthquake. The obtained strain distribution seems to be consistent with the overall distribution of damage to dwellings, which killed more than 43,000 people. Conclusions

The Bam Earthquake was yet another evidence of the high seismic vulnerability of adobe and unreinforced masonry structures. It also showed the very good seismic performance of confined masonry. Although it is possible to ban the use of adobe as a construction material, which was actually done by the Iranian Government, this measure is inapplicable, as many people with limited resources will continue to use it. Several constructions practices for improving the seismic performance of new adobe structures have already been devised as well as retrofitting methods for existing structures. Unfortunately, these have not been implemented due to a lack of appropriate information spreading campaigns. This fact underscores once more the stress that should be put not only on technical issues of earthquake engineering but also on the social ones.

REFERENCES

- Azuma, T., Goto, H., Konagai, K. And Sadr, A. (2002). "Surface faulting and liquefaction related to the Changureh (Avaj) earthquake, Iran, June 22, 2002," AGU 2002 Fall Meeting, Moscone Center, San Francisco, California, USA.
- Chang, T.U., Cotton F., Tsai, Y.B. and Angelier, J. (2004). "Quantification of hanging-wall effects on ground motion: some insights from the 1999 Chi-Chi Earthquake," *Bulletin of the Seismological Society of America*, 94(6), 2186-2197.
- "Handbook for designing port facilities reflecting seismic directivity (CD ROM)," Port and Airport Research Institute, 2003.
- Inagaki, H., Iai, S. and Sugano T., Yamazaki, H. and Inatomi, T. (1996): "Performance of caisson type quay walls at Kobe Port," *Special Issue of Soils and Foundations*, 119-136.
- NASA: Destructive earthquake near Bam, 2004, http://www.parstimes.com/spaceimages/bam_landsat.html (Photo, taken on October 1, 1999).
- National Cartographic Center of Iran, Damage distribution to dwellings, Bam, 2004.
- Nozu, A. Iai, S. and Iwan, W.D. (2001). "A Study on Predominant Direction of Near-source Ground Motion and It's Application," *Report of Port and Airport Research Institute*, 40(1), 107-167.
- Nozu, A. (2004). "Velocity pulse and Fling step," Presentation in a meeting of "Technical Committee for Fault-related Geotechnical Issues about Civil-infrastructures," Japan Geotechnical Society.
- Kikuchi and Yamanaka, 2002, ERI, http://www.eri.u-tokyo.ac.jp/EIC/EIC_News/020622.html.
- Konagai, K. et al. (2003), "Provisional Report of the June 22, 2002, Changureh Earthquake, Iran," JSCE website: <http://www.jsce.or.jp/report/15/02/contents.htm>.
- Konagai, K., Yoshimi, M., Meguro, K., Yoshimura, M., Mayorca, P., Takashima, M., Farahani, A., Tahghighi, H. and Keshavarz, M.: Strain induced in cracked utility poles and damage to dwellings from the Dec. 26. 2003, Bam Earthquake, *Bull., Earthquake Research Institute*, University of Tokyo, **79(3/4)**, 59-68, 2004.
- Walker, R., J., and Baker, C., (2003). "Surface Expression of Thrust Faulting in Eastern Iran: Source Parameters and Surface Deformation of the 1978 Tabas and 1968 Ferdows Earthquake Sequences," *Geophysical Journal International*, **152**, 749-765.

Chapter 7

FAULT PROVISIONED DESIGN EXAMPLES

7.1 MITIGATION MEASURES, after Bray, 2001, Hamada, 2003

A few case histories where the possibility of fault surface rupture or fault dislocation has been considered during the design process and with special construction features are summarized below. (For earlier case histories and reviews see Bray (2001) and references therein.)

The last part of Bray (2001) contains an illustrative fault rupture mitigation case history for a reverse and normal fault. He concludes from a thorough numerical and experimental investigation that the hazards can be reduced by using compacted fill and:

- Increasing the height of the compacted fill
- Increasing the ductility of the compacted fill
- Installing soil-reinforcement within the compacted fill

If a reduction of the required compacted fill height is desired, a combination of compacted fill and e.g. post-tensioned slabs instead of standard concrete foundation slabs can be used. Reinforced slabs performed significantly better than un-reinforced slabs during the 1992 Landers earthquake. Bray also writes that a grade beam foundation system is another means of limiting the transfer of ground strain to a building foundation.

Hamada (2003) gives a few examples of remediate measures and designs of lifelines against fault-induced ground surface ruptures.

7.2 WATER SUPPLY OF EAST BAY MUNICIPAL UTILITY DISTRICT, CALIFORNIA, U.S.

The first example is from EBMUD (East Bay Municipal Utility District) in California, U.S. Its main reservoir lake Pardee located about 100 km to the east of the service area (see **Fig. 7.1**) with which it is connected through a trunk line of 60 inch (1.5 m) diameter steel pipe crossing two active faults, the Hayward Fault and the Concord Fault. Particularly, the predicted activity of the Hayward fault is very high and the probability of magnitude 7.0 earthquake within next 20 years is estimated to 35 %. Therefore, EBMUD is constructing a new trunk line, the Southern Loop (**Fig. 7.1**), to increase the redundancy of the water network. Thereto, at the fault-crossing point, emergency shut-down valves were installed and temporary hoses were stored in the nearby to quickly restore the water supply after the earthquake (**Fig. 7.2**).

- The Los Angeles Department of Water and Power also reported the following countermeasures for its water supply system against the San Andreas fault and the other active faults:
- Many large reservoirs were constructed on the west side (Los Angeles side) of the San Andreas Fault to provide water storage for the city in the case of a rupture of the tunnel crossing the fault.

- A new trunk line with high strength pipe and joints was constructed in the Mission Hills fault area to increase the redundancy of the water supply.
- The Terminal Hill Tunnel on the Second Los Angeles Aqueduct (under design) will be constructed with
 - enough space between the inside pipe and outer tunnel to accommodate the design rupture displacements and allowing access after earthquakes,
 - protective pipe coating to protect against spalled off concrete segments
 - emergency shut-off by automatic valve operation.

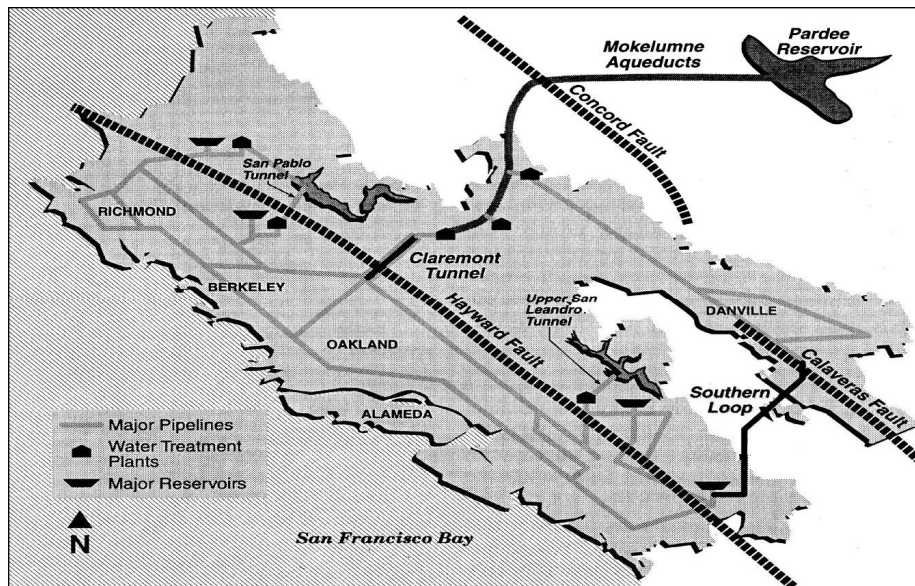


Fig. 7.1: East Bay Municipal Utility District with its main reservoir Pardee and the Southern Loop in the right bottom part of the figure, from Hamada (2003) after Diemer (1998).

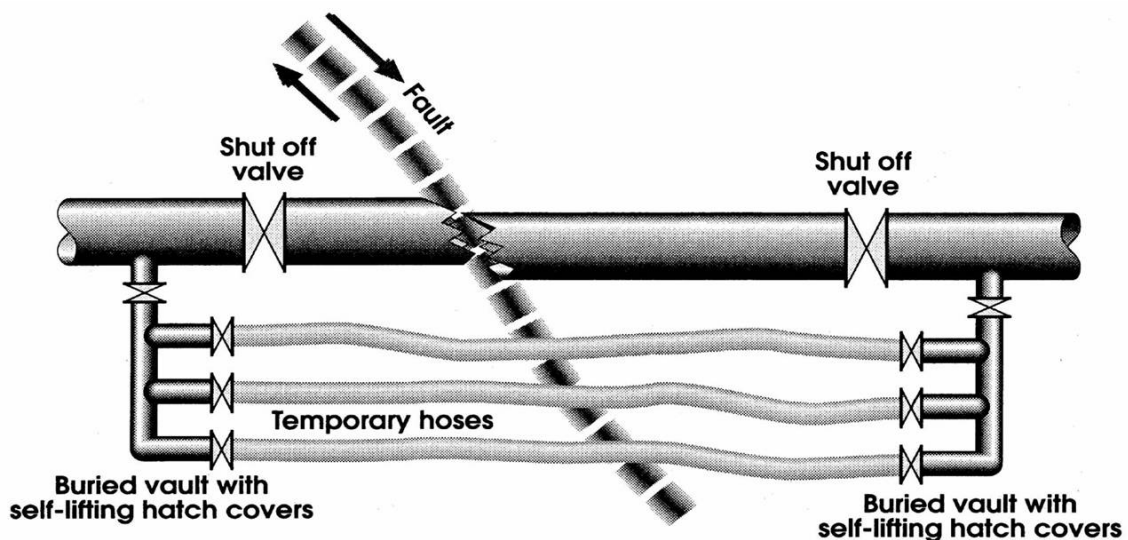


Fig. 7.2: East Bay Municipal Utility District redundancy measures for fault crossing pipe line from Hamada (2003) after Diemer (1998)

7.3 TOKYO, JAPAN – SAKHALIN, RUSSIA PIPELINE

Location: off-shore, Shirako, Chiba, Japan

The Japan-Sakhalin Gas Pipeline under design in 2003, connects the Russian Sakhalin islands with the Tokyo area through the Japan sea, crossing the Hokkaido Island (Japan) and the Pacific Ocean as shown in **Fig. 7.3**.

With 1100 km total length of which about 1,000 km is offshore and the rest on land. Steel pipes of 65 to 70 cm diameter resting on the seabed or buried in the ground in the active seismic zone along the Pacific Ocean can deliver about 800 million cubic feet natural gas per day. Even though the route of the pipeline was basically selected not to cross any active faults it was found after a more detailed route survey that the designed pipeline route crosses three active faults. The pipeline crosses an active normal fault (**Fig. 7.4**) off Chiba prefecture, where an approximately 2 meter vertical seabed deformation was observed and the average displacement rate has been estimated 22cm/1000 years. **Fig. 7.4** gives only information about the vertical fault movement; Information about movement in the horizontal direction is not available from the route survey.

An FEM analysis with shell and infinite elements of the pipe-soil-fault interaction for a fault displacement of 5 meters resulted in a maximum strain of about 1.5% which is less than the current design code's allowable strain.

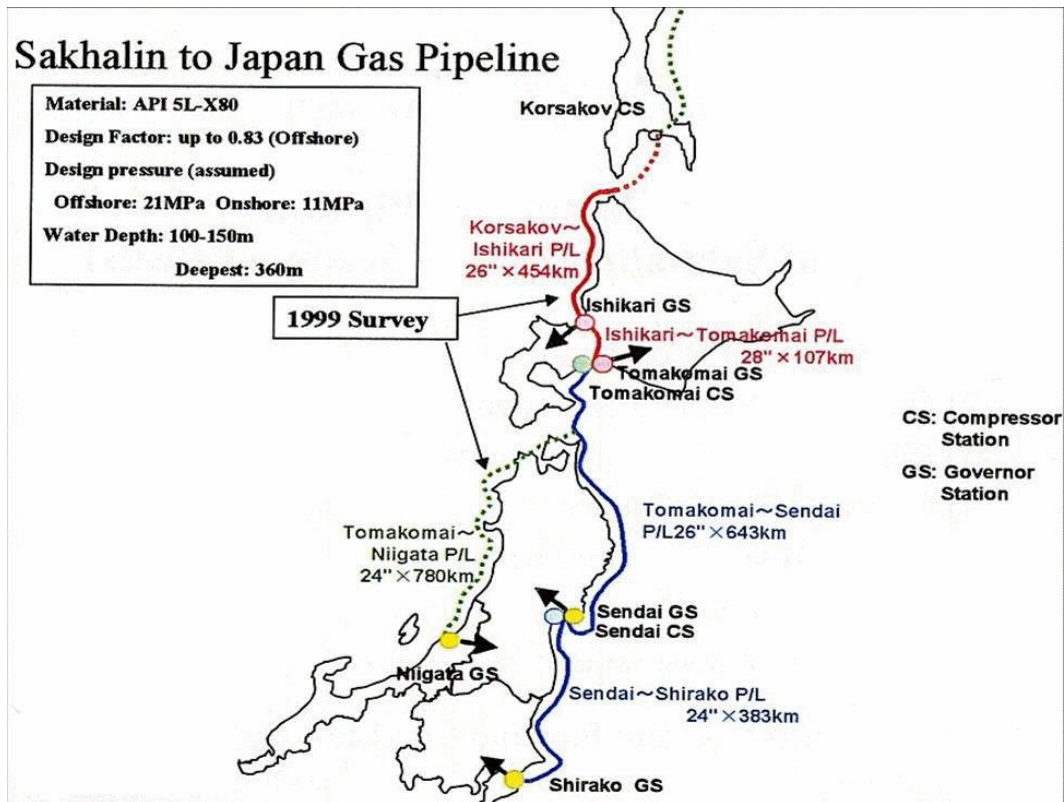


Fig. 7.3: Gas pipe line between Tokyo, Japan and Sakhalin islands, Russia after Hamada (2003)

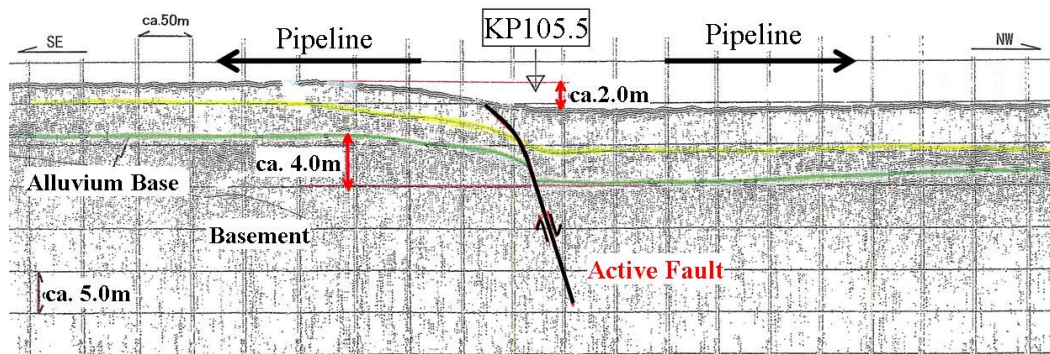


Fig. 7.4: The pipe line crosses an active normal fault off shore of Chiba prefecture to the east of Tokyo after Hamada (2003)

7.4 COUNTERMEASURES FOR SHINKANSEN (bullet train) STATION AND BRIDGE

Location: 34° 42'24"N, 135° 11'46"E

During excavation for the construction of the foundation of the Shinkansen Shin-Kobe station an active fault was found as shown in figures 22 and 23. However, it was impossible to change of the location of the station and of the route because of the limited construction space and time. The vertical fault movement was estimated to more than 0.7 meters during the last ten thousand years from geological inspections and the possible fault movement during the lifetime of the elevated bridges was estimated to less than 5cm. In order to allow for this fault movement, movable shoes with a maximum displacement capacity of 15 cm were installed between the platform structures and railway bridges as shown in **Fig. 7.7**.

Furthermore, the platform slabs were connected to the concrete piers with hinges to allow for vertical and rotational displacements and to reduce structural damage. The behavior during the 1995 Kobe earthquake was not reported on.

Another shinkansen example is a steel truss bridge crossing the Fuji river strike-slip fault in Shizuoka prefecture. The designers calculated the bridge deformation due to the estimated fault movement and assumed buckling of certain members. Spares were fabricated and stored in the vicinity of the bridge.

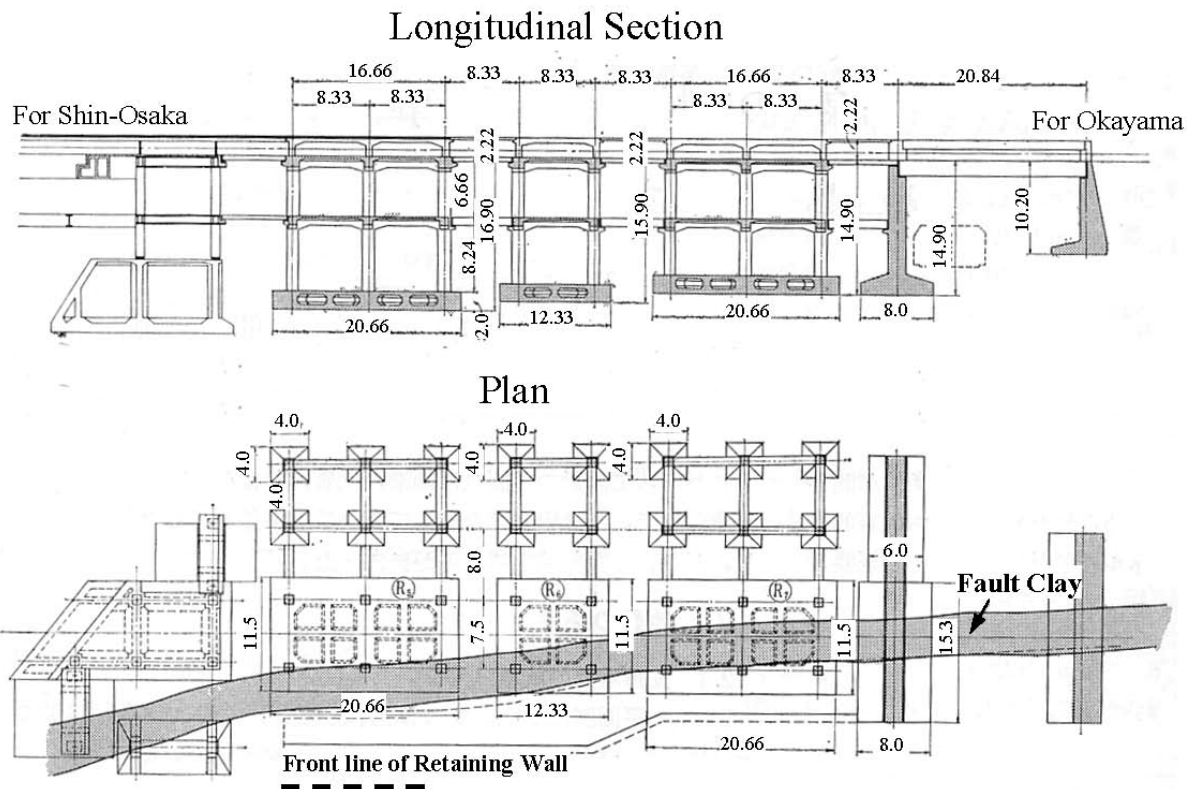


Fig. 7.5: Drawing of Shin-Kobe station showing the location of fault clay, from Hamada (2003) after Morishige (1970)

Conclusions in Hamada's paper

Hamada concludes that for lifeline networks such as water, sewer, gas and electricity which are generally distributed in a wide area it seems impossible to escape from all fault crossings. Furthermore, in the case of railway and highway it is difficult to change the route when the active faults were found during the construction, because of the financial and social problems.

Because of thick alluvial and diluvial deposits in Japan the identification of locations and magnitudes of the fault-induced ground surface ruptures with enough accuracy is difficult. Therefore, it does not seem realistic to restrict the construction of the lifeline networks by public regulations.

He also writes that it is almost impossible to avoid any damage to structures against large ground surface ruptures. However, in the case of lifeline systems such as water, electricity and gas, it is possible to increase the redundancy of the network and to develop system and facilities which can be easily and quickly restored having been damaged or destroyed by the ground deformation.

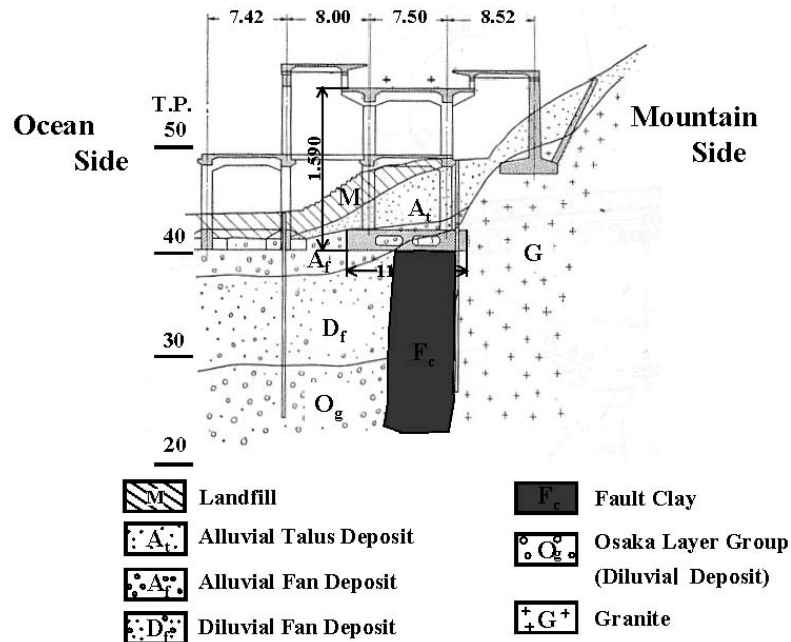


Fig. 7.6: Cross section of Shin-Kobe station showing the location of fault clay from Hamada (2003) after Morishige (1970)

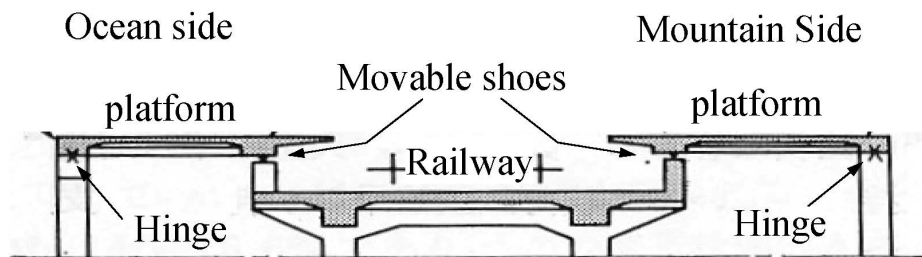


Fig. 7.7: Drawing of Shin-Kobe station showing the location of fault clay from Hamada (2003) after Morishige (1970)

7.5 FREEWAY PROJECT SAN BERNARDINO, CALIFORNIA, 2002

Location: 34° 08' 43"N, 117° 19' 09"W

Gloyd et. al. (2002) gives an interesting example of a freeway project San Bernardino, California, in which historical evidence of both vertical and horizontal ground fault ruptures was found while trenching during the final design phase. A state-of-the-art combination of deterministic and probabilistic (see Youngs (2003) for a discussion on PFDHA) approach was taken.

The paper gives hands on detail on how the estimated future displacement along the fault ruptures are dealt with in different load cases when designing several new bridges located in the area. Figure 43 shows different type of loading mechanisms due to a longitudinal and vertical fault displacement and how they cause hinges in the superstructure. Here follows a list of the design considerations for different parts of the structure as given in Gloyd et al (2002).

- Superstructures
 - Take advantage of inherent displacement and flexural capacity of well-detailed, ductile concrete members. Strengthen and/or detail critical superstructure regions for additional demands caused by vertical displacements.

- Strengthening measures can include additional mild steel reinforcement, increased pre-stress force, thickened slabs and girders and increased concrete strength
- If it is not practicable to provide sufficient strength to resist the flexural demands elastically, then adequate ductility must be ensured by proper detailing and verified with a ductility analysis
- Measures to increase ductility can include thickened slabs with seismic ties to enhance confinement and including mild steel reinforcement in top and bottom slabs
- Consider using secondary systems to support dead load of superstructure
- Column Design
 - Consider the horizontal displacement demands from ground shaking in combination with the demands from the surface displacements from fault rupture.
 - Consider the effects of the vertical displacements on the columns in the form of increased axial loads and moment demands from the superstructure.
 - Consider the effects of tension demands on the columns from uplift of the superstructure at adjacent support, or downward vertical displacement of the ground beneath the column. These effects include reduced shear and moment capacity.
 - Consider rotational demands on the columns from horizontal displacements at the footing or within the pile group.
 - Consider demands on bent caps from vertical column displacements; If possible use only 2 column caps reduce possible increase in flexural demands
- Abutments
 - Providing additional seat width to accommodate the increased displacement demands from the fault rupture event and
 - Designing the abutment for increased vertical forces from uplift of the abutment or downward displacement at the adjacent support.

They conclude that with the above the design they feel the bridges can be designed to accommodate displacement demand due to a fault surface rupture but the best solution is still to avoid construction nearby a fault if possible.

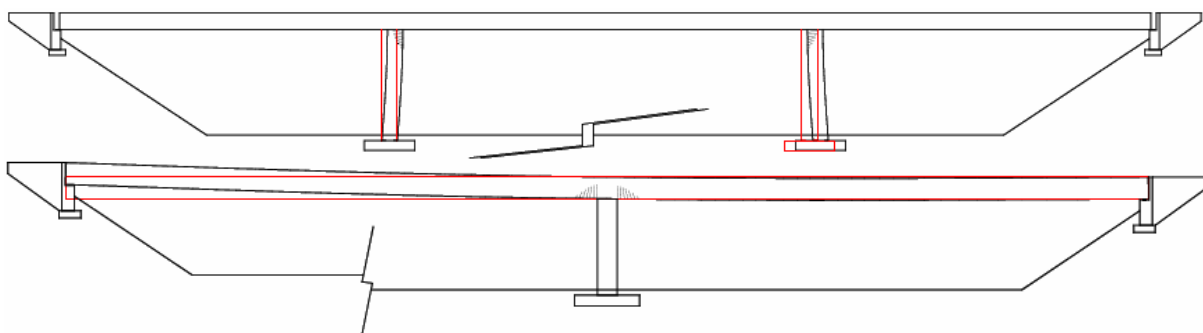
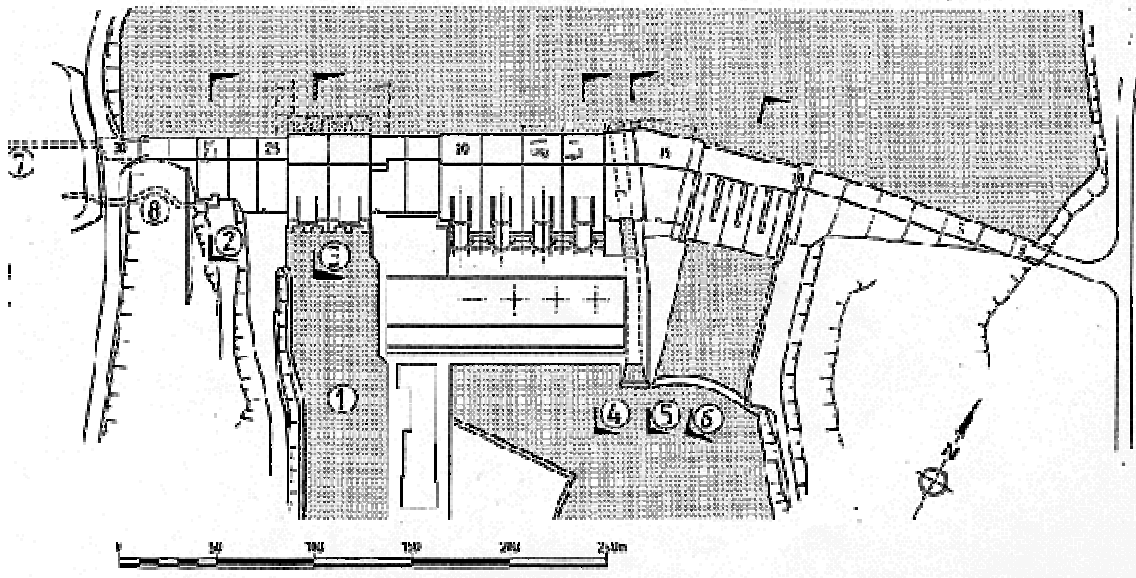


Fig. 7.8: Two different mechanisms introduced by longitudinal and vertical fault displacements after Gloyd et al (2002)

7.6 CLYDE DAM IN NEW ZEALAND, after Hatton et al (1987) and Hatton et al (1991)

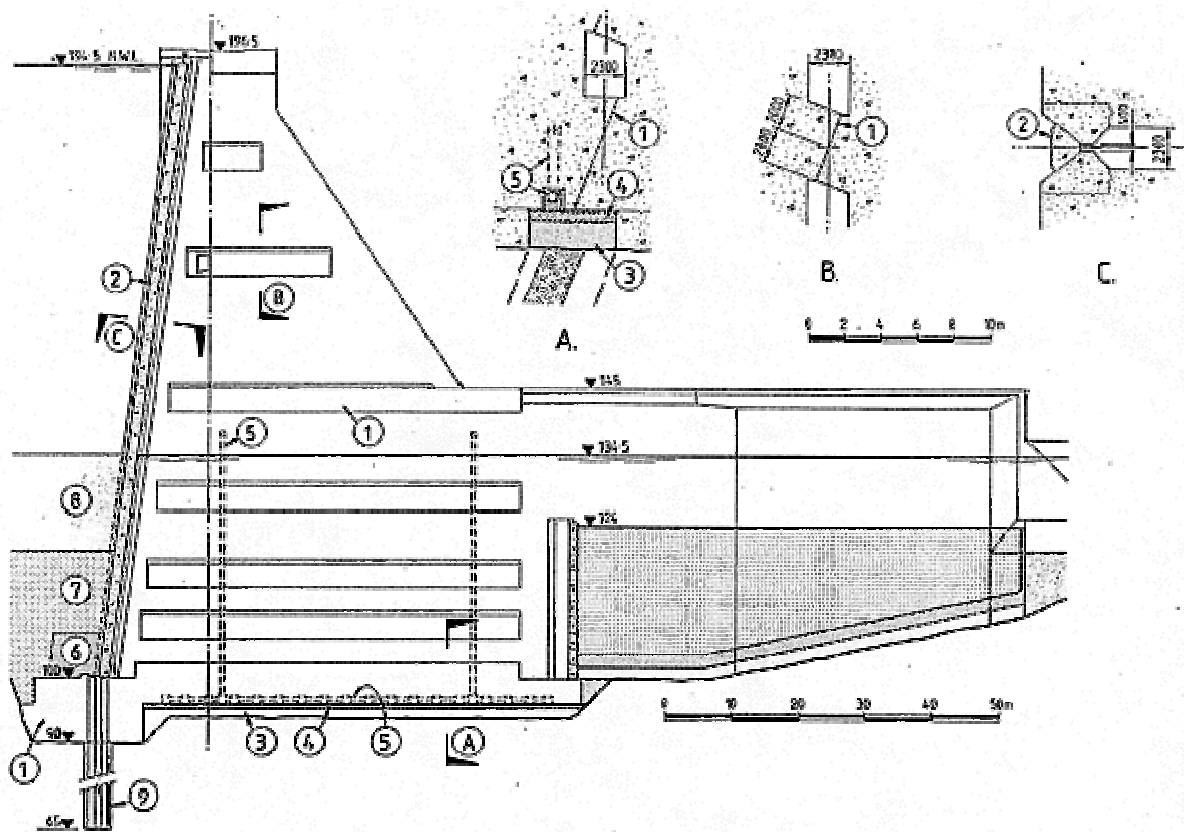
Location: 45° 10' 47"S, 169° 18' 19"E

A 100 meter high concrete gravity dam was completed at the end of 1980's at the city of Clyde on the Clutha river on the South island of New Zealand (**Fig. 7.9**). The dam is located at the exit of the Cromwell Gorge at the southern end of the Dunstan mountain range. Evidence exists of late quaternary deformation, some 3000-5000 years ago, along segments of the Dunstan fault which nearest segment is 3 km from the dam. A major rupture on this fault could produce a magnitude 7.0-7.5 (Ms) with up to 0.55g accelerations at Clydel and some 0.2 m accompanying secondary movements of the River Channel fault which crosses the dam site. This fault, which is probably a normal dis-slip fault with left lateral component has moved before and such movements on the fault could have detrimental effects on the dam. To this end a slip joint, with a wedge plug for water tightness, (**Fig. 7.10**) that can accommodate 2 meter lateral and 1 meter dip-slip displacements was introduced in the dam above the fault. In the event of movement on the River Channel fault the wedge plug on the upstream side can move to limit the flow through the joint. The opening of 0.4 meter shown in the detailed **Fig. 7.11** is necessary to allow for a possible reverse fault movement. To prevent possible erosion of the fault material, filter and drainage system installed along the fault beneath the dam blocks



- | | | |
|-------------------------|------------------------------|--------------------------------|
| 1. Diversion channel | 2. Right abutment section | 3. Diversion block section |
| 4. Intake block section | 5. River Channel Fault joint | 6. Spillway and stilling basin |
| 7. Grouting Adit | 8. Drainage Adit | |

Fig. 5.6: Clyde dam with a slip Joint against Fault Movement in New Zealand



- | | | |
|---------------------|-----------------------------|-----------------|
| 1. Contact surfaces | 2. Wedge plug | 3. Filter zone |
| 4. Drainage zone | 5. Drainage pipe | 6. Riprap |
| 7. Gravel blanket | 8. Low permeability blanket | 9. Cutoff shaft |

Fig. 7.10: River channel fault slip joint

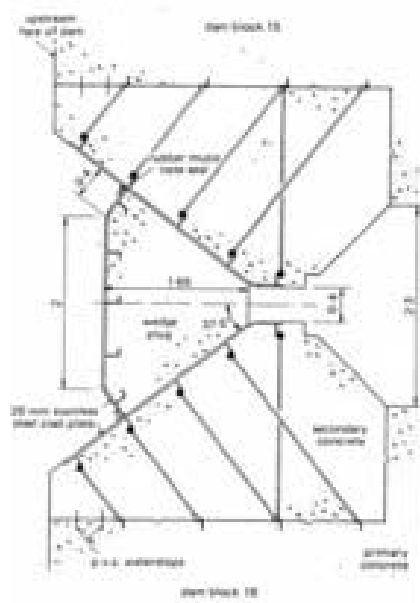


Fig. 7.11: Details of the wedge plug of Clyde dam slip joint

7.7 FLEXIBLE ALASKAN PIPELINE

Location: 63° 23'00"N, 145° 44'00"E

Earthquake: Nov. 3, 2002, Denali Fault Earthquake, USA, M=7.9

There have been several studies on pipe line interaction with faults going back to the designs of the Trans-Alaskan pipeline (Newmark and Hall, 1975). A comprehensive compilation O'Rourke and Liu (1999) contains many design criteria and procedures and references to earlier work. A recent study suggests a new simplified design Takada et al (2001) and a search in the proceedings of the 13th World Conference on Earthquake Engineering results in some 30 papers though there are only a few that considers dip-slip faulting (one example given in the next section).

Though pipeline fault interaction is only partially related to the current study this section was included because of the great performance of the Trans-Alaskan pipeline during the Denali fault earthquake showing that through thorough geological investigations and clever design, important lifelines can be constructed to survive a large fault induced deformations (**Fig. 7.12**).

The 7.9M_w earthquake that occurred in south-central Alaska on November 3, 2002 ruptured an approximately 350-km long segment along Susitna Glacier, Denali, and Totschunda faults shown in figure 46. The epicenter is located about 88 km west of the Trans-Alaska Pipeline which were subjected to violent ground shaking approaching or exceeding design criteria, and liquefaction was observed at a number of locations along the pipeline. At the fault crossing the pipeline displaced over 5 meters laterally and almost 1 meter vertically (see **Fig. 7.13**). Despite these severe loading conditions there was only minor damage to the pipeline and it performed as designed and no oil was spilled. This excellent performance was due to accurate and conservative ground motion estimates, accurate and conservative fault displacement parameters, and innovative structural design.

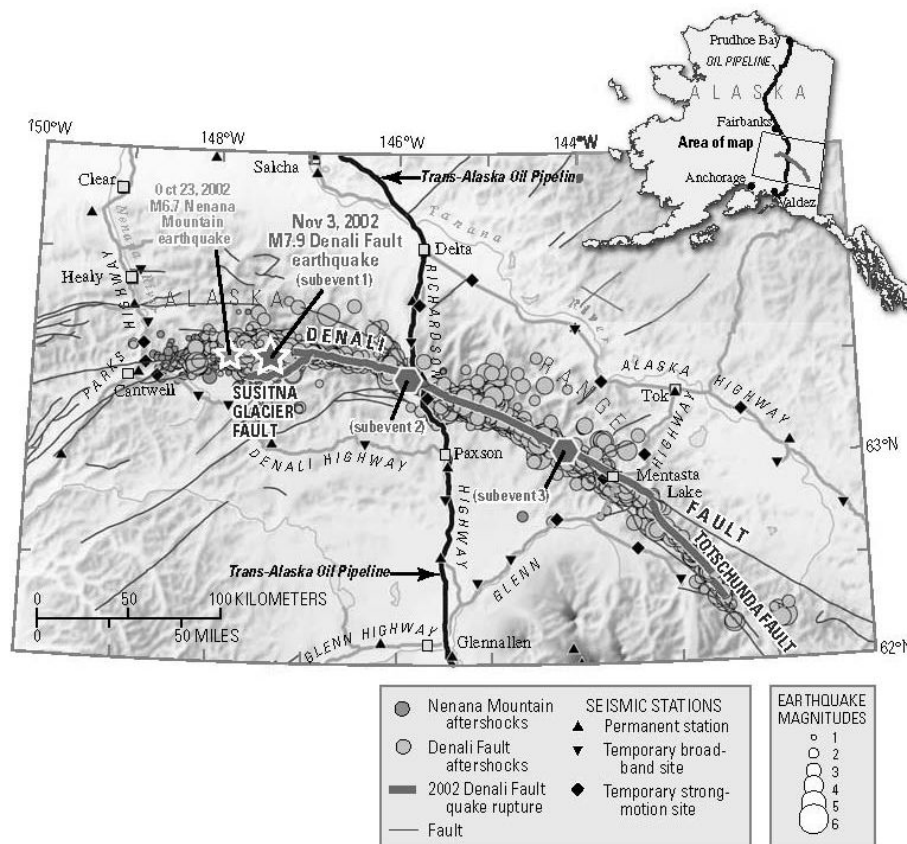


Fig. 7.12: Overview of the Susitna thrust fault (earlier unknown), and the Denali and Totschunda strike-slip faults after USGS (2003)

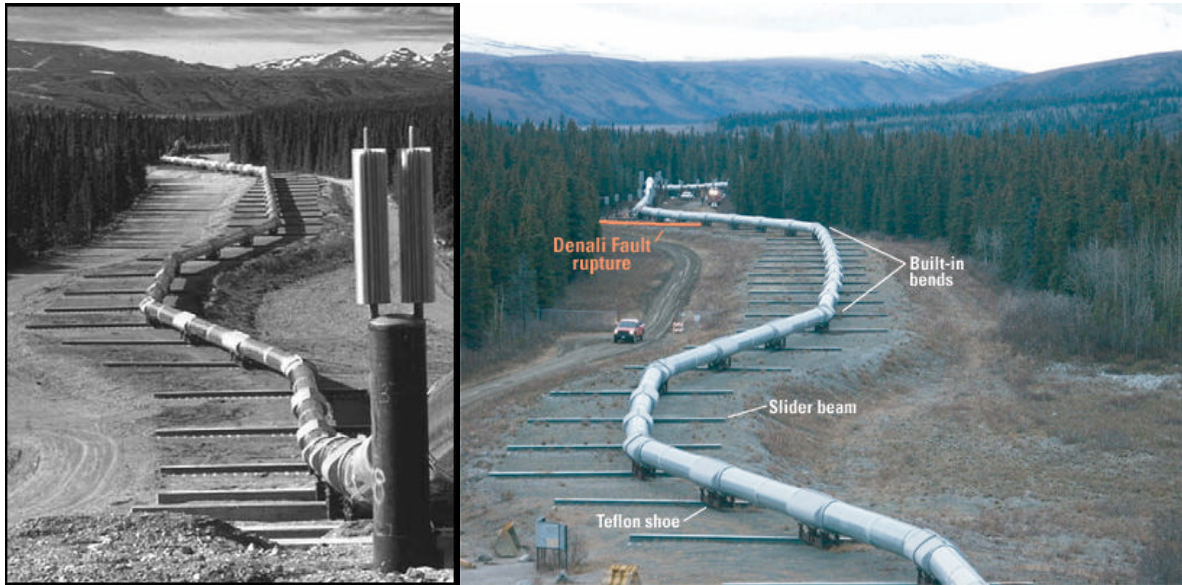


Fig. 7.13: Trans-Alaskan pipeline at the Denali fault crossing (Hall et al., 2003)
Photo right: US Geological Survey Fact Sheet 014-03 (2003)

REFERENCES

- Bray, J. D. (2001). "Developing mitigation measures for the hazards associated with earthquake surface fault rupture," *Seismic Fault Induced Failures*, Workshop, JSPS (Konagai, K., Hori, M. and Meguro, K., eds.), 55–80.
- Diemer, D. (1998). "Anti-seismic measures on water supply in California," *Proceedings of IWSA International Workshop on Anti-Seismic Measure on Water Supply*, 1–21.
- Gloyd, S., Fares, R., Sanchez, A. and Trinh, V. (2002). "Designing ordinary bridges for ground fault rupture," *Proceedings of third national conference & workshop on bridges & highways*.
- Hamada, M. (2003). "Measures and designs of lifelines against fault-induced ground surface ruptures," *Seismic Fault Induced Failures*, Workshop, JSCE (Konagai, K., Hori, M., Meguro, K. and Koseki, J., eds.), 119–130.
- Hatton, J. W., Black, J. C. and Foster, P. F. (1987). "New Zealand's Clyde power station," *Water power & Dam Construction*, 15–20.
- Hatton, J. W., Foster, P. F. and Thomson, R. (1991). "The influence of foundation conditions on the design of clyde dam," *16th Conference on large dams*, 157–177.
- Newmark, N. and Hall, W. J. (1975). "Pipeline design to resist large fault displacement," *Proceedings U.S. National Conference on Earthquake Engineering*, ASCE Technical Council on Lifeline Earthquake Engineering, 416–425.
- Morishige, R. (1970). "A special construction of sanyo shinkansen," *Bulletin of The Design Office of Japan National Railway*, 23.
- O'Rourke, M. J. and Liu, X. (1999). "Response of buried pipelines subject to earthquake effects," *MCEER Monograph*, 3, Multidisciplinary center for Earthquake Engineering Research.
- Takada, S., Hassani, N. and Fukuda, K. (2001). "A new proposal for simplified design of buried steel pipes crossing active faults," *Earthquake engineering and structural dynamics*, 30, 1243–1257.
- U.S.G.S (2003). "Rupture in south-central Alaska - the Denali fault earthquake of 2002," *USGS Fact*

Sheet 014-03, 4.

Youngs, R. e. a. (2003). “A methodology for probabilistic fault displacement hazard analysis (pfdha),”
Earthquake Spectra, **19(1)**, 191–219.

Chapter 8

KEY POINTS FOR RATIONAL DESIGNS

8.1. INTRODUCTION

One of the important aims of this JSPS project was to discuss the possible measures for minimizing losses of life and damage to a variety of structures, and it was timely that the Japan Geotechnical Society (JGS) organized “Technical Committee for Fault-related Geotechnical Issues about Civil-infrastructures”. The following keywords symbolize the essence of the discussions made among both the JSPS project members and JGS Technical Committee members.

8.2. SEQUENTIAL APPEARANCE OF THRUST FAULT RUPTURE PLANES

Key parameter: $\theta - (\pi/4 - \phi/2)$, where θ = dip angle of bedrock wedge, and ϕ = either internal friction angle or dilation angle of its overburden soil.

Fault zoning is inevitable because few structures can sustain the deformations induced by a fault rupture. On the other hand, complete restriction of development within a fault zone is too much conservative and impossible in reality. In California, USA, a law to restrict developments within fault hazard zones has been enacted since the early 1970s. The ‘Alquist–Priolo Fault Zoning act’ (California Geological Survey, 2002) requires the State Geologists to establish regulatory zones (Earthquake Fault Zones) around the surface traces of active faults. Before a project is permitted, a geological investigation is required, and the construction of a building is permitted only if the building is located more than 50 feet off a fault trace. A similar zoning act has been enacted in Auckland, New Zealand (Wellington Regional Council, 2002).

It is, however, noted that these laws in California and New Zealand deal with strike-slip faults, while about two thirds of active faults in Japan are thrust faults. As contrasted with strike-slip faults, a bundle of thrust faults make up a ‘wider brush’ with many fault traces hidden in areas off the most suspicious line recognized from surface configuration.

This can be due to the fact that a fault rupture plane propagated up through overburden soil strata meets the ground surface at some different angle from the dip of its bedrock wedge. Cole and Lade (1984) conducted a series of experiments on dense and loose sand in a glass-walled fault test box to investigate the shapes and locations of failure surfaces that may occur in alluvium overlying active dip-slip faults. Analogue models are representative of a natural prototype if they are properly scaled and if the materials used show a similar rheological behavior as the natural prototype. This requires the proper scaling of surface forces (stresses) in relation to body forces (due to gravity). Sands have been considered to be appropriate materials for describing prototype rocks with quite small contribution of cohesions to overall shear strength. Cole and Lade reported that a rupture plane propagates from the

thin end of its bedrock wedge along the upper extension of the wedge's dip and meets the surface at about $45^\circ + \phi/2$ for active conditions and $45^\circ - \phi/2$ for passive conditions. The angle ϕ can be the internal friction angle of the soil in consideration of static equilibrium. However, Cole and Lade suggested that it is rather closer to the dilation angle.

Ueta [8] suggested that the appearing sequence of rupture planes could depend largely on the relation between ϕ and the dip-angle, θ , of the distinct bedrock wedge. For this reference, Fig. 8.2 shows bedrock fault wedges, which cut in the surface soil models, shoot several rupture planes (shear bands) up through the soils [9,10]. Among these rupture planes, those formed in the earlier stage die out before reaching the ground surface; while those formed in the later stage, where the bedrocks are closer to the ground surface, reach the ground surface in such a way that the plane meets the ground surface at about an angle of $\pi/4 - \phi/2$. Therefore, as the difference between bedrock wedge angle θ and $\pi/4 - \phi/2$ becomes larger, newly formed rupture planes will branch further off the older ones, and eventually a bundle of rupture planes make up a wider brush. Moreover, the appearing sequence of rupture planes could depend largely on the relation between ϕ and θ (Fig. 8.2).

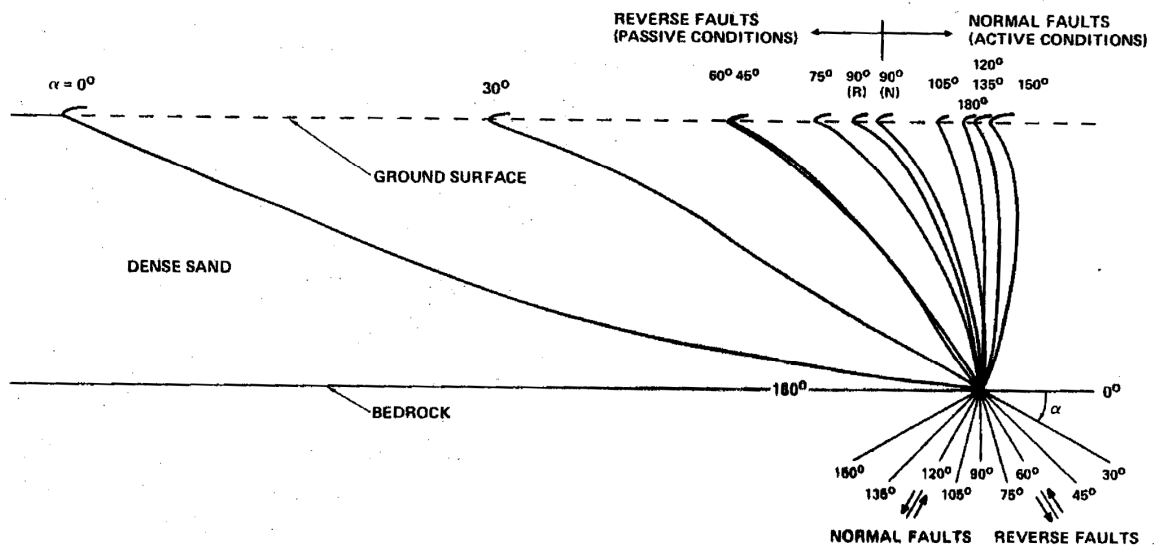


Fig. 8.1: Line drawings of primary failure surfaces observed in tests on dense sand (Cole and Lade, 1984):

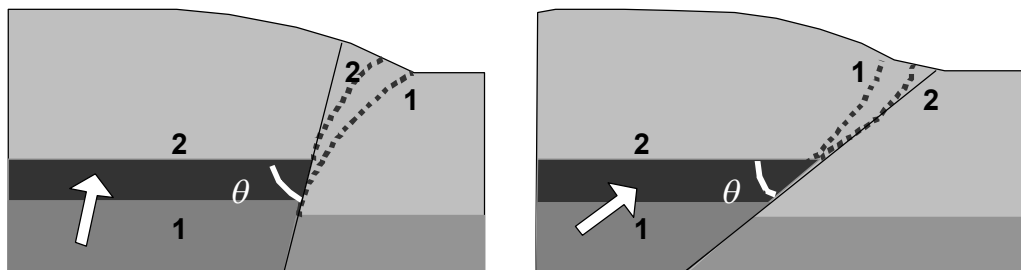
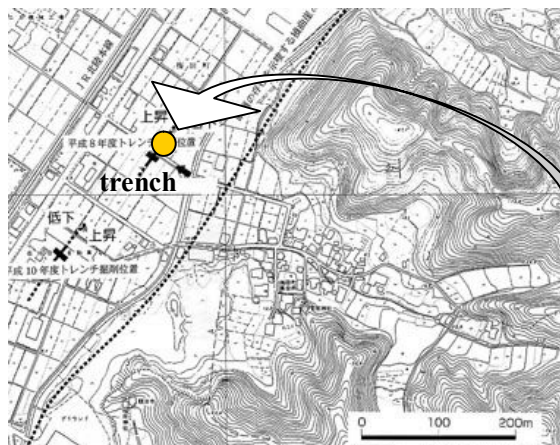


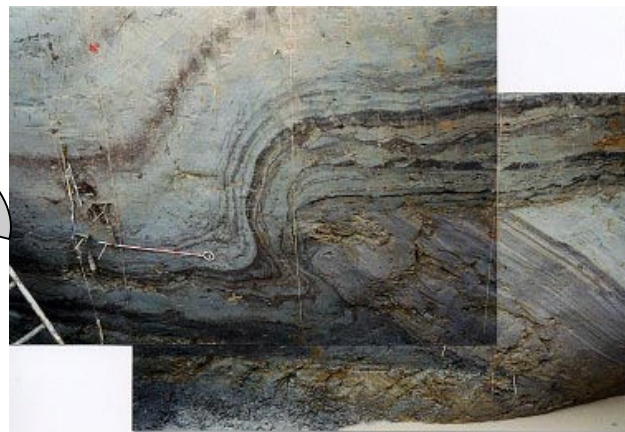
Fig. 8.2: Possible appearing sequence of fault rupture planes (after Ueta, 2003).

Fig. 8.3 shows the location of a newly found Morimoto fault trace and photos of a trench excavated across it. The fault was found about 100 m off the estimated linear boundary (broken line in **Fig. 8.3(a)**) between the Kanazawa plain and its eastern hills. A base mud rock is cutting sharp into an overlying soft soil deposit, while the soil deposit is gently bent over the base rock wedge. Before the trench excavation, there was no clear evidence on the ground surface indicating the presence of this hidden fault. It is noted here that the right-hand side of the base rock (hanging wall) that had pushed about 1 m up into the surface soil deposit was not on the mountain side but on the flat land side. Assuming that a soil wedge was pushed up and we were looking at just one side of the wedge, this fact suggests the presence of another new fault hidden further away from the mountains, and actually, this new fault was found in 2001 about 500m off the mountains (Nakata and Imaizumi, 2002). This indicates that the width of 300m for the Fault Hazard Zone may not be wide enough.

From these mentioned above, a thrust fault zone, along a boundary between mountains and a flat land, may be determined in such a way that **“the zone shall cover about several hundreds meters wide the flat land with the fault trace put aside along the zone’s edge”**. This does not necessarily mean the exterior area on the mountains side is safer than that on the flatland side. As for intense shakes are concerned, it is quite often that the shake is very intense on the hanging wall side. It is also to be noted that soft soil deposits are often responsible for amplifying base input motions. “Earthquake Fault Zones” are just for accounting for considerable deformations of soils.



(a) Location of a fault trace found 100 m off the estimated linear boundary (broken line) between the Kanazawa plain and its eastern hills



(b) South trench wall (Photo by Sangawa)



(c) Trench walls showing seaside-up movement (Photo from Ishiwatari, A., <http://earth.s.kanazawa-u.ac.jp/ishiwata/labo/morimotoUS.html>)

Fig. 8.3: Trench excavated across Morimoto fault (N36 37'28", E136 42'15")

8.3. SOIL STRAIN PAPERETER DETERMINING RESTRICTION LEVEL

Key parameter: $\zeta = D/\gamma_y H$, where D = dislocation of the base rock, γ_y = soil's failure strain and H = thickness of the soil deposit.

As a bedrock rupture propagates up through overlying soil material, strains will spread and decrease. The overall strain induced within the surface soil deposit will be represented by D/H where D = dislocation of the base rock and H = thickness of the soil deposit. If the material is brittle, the distance that the base rock rupture propagates will be large, while in a soft overlying material strains will be absorbed. Thus, comparing D/H with the soil's failure strain γ_y will provide necessary information for possible remedial measures for fault-inflicted damage to civil infrastructures. Bray (1994) found through both his numerical and experimental studies that at a specified amount of bed rock fault displacement, the height that the shear rupture will propagate up into the overlying soil can be related to the failure strain of the soil as shown in **Fig. 8.4**. The curve in **Fig. 8.4** seemingly exhibits some hyperbolic feature, and the product of the normalized height H/D by the soil's failure strain γ_y is about 100%. This means that the shear rupture reaches the overlying ground surface when $\zeta (= D/\gamma_y H)=1.0$.

The parameter $\zeta = D/\gamma_y H$ thus can determine the restriction levels for projects in a fault zone.

As for important civil infrastructures, numerical simulations are necessary to ensure that the restrictions and/or measures taken will be effective.

A possible D value may be determined from either:

- (1) the maximum credible dislocation observed at nearby trenches, outcrops etc., or
- (2) the possible maximum dislocation of an asperity that has ever been estimated for an event in the concerned fault system.

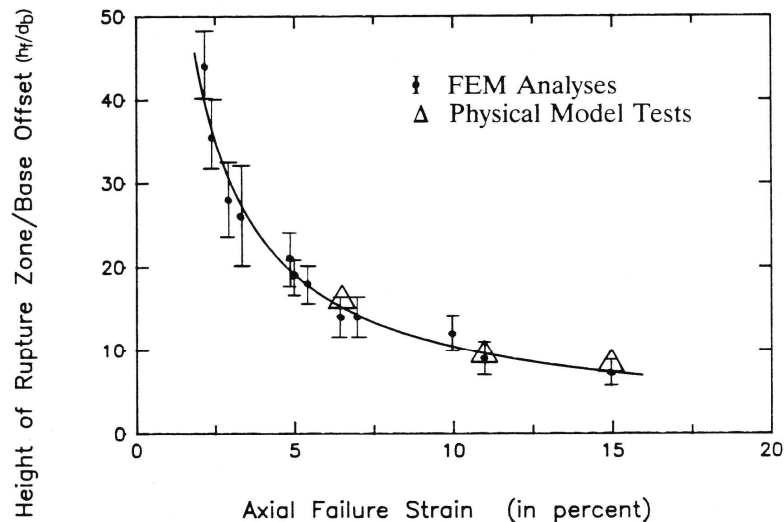


Fig. 8.4 Normalized height of shear rupture zone in soil overlying base rock fault as a function of soil's failure strain (after Bray et al. 1994)

8.4 SEQUENCE OF DYNAMIC AND STATIC SOIL DEFORMATIONS

As has been described in Chapter 2, the Bauweishan section of the Highway #3 suffered seismic fault dislocation during its construction. Some pile caps sustained their piers, while the others did not. Many piles loaded with piers were cracked around their top ends immediately beneath their caps, while those without piers did not suffer serious cracking at their top ends (Figs. 8.5 and 8.6). For the latter piles, clusters of major cracks were found rather deeper locations, which were closer to the boundary between the deeper clay layer with sheared marks and shallower and stiffer soil sediment above it (Fig. 8.6). This fact suggests that the piles bearing superstructures can be cracked due to inertia forces from their superstructures, while for those without superstructures, soil deformations can be the major cause of cracking (kinematic interaction).

Taking into account fault rupturing process, the piles could have experienced dynamic inertia interaction first, which was then followed by rather slow kinematic interaction due to fault-induced large soil deformation (see Fig. 8.7). Eventually pile-cap interface cracked due to the inertia interaction can be moment-free, and the pile cap will be moved by the piles experiencing slow and steady soil deformations. To discuss possible pile caps movements near a seismic fault, which movements can affect the function of their viaduct; due attentions should be paid to this scenario.

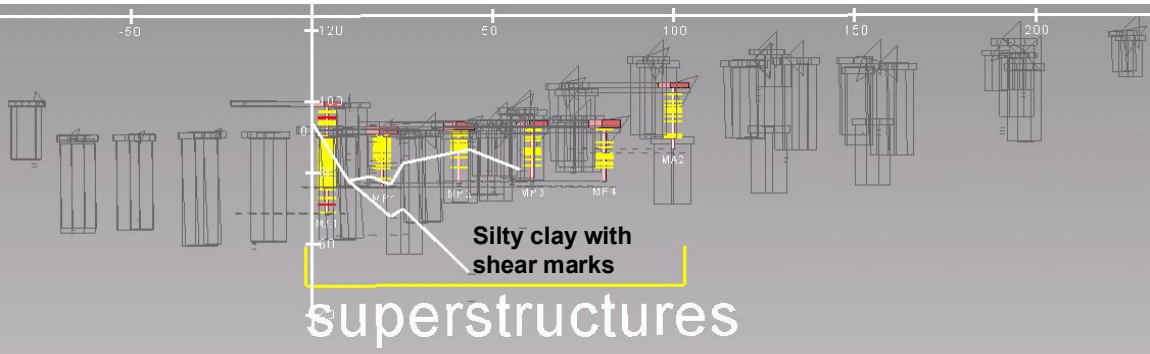


Fig. 8.5 (same as Fig. 2.17): Location of cracks in cores from piles for the main viaduct piers and abutments looking from south to north in the direction of along the estimated fault trace: Cracks are densely distributed within the surface stratum of natural sand and gravel covered up with fills from the time of construction. These piles sustained piers when the Chi-Chi Earthquake occurred.

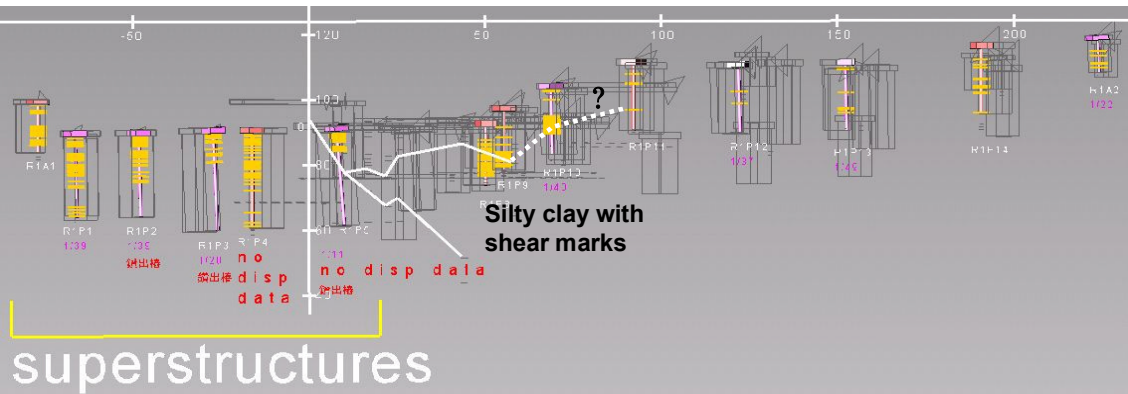
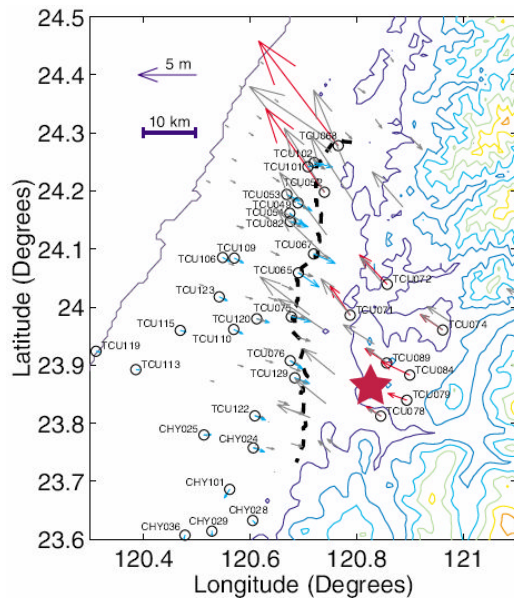


Fig. 8.6 (same as Fig. 8.17): Location of cracks in cores from piles for the Ramp #1 viaduct piers and abutments looking from south to north in the direction of along the estimated fault trace: It is remarkable that piles near the estimated fault, regardless of their locations on either hanging wall side or foot wall side, were severely cracked. However those on the hanging wall side appeared rather deeper locations and seemingly close to boundary between the surface stratum and the silt-clay wedge with shear marks. Note those on the hanging wall side sustained no pier when the earthquake occurred.



Above: Peak integrated strong-motion displacement (red and blue arrows) and final GPS displacement (gray arrows). (Oglesby and Day, 2001).

Right: Acceleration Velocity and displacement time histories at TCU068, red circle in the map above. (Lee et al., 1999).

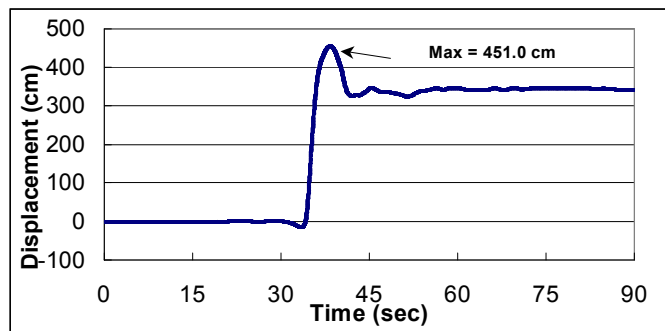
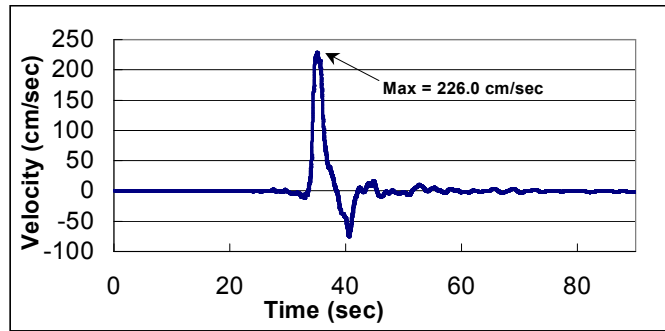
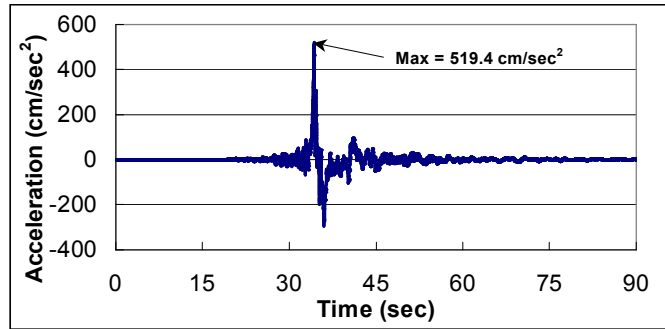


Fig. 8.7: Acceleration Velocity and displacement time histories of the record obtained at Shihkan (TCU068,) during the 1999 Chi-chi, Taiwan earthquake: Among many stations in Taiwan, TCU068 and TCU06 were located on the hanging wall at distances less than 1 km from the fault rupture plane. Though they were several tens kilometers north of Bauweishan viaduct, they show important features of near fault data on the hanging wall. The peak ground displacement (PGD) of 0.451m appears at 37.82s following the PGA of 519.4cm/s² at 34.12s and the PGV of 226.0cm/s at 34.88s.

8.5. ACTIVE LENGTH OF UNDERGROUND PIPES AND TUNNELS

As described above, an embedded foundation is often very flexible, and follows closely the motion of the surrounding soil. There will be an analogy between a tunnel crossing a fault and a pile subjected to a lateral loading (Fig. 8.8). Under lateral loading, the horizontal deflection of a pile decreases with increasing depth. In practice, most laterally loaded piles are indeed ‘flexible’ in the sense that they are not deformed over their entire lengths. Instead, pile deflections become negligible below an active length (or effective length) L_a . The active length, an important parameter in the design of a pile foundation, depends largely on the ratio of the pile stiffness EI (= number of piles grouped together $\times EI$ for a single pile) for flexural deformation and the soil stiffness G , and is proportional to $\sqrt[4]{EI/G}$. From Fig. 8.8, one can see that the pile cap displacement can correspond to the fault dislocation D applied to a tunnel. Thus, the overall strain induced within the tunnel will be represented by D/L_a . Necessary measures can be determined with this D/L_a as an index.

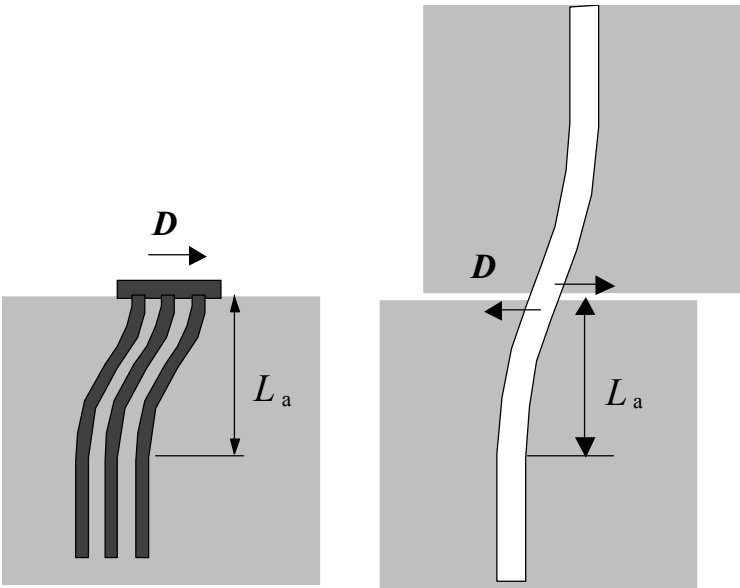


Fig. 8.8: Analogy between a pile foundation and tunnel subjected to fault dislocation (Konagai, 2004)

REFERENCES

- Bray, J.D., Seed, R.B. and Seed, H.B. (1994). "Analysis of earthquake fault rupture propagation through cohesive soil," *Journal of Geotechnical Engineering*, ASCE, **120(3)**, 562-580.
- California Geological Survey (2002). "Alquist Priolo Earthquake Fault Zones," California Department of Conservation, <http://www.consrv.ca.gov/cgs/rghm/ap/index.htm>.
- Cole, D.A. Jr. and Lade, P.V. (1984). "Influence zones in alluvium over dip-slip faults," *Journal of Geotechnical Engineering*, ASCE, **110(5)**, 599-615."
- Ishiwatari, A. (1998). "Morimoto fault," <http://earth.s.kanazawa-u.ac.jp/ishiwata/labo/morimotoUS.html>.
- Konagai, K.(2005). "Data archives of seismic fault-induced damage," *Soil Dynamics and Earthquake Engineering*, **25(7-10)**, 559-570.
- Lee, W. H. K., T. C. Shin, K. W. Kuo, and K. C. Chen (1999). CWB free-field strong-motion data from the 921 Chi-Chi earthquake, digital acceleration files on CD-ROM, prepublication version (December 6, 1999), Seismology Center, Central Weather Bureau, Taipei, Taiwan, Vol. 1.
- Oglesby, D.D. and Day, S.M. (2001). "Fault geometry and dynamics of the 1999 Chi-Chi (Taiwan) Earthquake," *Bulletin of the Seismological Society of America*, **91(5)**, 1099–1111.
- Ueta, K. (2003). "Evolution of Fault Systems and its Associated Geomorphic Structures: Strike-Slip and Dip-Slip Fault Model Test and Field Survey," *American Geophysical Union, 2003 Fall Meeting*, T22B-0507.
- Wellington Regional Council (2002). "Hazard management," <http://www.wrc.govt.nz/em/hazrep.htm>.

Appendix

BOREHOLE DATA AT BAUWEISHAN

A1.1 LOCATIONS OF BOREHOLES

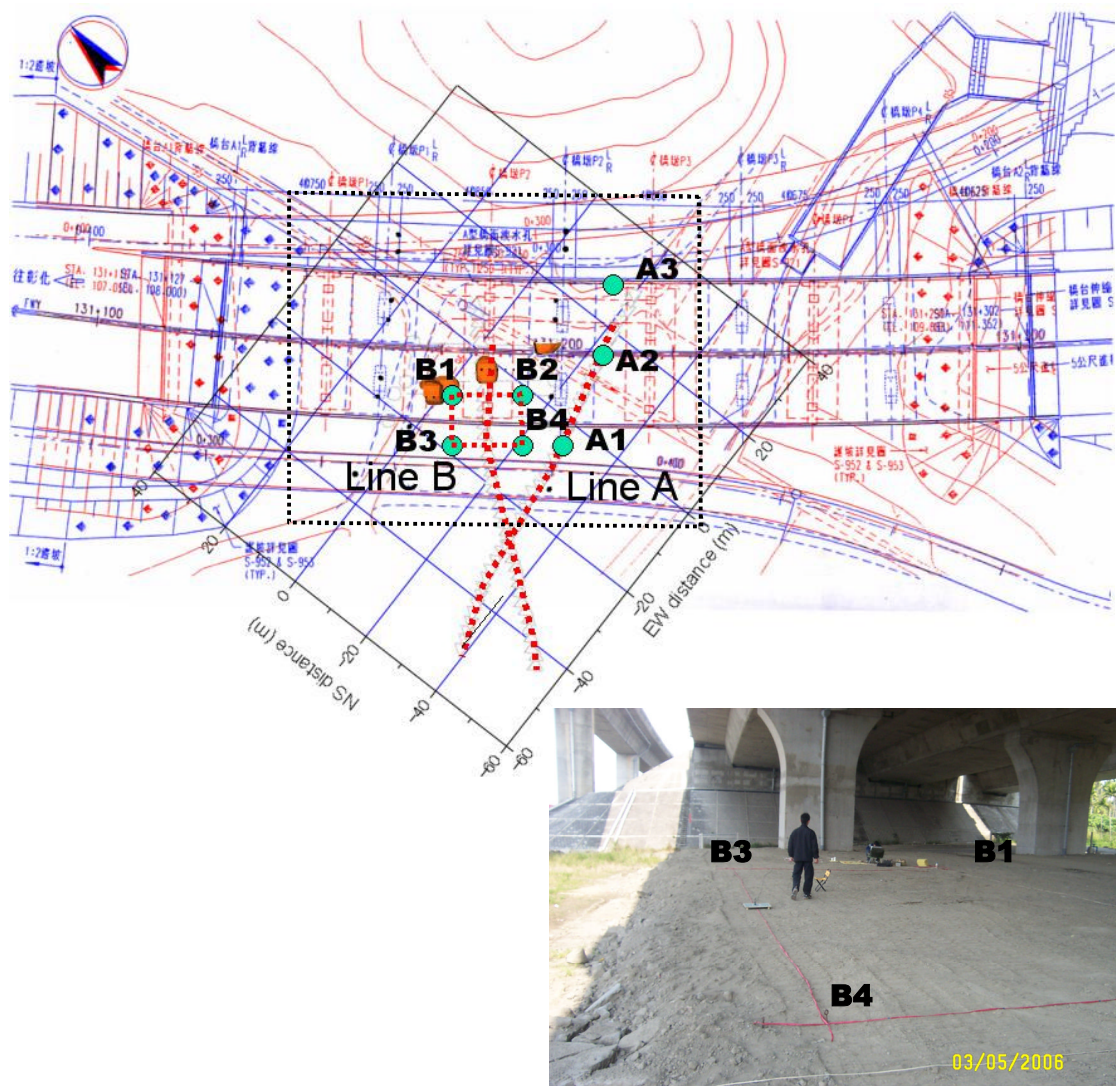


Fig. A1.1 (same as **Fig. 2.3**): Locations of boreholes: Red and blue drawings are original and post-earthquake plans of viaducts. Orange blocks immediately above are high electric-resistivity zones located in the electric resistivity tomography exploration.



Fig. A1.2: Borholings at A1, A2 and A3



Fig. A1.3: Borholings at B1, B2, B3 and B4

A1.2 BOREHOLE A1

Soil profile

Project: Baweishan Viaduct Geophysical Survey Plan

Bore No: A-1

Method: Percussion Drilling

Inclination: 90°

Total Depth: 31m

Water Level: GL-10.05m

Date: Jan.11.'06 ~ Jan .12.'06

SAMPLE NO	DEPTH (m)	CORE RECOVERY (%)	SPT DEPTH		N VALUE	WEATHER CONDITION	RQD (%)	GRAPHIC LOG	GEOLOGICAL DESCRIPTION
			BEGIN (m)	END (m)					
S-1	1	—	1.05	1.50	5+8+7	—	—	[Cross-hatched pattern]	0.0~2.9m Soil Filled
S-2	2	—	2.55	3.00	4+5+5	—	—		2.9m
S-3	3	—	4.05	4.50	3+3+4	—	—	[Dotted pattern]	2.9~10.7m Sandy silt, yellowish brown, with trace of gravels.
S-4	4	—	5.55	6.00	3+4+5	—	—		
S-5	5	—	7.05	7.50	2+3+3	—	—		
S-6	6	—	8.55	9.00	4+5+3	—	—		
	7	—				—	—		
	8	—				—	—		
	9	—				—	—		
	10	—				—	—		

W0: Fresh **W3: Highly weathered**
W1: Slightly weathered **W4: Completely weathered**
W2: Moderately weathered

Borehole No: A-1(sheet No: 1 / 4)

Project: Baweishan Viaduct Geophysical Survey Plan

Bore No: A-1

Method: Percussion Drilling

Inclination: 90°

Total Depth: 31m

Water Level: GL-10.05m

Date: Jan.11.'06 ~ Jan .12.'06

SAMPLE NO	DEPTH (m)	CORE RECOVERY (%)	SPT DEPTH (m)		N VALUE	WEATHER CONDITION	RQD (%)	GRAPHIC LOG	GEOLOGICAL DESCRIPTION
			BEGIN	END					
S-7	10.05	10.50	5+7+5	—	—	—	2.9~10.7m	Sandy silt, yellowish brown, with trace of gravels.	
	10.7	12.1					10.7~12.1m	Sandy silt or clay, grayish.	
S-8	11.55	12.00	3+3+3				12.1~17.3m	Siltstone, grayish.	
	17.3	26.4					17.3~26.4m	Mudstone, grayish.	

W0: Fresh **W3: Highly weathered**
W1: Slightly weathered **W4: Completely weathered**
W2: Moderately weathered **Borehole No: A-1(sheet No: 2 / 4)**

Project: Baweishan Viaduct Geophysical Survey Plan

Bore No: A-1

Method: Percussion Drilling

Inclination: 90°

Total Depth: 31m

Water Level: GL-10.05m

Date: Jan.11.'06 ~ Jan.12.'06

SAMPLE NO	DEPTH (m)	CORE RECOVERY (%)	SPT DEPTH (m)		N VALUE	WEATHER CONDITION	RQD (%)	GRAPHIC LOG	GEOLOGICAL DESCRIPTION
			BEGIN	END					
	21	—				—	—	17.3~26.4m Mudstone, grayish.	
	22	—				—	—		
	23	—				—	—		
	24	—				—	—		
	25	—				—	—		
	26	—				—	—		
	27	—				—	—	26.4~31.0m Gravel with sand, yellowish brown.	
	28	—				—	—	26.4m	
	29	—				—	—		
	30	—				—	—		

W0: Fresh

W3: Highly weathered

W1: Slightly weathered

W4: Completely weathered

W2: Moderately weathered

Borehole No: A-1(sheet No: 3 / 4)

Project: Baweishan Viaduct Geophysical Survey Plan

Bore No: A-2


Method: Rotary Drilling

Inclination: 90°

Total Depth: 50m

Water Level: GL-9.5m

Date: Jan.17.'06 ~ Jan .22.'06

SAMP LE NO	DEPTH (m)	CORE RECO- VERY (%)	SPT DEPTH		N VALUE	WEATHE R CONDI- TION	RQD (%)	GRA- PHIC LOG	GEOLOGICAL DESCRIPTION
			BEGIN	END					
			(m)						
	100					W0	100		7.8~42.4m Shear Zone.
	110					W0	100		
	120					W0	90		
	130					W0	100		
	140					W0	100		
	150					W0	90		
	160					W0	90		
	170					W0	80		
	180					W0	70		
	190					W0	70		
	200					W0	70		
<p> W0: Fresh W3: Highly weathered W1: Slightly weathered W4: Completely weathered W2: Moderately weathered Borehole No: A-2(sheet No: 2 / 5) </p>									

Project: Baweishan Viaduct Geophysical Survey Plan

Bore No: A-2

Method: Rotary Drilling

Inclination: 90°

Total Depth: 50m

Water Level: GL-9.5m

Date: Jan.17.'06 ~ Jan .22.'06

SAMPLE NO	DEPTH (m)	CORE RECOVERY (%)	SPT DEPTH		N VALUE	WEATHER CONDITION	RQD (%)	GRAPHIC LOG	GEOLOGICAL DESCRIPTION
			BEGIN	END					
			(m)						
	100					W0	80		7.8~42.4m Shear Zone.
21	100				W0	70			
22	100				W0	80			
23	100				W0	90			
24	100				W0	70			
25	100				W0	100			
26	100				W0	80			
27	100				W0	100			
28	100				W0	90			
29	100				W0	90			
30	100				W0	90			

W0: Fresh **W3: Highly weathered**
W1: Slightly weathered **W4: Completely weathered**
W2: Moderately weathered **Borehole No: A-2(sheet No: 3 / 5)**

Bore No: A-2

Method: Rotary Drilling

Inclination: 90°

Total Depth: 50m

Water Level: GL-9.5m

Date: Jan.17.'06 ~ Jan .22.'06

SAMP LE NO	DEPTH (m)	CORE RECO- VERY (%)	SPT DEPTH		N VALUE	WEATHE R CONDI- TION	RQD (%)	GRA- PHIC LOG	GEOLOGICAL DESCRIPTION
			BEGIN	END					
			(m)						
								7.8~42.4m Shear Zone.	
	100					100			
31									
	100					80			
32									
	100					90			
33									
	100					85			
34									
	100					70			
35									
	100					80			
36									
	100					100			
37									
	100					100			
38									
	100					70			
39									
	100					100			
40									

W0: Fresh W3: Highly weathered
W1: Slightly weathered W4: Completely weathered
W2: Moderately weathered Borehole No: A-2(sheet No: 4 / 5)

Project: Baweishan Viaduct Geophysical Survey Plan

Bore No: A-2


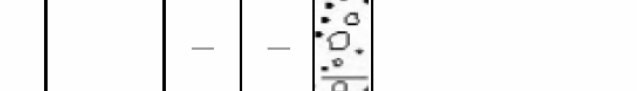
Method: Rotary Drilling

Inclination: 90°

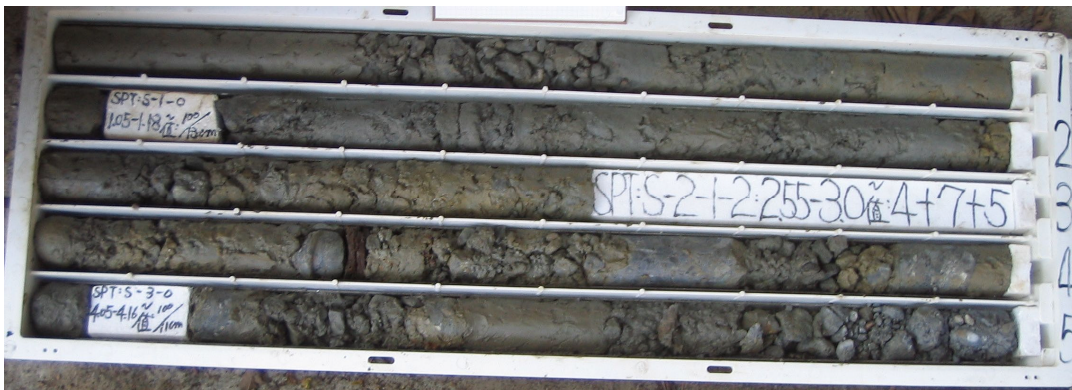
Total Depth: 50m

Water Level: GL-9.5m

Date: Jan.17.'06 ~ Jan .22.'06

SAMPLE NO	DEPTH (m)	CORE RECOVERY (%)	SPT DEPTH (m)		N VALUE	WEATHER CONDITION	RQD (%)	GRAPHIC LOG	GEOLOGICAL DESCRIPTION
			BEGIN	END					
	100					W0	90		7.8~42.4m Shear Zone.
41	100					W0	55		
42	—					—	—		42.4~50.0m Gravel with sand, yellowish brown.
43	—					—	—		
44	—					—	—		
45	—					—	—		
46	—					—	—		
47	—					—	—		
48	—					—	—		
49	—					—	—		
50	—					—	—		
50.0m									
END OF BORING									
W0: Fresh					W3: Highly weathered				
W1: Slightly weathered					W4: Completely weathered				
W2: Moderately weathered					Borehole No: A-2(sheet No: 5 / 5)				

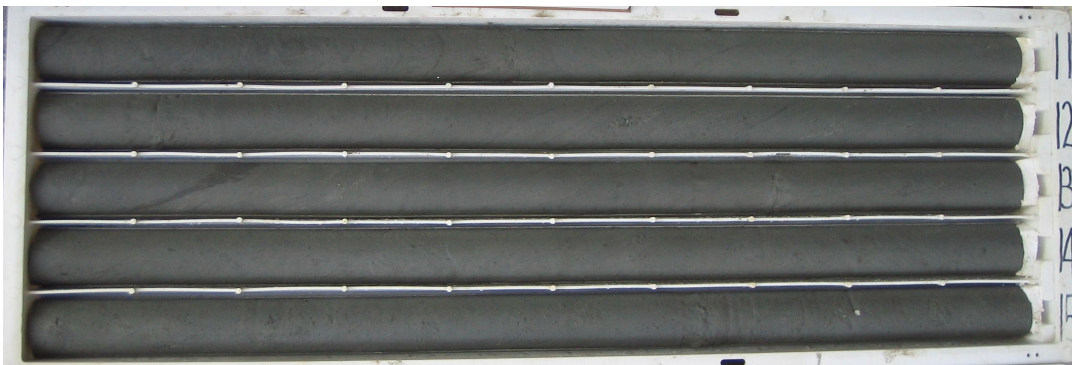
Photos of samples



A2: 1-5 m



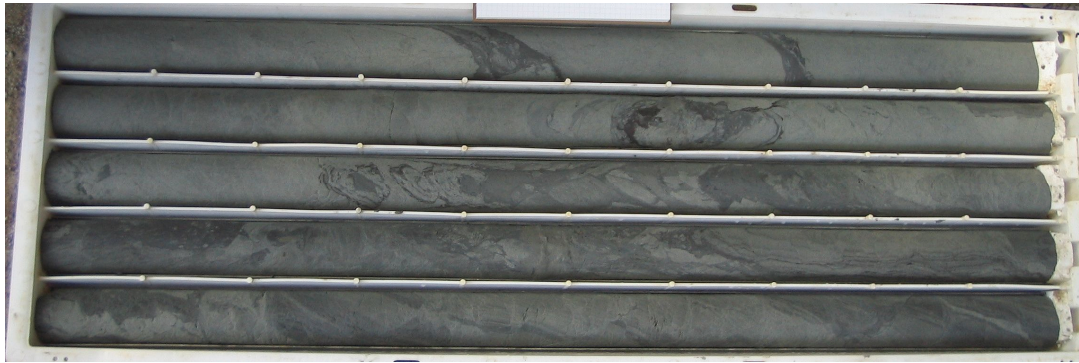
A2: 6-10 m



A2: 11-15 m



A2: 16-20 m



A2: 21-25 m



A2: 26-30 m



A2: 31-35 m



A2: 36-40 m



A2: 41-45 m



A2: 46-50 m

A1.4 BOREHOLE A3

Soil Profile

Project: Baweishan Viaduct Geophysical Survey Plan

Bore No: A-3



Method: Rotary Drilling

Inclination: 90°

Total Depth: 31m

Water Level: GL-4.0m

Date: Jan.05.'06 ~ Jan .07.'06

SAMPLE NO	DEPTH (m)	CORE RECOVERY (%)	SPT DEPTH		N VALUE	WEATHER CONDITION	RQD (%)	GRAPHIC LOG	GEOLOGICAL DESCRIPTION		
			BEGIN (m)	END (m)							
S-1	1	—	1.05	1.33	100/13cm	—	—		0.0~9.08m Soil Filled (Including R.C, gravels, clay and silt,...)		
	2	—	2.55	3.00	3+4+3	—	—				
S-2	3	—	4.05	4.50	5+3+4	—	—				
	4	—	5.55	5.65	100/10cm	—	—				
S-3	5	—	7.05	7.50	3+3+3	—	—				
	6	—	8.55	9.00	2+4+3	—	—				
S-4	7	—	100			W2	60				9.08~10.52m Silt, yellowish brown, with trace of gravels.
	8	—									
S-5	9	—									9.08m
S-6	10	—									

W0: Fresh

W1: Slightly weathered

W2: Moderately weathered

W3: Highly weathered

W4: Completely weathered

Borehole No: A-3(sheet No: 1 / 4)

Project: Baweshan Viaduct Geophysical Survey Plan

Bore No: A-3

Method: Rotary Drilling

Inclination: 90°

Total Depth: 31m

Water Level: GL-4.0m

Date: Jan.05.'06 ~ Jan .07.'06

SAMPLE NO	DEPTH (m)	CORE RECOVERY (%)	SPT DEPTH (m)		N VALUE	WEATHER CONDITION	RQD (%)	GRAPHIC LOG	GEOLOGICAL DESCRIPTION
			BEGIN	END					
S-7	100	100	10.05	10.32	19+100/12cm	W1	50		Silt, yellowish brown, with trace of gravels. 10.52m
S-8	100	100	11.55	11.68	100/13cm	W0	50		10.52~15.0 m Siltstone, grayish.
	100	100				W0	75		
	100	100				W0	60		
	100	100				W0	55		
	100	100				W0	45		
	100	100				W0	70		15.0~31.0m Shear Zone.
	100	100				W0	70		
	100	100				W0	60		
	100	100				W0	70		
	100	100				W0	70		

W0: Fresh

W1: Slightly weathered

W2: Moderately weathered

W3: Highly weathered

W4: Completely weathered

Borehole No: A-3(sheet No: 2 / 4)

Project: Baweishan Viaduct Geophysical Survey Plan

Bore No: A-3

Method: Rotary Drilling

Inclination: 90°

Total Depth: 31m

Water Level: GL-4.0m

Date: Jan.05.'06 ~ Jan .07.'06

SAMPLE NO	DEPTH (m)	CORE RECOVERY (%)	SPT DEPTH		N VALUE	WEATHER CONDITION	RQD (%)	GRAPHIC LOG	GEOLOGICAL DESCRIPTION
			BEGIN	END					
			(m)						
	100					W0	55		15.0~31.0m Shear Zone.
21	100				W0	80			
22	100				W0	60			
23	100				W0	90			
24	100				W0	100			
25	100				W0	70			
26	100				W0	90			
27	100				W0	80			
28	100				W0	80			
29	100				W0	100			
30									

W0: Fresh

W1: Slightly weathered

W2: Moderately weathered

W3: Highly weathered

W4: Completely weathered

Borehole No: A-3(sheet No: 3 / 4)

Project: Baweishan Viaduct Geophysical Survey Plan

Bore No: A-3

Method: Rotary Drilling

Inclination: 90°

Total Depth: 31m

Water Level: GL-4.0m

Date: Jan.05.'06 ~ Jan .07.'06

SAMPLE NO	DEPTH (m)	CORE RECOVERY (%)	SPT DEPTH		N VALUE	WEATHER CONDITION	RQD (%)	GRAPHIC LOG	GEOLOGICAL DESCRIPTION
			BEGIN	END					
			(m)						
	100					W0	100		15.0~31.0m Shear Zone.
	31								31.0m
									END OF BORING
	32								
	33								
	34								
	35								
	36								
	37								
	38								
	39								
	40								
W0: Fresh		W3: Highly weathered							
W1: Slightly weathered		W4: Completely weathered							
W2: Moderately weathered								Borehole No: A-3(sheet No: 4 / 4)	

Photos of samples



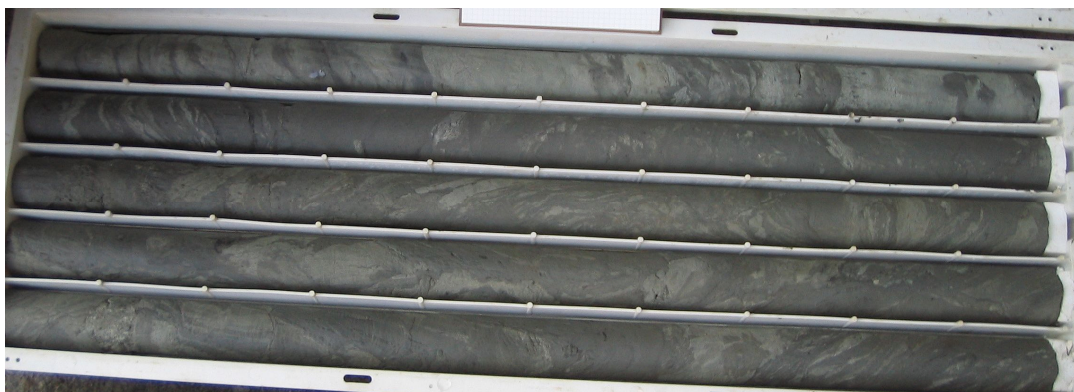
A3: 1-5 m



A3: 6-10 m



A3: 11-15 m



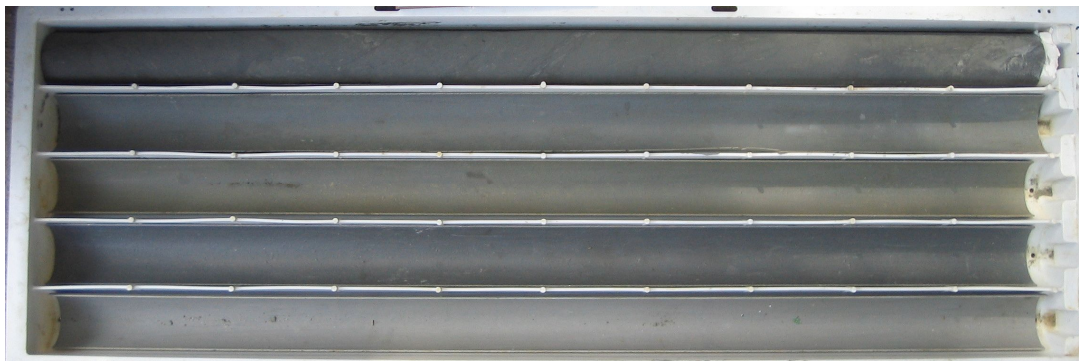
A3: 16-20 m



A3: 21-25 m



A3: 26-30 m



A3: 30-31 m

A1.5 BOREHOLE B1

Soil Profile

Project: Baweishan Viaduct Geophysical Survey Plan

Bore No: B-1



Method: Percussion Drilling

Inclination: 90°

Total Depth: 31m

Water Level: GL-9.7m

Date: Jan.08.'06 ~ Jan .09.'06

SAMPLE NO	DEPTH (m)	CORE RECOVERY (%)	SPT DEPTH		N VALUE	WEATHER CONDITION	RQD (%)	GRAPHIC LOG	GEOLOGICAL DESCRIPTION
			BEGIN (m)	END (m)					
S-1	1	—	1.05	1.50	4+6+8	—	—		0.0~4.8m Soil Filled (Including R.C , rock, clay and sily,...)
S-2	2	—	2.55	3.00	5+7+5	—	—		
S-3	3	—	4.05	4.50	6+7+10	—	—		
S-4	4	—	5.55	6.00	2+2+3	—	—		4.8~11.6m Sandy silt, yellowish brown, with trace of gravels.
S-5	5	—	7.05	7.50	3+3+4	—	—		
S-6	6	—	8.55	9.00	4+6+6	—	—		
S-7	7	—				—	—		
S-8	8	—				—	—		
S-9	9	—				—	—		
S-10	10	—				—	—		

W0: Fresh

W1: Slightly weathered

W2: Moderately weathered

W3: Highly weathered

W4: Completely weathered

Borehole No: B-1(sheet No: 1 / 4)

Project: Baweishan Viaduct Geophysical Survey Plan

Bore No: B-1

Method: Percussion Drilling

Inclination: 90°

Total Depth: 31m

Water Level: GL-9.7m

Date: Jan.08.'06 ~ Jan .09.'06

SAMP LE NO	DEPTH (m)	CORE RECO- VERY (%)	SPT DEPTH		N VALUE	WEATHE R CONDI- TION	RQD (%)	GRA- PHIC LOG	GEOLOGICAL DESCRIPTION
			BEGIN (m)	END (m)					
S-7	11	—	10.05	10.50	5+6+8	—	—	4.8~11.6m Sandy silt, yellowish brown, with trace of gravels.	
S-8	12	—	11.55	12.00	3+3+3	—	—	11.6~12.75m Silty clay, grayish.	
S-9	13	—	13.05	13.48	12+23+100/13cm	—	—	12.75~31.0m Gravel with silt and sand, yellowish brown.	
S-10	15	—	14.55	14.79	43+100/9cm	—	—		
S-11	16	—	16.05	16.12	100/7cm	—	—		
S-12	18	—	17.55	17.67	100/12cm	—	—		
S-13	19	—	19.05	19.44	39+67+100/9cm	—	—		
	20	—							

W0: Fresh **W3: Highly weathered**
W1: Slightly weathered **W4: Completely weathered**
W2: Moderately weathered

Borehole No: B-1(sheet No: 2 / 4)

Project: Baweishan Viaduct Geophysical Survey Plan

Bore No: B-1

Method: Percussion Drilling

Inclination: 90°

Total Depth: 31m

Water Level: GL-9.7m

Date: Jan.08.'06 ~ Jan .09.'06

SAMPLE NO	DEPTH (m)	CORE RECOVERY (%)	SPT DEPTH		N VALUE	WEATHER CONDITION	RQD (%)	GRAPHIC LOG	GEOLOGICAL DESCRIPTION		
			BEGIN	END							
			(m)								
									12.75~31.0m Gravel with silt and sand, yellowish brown.		
	31								31.0m		
	32								END OF BORING		
	33										
	34										
	35										
	36										
	37										
	38										
	39										
	40										
W0: Fresh			W3: Highly weathered								
W1: Slightly weathered			W4: Completely weathered								
W2: Moderately weathered			Borehole No: B-1(sheet No: 4 / 4)								

Project: Baweishan Viaduct Geophysical Survey Plan

Bore No: B-2

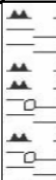
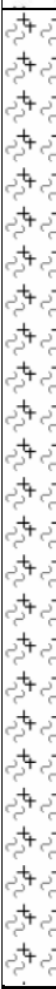
Method: Rotary Drilling

Inclination: 90°

Total Depth: 31m

Water Level: GL-10.0m

Date: Jan.11.'06 ~ Jan .15.'06

SAMPLE NO	DEPTH (m)	CORE RECOVERY (%)	SPT DEPTH (m)		N VALUE	WEATHER CONDITION	RQD (%)	GRAPHIC LOG	GEOLOGICAL DESCRIPTION						
			BEGIN	END											
S-7	100		10.05	10.50	2+2+3	W0	40		Silty clay, grayish. 10.6~11.5m Sandy silt or clay, grayish brown, with trace of gravels						
	110												10.6m		
S-8	100		11.55	11.68	100/13cm	W0	50		11.5~24.4m Shear Zone						
	110														11.5m
	120														
	130														
	140														
	150														
	160														
	170														
	180														
	190														
200															

W0: Fresh

W3: Highly weathered

W1: Slightly weathered

W4: Completely weathered

W2: Moderately weathered

Borehole No: B-2(sheet No: 2 / 4)

Project: Baweishan Viaduct Geophysical Survey Plan

Bore No: B-2

Method: Rotary Drilling

Inclination: 90°

Total Depth: 31m

Water Level: GL-10.0m

Date: Jan.11.'06 ~ Jan .15.'06

SAMPLE NO	DEPTH (m)	CORE RECOVERY (%)	SPT DEPTH		N VALUE	WEATHER CONDITION	RQD (%)	GRAPHIC LOG	GEOLOGICAL DESCRIPTION
			BEGIN	END					
			(m)						
	100					W0	40		Shear Zone
21						W0	80		
22						W0	90		
23						W0	100		
24									24.4m
25									24.4~31.0m Gravel with sand and silt.
26									
27									
28									
29									
30									

W0: Fresh

W3: Highly weathered

W1: Slightly weathered

W4: Completely weathered

W2: Moderately weathered

Borehole No: B-2(sheet No: 3 / 4)

Project: Baweishan Viaduct Geophysical Survey Plan

Bore No: B-2

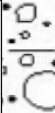
Method: Rotary Drilling

Inclination: 90°

Total Depth: 31m

Water Level: GL-10.0m

Date: Jan.11.'06 ~ Jan .15.'06

SAMPLE NO	DEPTH (m)	CORE RECOVERY (%)	SPT DEPTH		N VALUE	WEATHER CONDITION	RQD (%)	GRAPHIC LOG	GEOLOGICAL DESCRIPTION
			BEGIN	END					
			(m)						
	31	—				—	—	 24.4~31.0m Gravel with sand and silt.	31.0m
	32							END OF BORING	
	33								
	34								
	35								
	36								
	37								
	38								
	39								
	40								
W0: Fresh		W3: Highly weathered							
W1: Slightly weathered		W4: Completely weathered							
W2: Moderately weathered		Borehole No: B-2(sheet No: 4 / 4)							

Photos of samples



B2: 1-5 m



B2: 6-10 m



B2: 11-15 m



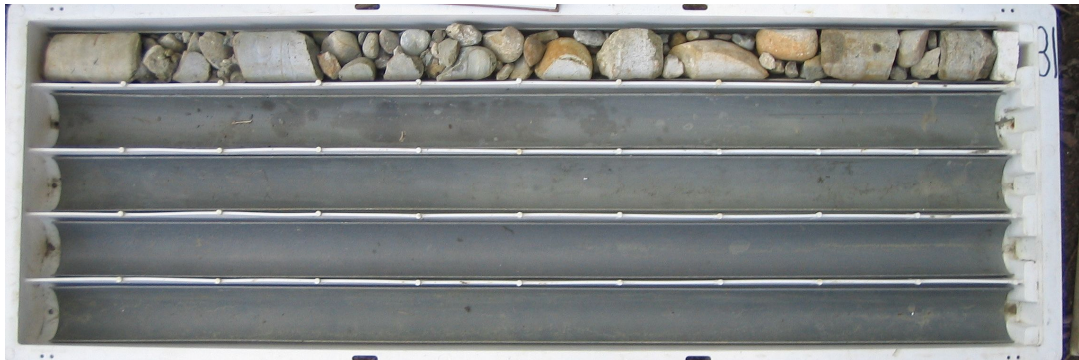
B2: 16-20 m



B2: 21-25 m



B2: 26-30 m



B2: 30-31 m

A1.7 BOREHOLE B3

Soil Profile

Project: Baweishan Viaduct Geophysical Survey Plan

Bore No: B-3



Method: Percussion Drilling

Inclination: 90°

Total Depth: 31m

Water Level: GL-9.5m

Date: Jan.05.'06 ~ Jan .09.'06

SAMP LE NO	DEPTH (m)	CORE RECO- VERY (%)	SPT DEPTH		N VALUE	WEATHE R CONDI- TION	RQD (%)	GRA- PHIC LOG	GEOLOGICAL DESCRIPTION
			BEGIN (m)	END (m)					
S-1	1	—	1.05	1.50	5+7+26	—	—	 0.0~2.3m Soil Filled: (Including RC, gravels, rock, clay and silt,...)	
S-2	2	—	2.55	3.00	2+2+3	—	—		
S-3	3	—	4.05	4.50	2+3+3	—	—	 2.3~11.85m Sandy silt, yellowish brown, with trace of 'gravels	
S-4	4	—	5.55	6.00	3+5+7	—	—		
S-5	5	—	7.05	7.50	3+3+3	—	—		
S-6	6	—	8.55	9.00	3+3+4	—	—		
	7	—				—	—		
	8	—				—	—		
	9	—				—	—		
	10	—				—	—		

W0: Fresh

W3: Highly weathered

W1: Slightly weathered

W4: Completely weathered

W2: Moderately weathered

Borehole No: B-3(sheet No: 1 / 4)

Project: Baweishan Viaduct Geophysical Survey Plan

Bore No: B-3


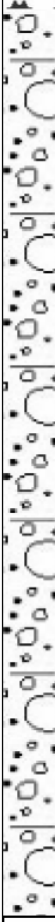
Method: Percussion Drilling

Inclination: 90°

Total Depth: 31m

Water Level: GL-9.5m

Date: Jan.05.'06 ~ Jan .09.'06

SAMPLE NO	DEPTH (m)	CORE RECOVERY (%)	SPT DEPTH		N VALUE	WEATHER CONDITION	RQD (%)	GRAPHIC LOG	GEOLOGICAL DESCRIPTION
			BEGIN (m)	END (m)					
S-7	11	—	10.05	10.50	3+3+3	—	—		Sandy silt, yellowish brown, with trace of gravels
S-8	12	—	11.55	12.00	3+4+3	—	—		11.85~12.3m Silty clay, grayish.
S-9	13	—	13.05	13.45	7+19+100/10cm	—	—		12.3~31.0m Gravel with sand and silt.
S-10	15	—	14.55	14.61	100/6cm	—	—		
S-11	16	—	16.05	16.33	42+100/13cm	—	—		
S-12	18	—	17.55	17.61	100/6cm	—	—		
S-13	19	—	19.05	19.19	100/14cm	—	—		
	20	—							

W0: Fresh

W3: Highly weathered

W1: Slightly weathered

W4: Completely weathered

W2: Moderately weathered

Borehole No: B-3(sheet No: 2 / 4)

Project: Baweishan Viaduct Geophysical Survey Plan

Bore No: B-3

Method: Percussion Drilling

Inclination: 90°

Total Depth: 31m

Water Level: GL-9.5m

Date: Jan.05.'06 ~ Jan .09.'06

SAM- PLE NO	DEPTH (m)	CORE RECO- VERY (%)	SPT DEPTH		N VALUE	WEATHE R CONDI- TION	RQD (%)	GRA- PHIC LOG	GEOLOGICAL DESCRIPTION
			BEGIN	END					
			(m)						
S-14	21	—	20.55	20.93	24+37+100/8cm	—	—		Gravel with sand and silt.
S-15	22	—	22.05	22.14	100/9cm	—	—		
S-16	24	—	23.55	23.66	100/11cm	—	—		
S-17	25	—	25.05	25.09	100/4cm	—	—		
S-18	27	—	26.55	26.62	100/7cm	—	—		
S-19	28	—	28.05	28.10	100/5cm	—	—		
S-20	30	—	29.55	29.61	100/6cm	—	—		

W0: Fresh **W3: Highly weathered**
W1: Slightly weathered **W4: Completely weathered**
W2: Moderately weathered **Borehole No: B-3(sheet No: 3 / 4)**

Project: Baweishan Viaduct Geophysical Survey Plan

Bore No: B-3

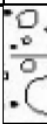
Method: Percussion Drilling

Inclination: 90°

Total Depth: 31m

Water Level: GL-9.5m

Date: Jan.05.'06 ~ Jan .09.'06

SAMPLE NO	DEPTH (m)	CORE RECOVERY (%)	SPT DEPTH		N VALUE	WEATHER CONDITION	RQD (%)	GRAPHIC LOG	GEOLOGICAL DESCRIPTION
			BEGIN	END					
			(m)						
	31	—				—	—		Gravel with sand and silt.
									31.0m
	32								END OF BORING
	33								
	34								
	35								
	36								
	37								
	38								
	39								
	40								
W0: Fresh		W3: Highly weathered							
W1: Slightly weathered		W4: Completely weathered							
W2: Moderately weathered		Borehole No: B-3(sheet No: 4 / 4)							

A1.8 BOREHOLE B4

Soil Profile

Project: Baweishan Viaduct Geophysical Survey Plan

Bore No: B-4

Method: Percussion Drilling

Inclination: 90°

Total Depth: 50m

Water Level: GL-9.9m

Date: Jan.10.'06 ~ Jan .11.'06

SAMPLE NO	DEPTH (m)	CORE RECOVERY (%)	SPT DEPTH		N VALUE	WEATHER CONDITION	RQD (%)	GRAPHIC LOG	GEOLOGICAL DESCRIPTION
			BEGIN (m)	END (m)					
									0.0~3.2m Soil Filled
S-1	1	—	1.05	1.50	6+7+9	—	—		
S-2	3	—	2.55	3.00	5+4+6	—	—		
S-3	4	—	4.05	4.50	2+3+3	—	—		
S-4	6	—	5.55	6.00	3+3+4	—	—		
S-5	7	—	7.05	7.50	4+3+4	—	—		
S-6	9	—	8.55	9.00	4+7+5	—	—		
	10								9.95m
W0: Fresh W1: Slightly weathered W2: Moderately weathered			W3: Highly weathered W4: Completely weathered						
Borehole No: B-4(sheet No: 1 / 4)									

Project: Baweishan Viaduct Geophysical Survey Plan

Bore No: B-4

Method: Percussion Drilling

Inclination: 90°

Total Depth: 50m

Water Level: GL-9.9m

Date: Jan.10.'06 ~ Jan .11.'06

SAMPLE NO	DEPTH (m)	CORE RECOVERY (%)	SPT DEPTH		N VALUE	WEATHER CONDITION	RQD (%)	GRAPHIC LOG	GEOLOGICAL DESCRIPTION
			BEGIN	END					
			(m)						
	21	—				—	—		Shear Zone
	22	—				—	—		21.3~31.0m Gravel with sand and silt.
	23	—				—	—		
	24	—				—	—		
	25	—				—	—		
	26	—				—	—		
	27	—				—	—		
	28	—				—	—		
	29	—				—	—		
	30	—				—	—		

W0: Fresh

W3: Highly weathered

W1: Slightly weathered

W4: Completely weathered

W2: Moderately weathered

Borehole No: B-4(sheet No: 3 / 4)

